CARBONATE CLUMPED ISOTOPE GEOCHEMISTRY

ASSESSMENT OF THE CLUMPED ISOTOPE COMPOSITION OF CALCITE FOR PALEOTHERMOMETERY

By CHRISTOPHER SPENCER, B.Sc.

A Thesis Submitted to the School of Graduate Studies in Partial Fulfilment of the Requirements for the Degree Master of Science

McMaster University

McMaster University MASTER OF SCIENCE (2015) Hamilton, Ontario (Geochemistry)

TITLE: Assessment of the Clumped Isotope Composition of Carbonates for Geothermometry

AUTHOR: Christopher Spencer, B.Sc. (McMaster University)

SUPERVISOR: Assistant Professor S.-T. Kim

NUMBER OF PAGES: 142.

PRELIMINARIES

ABSTRACT

Clumped isotope paleothermometry defines carbonate formation temperature based upon the relative abundance of the $^{13}C^{18}O^{16}O$ isotopologue within CO_2 (Δ_{47}) formed through phosphoric acid digestion of carbonates. When precipitated in equilibrium, resultant Δ_{47} values are inversely-proportional to growth temperature, where $^{13}C^{18}O^{16}O$ is more abundant at lower temperatures. To precisely define Δ_{47} values, a rigorous analytical protocol is required to: (1) minimize CO_2-H_2O isotope exchange during acid digestion; (2) purify CO_2 to remove contaminants; (3) quantify the raw Δ_{47} value using a mass spectrometer configured for *m/z* 44 – 49; and (4) normalize the raw Δ_{47} value to account for machine-specific isotopic scrambling and Δ_{47} vs. δ^{47} non-linearity. Amongst laboratories with well-established analytical protocols, substantial disagreement still exists between proposed clumped isotope calibrations at low temperatures. To investigate the source of this discrepancy, calcite was precipitated between 15 – 40 °C from a $HCO_3^-{}_{(aq)}$-dominated solution using an upgraded constant addition technique. This technique is the first to provide simultaneous control of $\delta^{18}O_{H2O}$ and $\delta^{13}C_{DIC}$ values of parent solution. Observed oxygen isotope fractionation between calcite and water is in agreement with Kim and O'Neil (1997), providing robust evidence of calcite precipitation in oxygen isotope equilibrium. Δ_{47} values were determined using McMaster's clumped isotope facility, yielding the following calibration:

$$\Delta_{47\text{-}RF} = 0.0351\ (\pm\ 0.0021) \times 10^6/T^2 + 0.2982\ (\pm\ 0.0233)$$

This calibration observes a similar temperature dependency to theoretical models as well as ‘*shallow*’ slope experimental studies. To provide context to experimental calibrations with ‘*steep*’ slopes, we consider the non-equilibrium isotope effects of CO_2 hydration/hydroxylation and HCO_3^- dehydration/dehydroxylation reactions on precipitating calcite. We propose that low temperature calcites primarily responsible for the ‘*steep*’ slopes of certain calibrations have partially inherited the disequilibrium isotope composition of DIC due to significant non-equilibrium isotope effects associated with the aforementioned CO_2 hydration/hydroxylation and HCO_3^- dehydration/dehydroxylation reactions.

ACKNOWLEDGEMENTS

I would first like to extend my gratitude to my supervisor, Dr. Sang-Tae Kim, for his continued encouragement, guidance and friendship over these past years. When I first met Dr. Kim in 2010, I admired his keen interest in geochemical investigation, and his determination to solve geochemistry's most perplexing questions. This admiration fueled my interesting in stable isotope geochemistry, and provided the necessary encouragement to complete my Master's. I cannot thank him enough for assisting me throughout this degree. I would also like to thank my committee members, Dr. Henry P. Schwarcz and Dr. Greg Slater for their feedback, and constructive criticism during revision of this thesis.

I must also thank and acknowledge the members of the McMaster Research Group for Stable Isotopologues, Martin Knyf, Mohammed El Shenawy, Jill Wyman, Nicolas Randazzo and Kesia Ie. Your friendship, support and laughter helped me through some considerably stressful isotopic challenges. Further, Alan Sawula and Ajit Nagi were fundamental members of the team that developed and testing McMaster's automated clumped isotope CO_2 purification system. I cannot thank them enough. Without their work, I would not have achieved the results presented in this thesis.

Finally, none of this would have been possible without the unconditional support of my family and loved ones. They understood the sacrifices associated with academic pursuits. I'm sorry for coming home late to so many meals, however it was most assuredly worth it! Thank you Nicole, James and Pippa, I could not have accomplished any of this without your love.

TABLE OF CONTENTS

CHAPTER 3: Deciphering clumped and oxygen isotope effects in the low temperature calcite-water system..77

LIST OF FIGURES

LIST OF TABLES

CHAPTER 1: Introduction

1.1. Evolution of the Carbonate-Water Oxygen Isotope Paleothermometer

Urey (1947)'s proposition of a temperature dependence between the oxygen isotope composition of carbonates and their parent water arguably represents one of the most significant discoveries in stable isotope geoscience. Early experimental and empirical confirmations of this carbonate-water oxygen isotope paleothermometer (e.g., McCrea, 1950; Epstein, 1951; O'Neil et al., 1969) enabled paleoclimate reconstructions of vast portions of Earth's history, in some cases extending as far back as the Cambrian period (Wadleigh and Veizer, 1992). Several conditions are required to precisely determine the formation temperature of carbonate. First, carbonates must precipitate in oxygen isotope equilibrium with respect to their parent water. Second, the oxygen isotope composition of the parent water must be measurable or reliably estimated. Finally, consideration must be given to mineral- and/or species-specific isotope effects, where differing carbonate minerals and/or biogenic carbonates can exhibit a unique carbonate-water oxygen isotope fractionation relationship.

The calcite-water oxygen isotope paleothermometer proposed by Kim and O'Neil (1997) provides an experimental depiction of oxygen isotope equilibrium precipitation, and has been substantiated by several experimental precipitation studies (e.g., Jiménez-López et al., 2001) and theoretical oxygen isotope fractionation models (e.g., Horita and Clayton, 2007; Chacko and Deines, 2008). This calibration has been applied to derive paleotemperature fluctuations as well as to estimate the oxygen isotope composition of ancient marine waters (McManus et al., 1999; Adkins et al., 2002; Garzione et al., 2008).

Possibly the most common complication when applying the oxygen isotope carbonate-water paleothermometer to ancient carbonates is the accurate estimation of the oxygen isotope composition of parent water. For oceanic carbonate records, the evolution of the oxygen isotope composition of ocean water was largely believed to be well-buffered by oxygen isotope cycling through the Earth's crust (Muehlenbachs and Clayton, 1976; Lécuyer and Allemand, 1999). However, more recent modeling of Earth's oxygen cycling suggests significant oxygen isotope composition changes may have occurred throughout Earth's history (Jaffrés et al., 2007).

Carbonates must also be screened for possible non-equilibrium isotope effects during formation and/or diagenetic alteration during preservation. In the carbonate-water system, non-equilibrium oxygen isotope effects can result from physicochemical properties of the parent solution (i.e., pH, salinity, and saturation state), precipitation rate, and the isotopic composition of dissolved inorganic carbon (DIC) (Kim and O'Neil, 1997; Kim et al., 2006; Dietzel et al., 2009). For example, oxygen isotope non-equilibrium isotope effects associated CO_2 hydration/hydroxylation can lower the oxygen isotope composition of precipitating carbonates relative to the equilibrium value (Clark et al., 1992). An opposite increase in the oxygen isotope composition of carbonates relative to the equilibrium value can be caused by non-equilibrium isotope effects associated with HCO_3^- dehydration/dehydroxylation, most prominent in CO_2 degassing systems (Clark and Lauriol, 1992). Diagenetic alteration can occur during the fossilization stages of biogenic carbonates, or through oxygen isotope exchange with water, mediated by the increased pressure from depositional loading of detritus (Veizer, 1992).

Although the carbonate-water oxygen isotope paleothermometer provides invaluable insight into Earth's paleoclimate history, its application can be complicated by non-equilibrium isotope effects during carbonate precipitation, diagenetic alteration of the carbonate mineral post-formation, and imprecise estimation of the oxygen isotope composition of parent water.

1.2. Discrepancies among Calibrations of the Calcite-Water Oxygen Isotope Paleothermometer

Several recent publications have observed substantially different calcite-water oxygen isotope fractionation in comparison to the Kim and O'Neil (1997) calcite-water oxygen isotope equilibrium curve (Figure 1). Most notably, Coplen (2007) reported a larger than expected oxygen isotope fractionation from a vein calcite precipitated at 33.7 °C in Devils Hole, Nevada. Through adoption of a similar temperature-dependence to Kim and O'Neil 1997), Coplen (2007) extrapolated the calcite-water fractionation of this Devils Hole calcite to provide a new calibration of the calcite-water oxygen isotope paleothermometer. Demény et al. (2010) reported similar findings to Coplen (2011) in 30 – 70 °C travertines collected near Egerszalók, Hungary and Tenerife, Spain. However, Demény et al. (2010) also collected calcites precipitated in cave pools between 10 – 25 °C from the Baradla Cave and the Csodabogyós Cave that conform more closely to the Kim and O'Neil (1997) calibration.

Elevated calcite-water oxygen isotope fractionation can be associated to a non-equilibrium isotope effect. For example, the oxygen isotope composition of a precipitating carbonate can partially inherit the oxygen isotope composition of HCO_3^- if precipitated rapidly from a HCO_3-dominated solution. Given that the oxygen isotope fractionation of HCO_3^--water is larger than that of calcite-water at equilibrium, calcites that partially inherit this isotopic signature would appear isotopically enriched relative to the expected equilibrium value. Alternatively, an elevated oxygen isotope composition can also relate to substantial evaporation, altering the oxygen isotope composition of the parent water. Coplen (1997) mitigates these concerns by providing evidence to support that Devils Hole calcite precipitated slowly, and in an environment of 100% relative humidity. The source of this discrepancy remains elusive; however, it constitutes further investigation to ensure the correct definition of the calcite-water oxygen isotope paleothermometer.

1.3. A New Paleothermometer Derived from the Clumped Isotope Composition of Carbonates

Carbonate clumped isotope geochemistry provides a new method of deriving carbonate formation temperature based upon the abundance of ^{13}O-^{18}O bonds preserved in carbonates (Eiler and Schauble, 2004; Ghosh et al., 2006; Dennis and Schrag, 2010). The abundance of ^{13}C-^{18}O bonds is temperature dependent, and is governed by the following homogeneous isotope exchange reaction:

$$Ca^{13}C^{16}O^{16}O^{16}O + Ca^{12}C^{18}O^{16}O^{16}O \leftrightarrow Ca^{13}C^{18}O^{16}O^{16}O + Ca^{12}C^{16}O^{16}O^{16}O \qquad (1)$$

In comparison to the carbonate-water oxygen isotope paleothermometer, the clumped isotope composition of carbonates is independent of the oxygen isotope composition of parent water. Furthermore, experimental observations suggest that the clumped isotope composition of a carbonate may still reflect equilibrium in cases where increased precipitation rate, solution pH or salinity produces non-equilibrium oxygen isotope effects (Tang et al., 2014). Consideration must still be given to diagenetic alteration of the clumped isotope signature of preserved carbonates. In calcites, digenetic alteration is likely insignificant in carbonates preserved for up to 100 Ma so long as they are not exposed to temperatures above 100 °C (Henkes et al., 2014).

Given the inherent constraints of the dual-inlet gas-source isotope ratio mass spectrometer (i.e., samples must be in a gaseous form), the direct analytical quantification of the clumped isotope composition of carbonates is not yet possible. Instead, Ghosh et al. (2006) discovered that the clumped isotope composition of CO_2 gas produced through phosphoric acid digestion of carbonates was reflective of carbonate formation temperature. For CO_2, this clumped isotope signature is quantified by the Δ_{47} value; defined as the relative abundance of the $^{13}C^{18}O^{16}O$ isotopologue relative to a predicted high temperature stochastic distribution of all CO_2 isotopologues. Precisely quantifying this Δ_{47} value is analytically challenging. This is largely due to the remarkably low abundance of this rare clumped isotope. The $^{13}C^{18}O^{16}O$ isotopologue typically constitutes ~ 45 ppm of a CO_2 gas. In comparison, conventional oxygen isotope analysis compares the ratio of $^{18}O/^{16}O$ (i.e., $^{12}C^{18}O^{16}O/^{12}C^{16}O^{16}O$) where the $^{12}C^{18}O^{16}O$ isotopologue typically accounts for ~ 4000 ppm of a CO_2 gas.

Carbonate precipitation experiments have defined the clumped isotope temperature dependence relationship for inorganic calcite, aragonite and siderite (Ghosh et al., 2006; Dennis and Schrag, 2010; Defliese et al., 2015; Fernandez et al., 2014). Empirical studies have defined this temperature dependence for various $CaCO_3$ records, inclusive to bivalves, brachiopods, deep sea and surface corals, fish otoliths, foraminifera, eggshells, travertines, and tufa (Ghosh et al., 2006, 2007; Grauel et al., 2013; Wacker et al., 2014; Kele et al., 2015). The temperature resolution of the carbonate clumped isotope paleothermometer is reliant on three primary components: (1) ensuring the aforementioned non-equilibrium isotope effects are minimal; (2) precisely defining the clumped isotope composition through a rigorous analytical protocol; and (3) application of the applicable carbonate clumped isotope paleothermometer calibration.

1.4. The Carbonate Clumped Isotope Calibration Discrepancy: What Constitutes True Carbonate Clumped Isotope Equilibrium?

Problematic to current carbonate clumped isotope paleothermometry, a disagreement exists between calibrations of the carbonate clumped isotope paleothermometer (Figure 2). Calibrations may be categorized by those exhibiting a *'shallow'* slope, and those exhibiting a *'steep'* slope (Figure 2). *'Shallow'* slope calibrations include the experimental calibrations of Dennis and Schrag (2010), Tang et al. (2014), and Defliese et al. (2015), the empirical calibrations of Eagle et al. (2013), Henkes et al. (2013), Petrizzo et al. (2014), and Wacker et al. (2014), and finally, the theoretical calibrations of Guo et al. (2009) and Hill et al. (2014). In comparison, the *‘steep’* slope calibrations include the experimental calibrations of Ghosh et al. (2006), Tripati et al. (2010), Zaarur et al. (2013), and Kluge et al. (2015), and the empirical calibrations of Thiagarajan et al. (2011) and Kele et al. (2015). Several calibrations which appear to conform to either category are excluded from this list as they are solely reported using a different Δ_{47} value normalization protocol, complicating their interpretation.

Proposed analytical sources of this discrepancy include several aspects of CO_2 purification (e.g., acid digestion temperature, H_2O-CO_2 exchange, etc.) and/or the method of normalization for the Δ_{47} value (Eagle et al., 2013; Wacker et al., 2014; Defliese et al., 2015). Instead, it is possible that either *’steep’* or *‘shallow’* slope carbonates may have partially inherited a non-equilibrium clumped isotope effect not yet characterized (Henkes et al., 2013). Resolution of this calibration discrepancy will presumably require either improved analytical techniques for quantifying the Δ_{47} value of carbonates, and/or in-depth assessment of the isotopic behavior of clumped isotopes in the carbonate-water system.

1.5. Figures

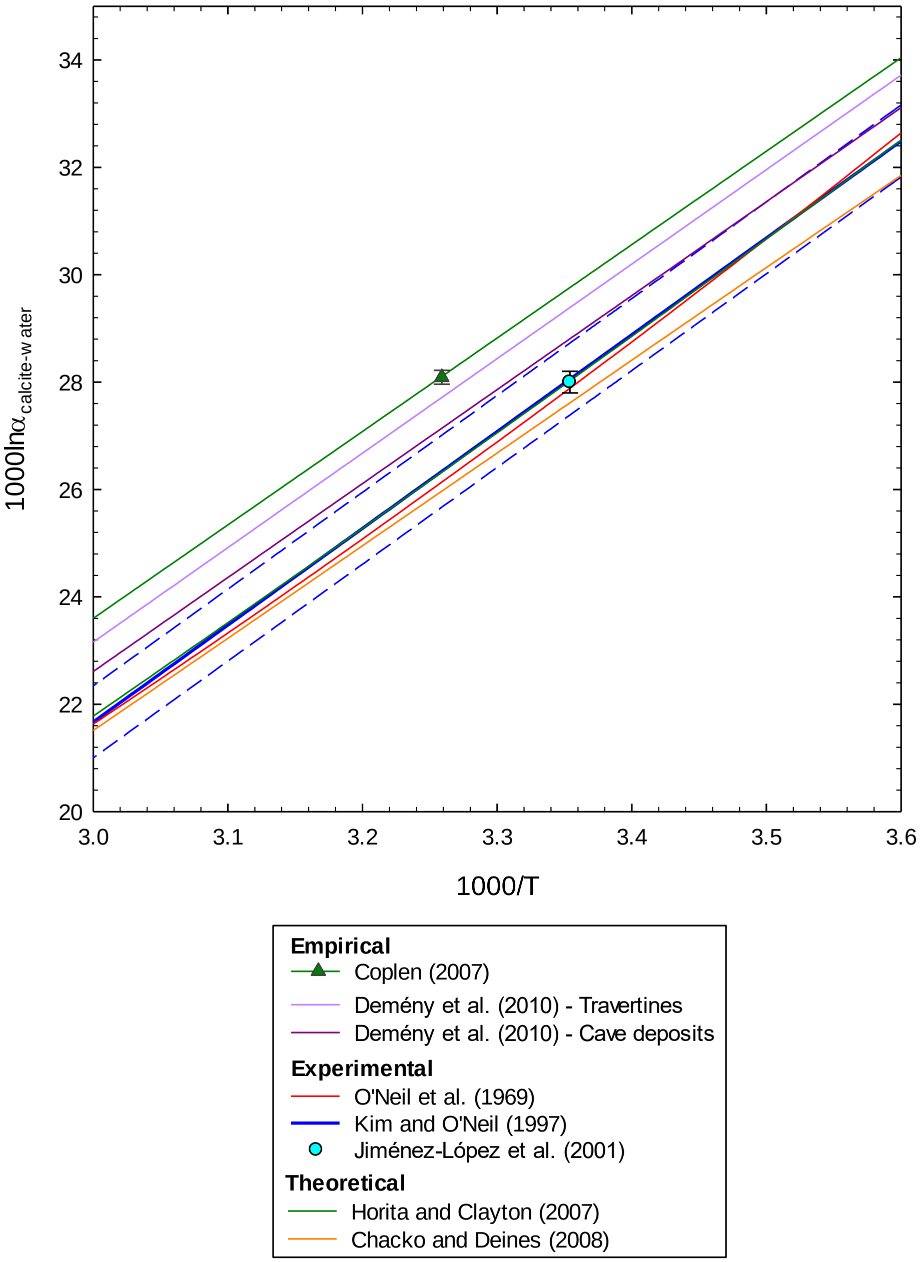

Figure 1: Compilation of calcite-water oxygen isotope fractionations factors and calibrations from empirical, experimental, and theoretical studies. Blue dashed lines represent the upper and lower boundaries of the analytical precision associated with the $1000\ln\alpha_{\text{calcite-water}}$ value relative to the Kim and O'Neil (1997) equilibrium curve. Values within this boundary are considered to reflect calcite-water oxygen isotope equilibrium.

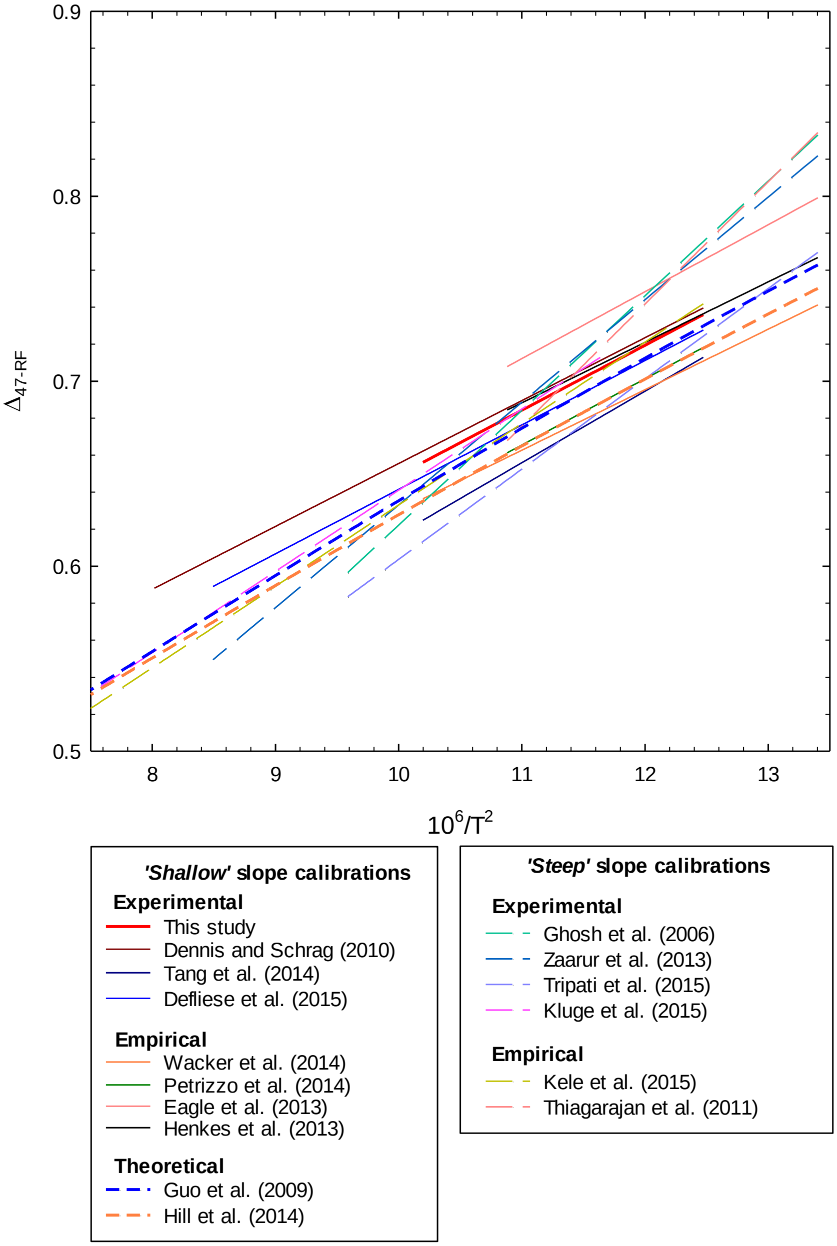

Figure 2: *'Shallow'* and *'steep'* calibrations of the $CaCO_3$ clumped isotope paleothermometer. 'This study' refers to findings discussed in Chapter 3. Ghosh et al. (2006), Dennis and Schrag (2010), Thiagarajan et al. (2011) and Eagle et al. (2013) have been re-projected to the absolute reference frame using a 2-point transfer function. Where applicable, calibrations are presented with a $\Delta_{25\text{-}Tacid}$ determined using Eq. 23 from Guo et al. (2009). Theoretical calibrations are projected using the Δ_{63}- Δ_{47} AFF = 0.280 ‰ defined by Tripati et al. (2015).

1.6. References

Adkins J. F., McIntyre K. and Schrag D. P. (2002) The salinity, temperature, and δ^{18}O of the glacial deep ocean. *Science* **298**, 1769–1773.

Chacko T. and Deines P. (2008) Theoretical calculation of oxygen isotope fractionation factors in carbonate systems. *Geochimica et Cosmochimica Acta* **72**, 3642–3660.

Clark I. D., Fontes J.-C., and Fritz P. (1992) Stable isotope disequilibria in travertine from high pH waters: Laboratory investigations and field observations from Oman. *Geochimica et Cosmochimica Acta* **56**, 2041–2050.

Clark I. D. and Lauriol B. (1992) Kinetic enrichment of stable isotopes in cryogenic calcites. *Chemical Geology* **102,** 217–228.

Coplen T. B. (2007) Calibration of the calcite-water oxygen-isotope geothermometer at Devils Hole, Nevada, a natural laboratory. *Geochimica et Cosmochimica Acta* **71**, 3948–3957.

Defliese W. F., Hren M. T. and Lohmann K. C. (2015) Compositional and temperature effects of phosphoric acid fractionation on Δ_{47} analysis and implications for discrepant calibrations. *Chemical Geology* **396**, 51–60.

Demény A., Kele S., and Siklósy Z. (2010) Empirical equations for the temperature dependence of calcite-water oxygen isotope fractionation from 10 to 70 °C. *Rapid Communications in Mass Spectrometry* **24**, 3521–3526.

Dennis K. J. and Schrag D. P. (2010) Clumped isotope thermometry of carbonatites as an indicator of diagenetic alteration. *Geochimica et Cosmochimica Acta* **74**, 4110–4122.

Dietzel M., Tang J., Leis A. and Köhler S. J. (2009) Oxygen isotope fractionation during inorganic calcite precipitation – Effects of temperature, precipitation rate and pH. *Chemical Geology* **268**, 107–115.

Eagle R.A., Eiler J.M., Tripati A.K., Ries J.B., Freitas P.S., Hiebenthal C., Wanamaker Jr. A. D., Taviana M., Elliot M., Marenssi S., Nakamura K., Ramirez P., and Roy K. (2013) The influence of temperature and seawater carbonate saturation state on ^{13}C-^{18}O bond ordering in bivalve mollusks. *Biogeosciences* **10**, 4591–4606.

Eiler J. M. and Schauble E. (2004) $^{18}O^{13}C^{16}O$ in Earth's atmosphere. *Geochimica et Cosmochimica Acta* **68**, 4767–4777.

Epstein S., Buchsbaum R., Lowenstam H., and Urey H. C. (1951) Carbonate-water isotopic temperature scale. *Bulletin of the Geological Society of America* **62**, 417–425.

Fernandez A., Tang J. and Rosenheim B. E. (2014) Siderite 'clumped' isotope thermometry: A new paleoclimate proxy for humid continental environments. *Geochimica et Cosmochimica Acta* **126**, 411–421.

Garzione C. N., Hoke G. D., Libarkin J. C., Withers S., Macfadden B., Eiler J., Ghosh P. and Mulch A. (2008) Rise of the Andes. *Science* **320**, 1304–1307.

Ghosh P., Adkins J., Affek H., Balta B., Guo W., Schauble E. A., Schrag D. and Eiler J. M. (2006) ^{13}C–^{18}O bonds in carbonate minerals: A new kind of paleothermometer. *Geochimica et Cosmochimica Acta* **70**, 1439–1456.

Ghosh P., Eiler J., Campana S. E., and Feeney R. F. (2007) Calibration of the carbonate 'clumped isotope' paleothermometer for otoliths. *Geochimica et Cosmochimica Acta* **71**, 2736–2744.

Grauel A.-L.. Schmid T. W., Hu B., Bergami C., Capotondi L., Zhou L. and Bernasconi S. M. (2013) Calibration and application of the 'clumped isotope' thermometer to foraminifera for high-resolution climate reconstructions. *Geochimica et Cosmochimica Acta* **108**, 125–140.

Guo W., Mosenfelder J. L., Goddard III W. A. and Eiler J. M. (2009) Isotopic fractionations associated with phosphoric acid digestion of carbonate minerals: Insights from first-principles theoretical modeling and clumped isotope measurements. *Geochimica et Cosmochimica Acta* **73**, 7203–7225.

Henkes G. A., Passey B. H., Wanamaker Jr., A. D., Grossman E. L., Ambrose Jr. W. G., and Carroll M. L. (2013) Carbonate clumped isotope compositions of modern marine mollusk and brachiopod shells. *Geochimica et Cosmochimica Acta* **106**, 307–325.

Henkes G. A., Passey B. H., Grossman E. L., Shenton B. J., Pérez-Huerta A., and Yancy T. E. (2014) Temperature limits for preservation of primary calcite clumped isotope paleotemperatures. *Geochimica et Cosmochimica Acta* **139**, 362–382.

Hill P. S., Schauble E. A. and Tripati A. K. (2014) Theoretical constraints on the effects of pH, salinity, and temperature on clumped isotope signatures of dissolved inorganic carbon species and precipitating carbonate minerals. *Geochimica et Cosmochimica Acta* **125**, 610–652.

Horita J. and Clayton R. N. (2007) Comment on the studies of oxygen isotope fractionation between calcium carbonates and water at low temperatures by Zhou and Zheng (2003; 2005). *Geochimica et Cosmochimica Acta* **71**, 3131–3135.

Jiménez-López C., Cabellero E., Huertas F. J. and Romanek C. S. (2001) Chemical, mineralogical and isotope behavior, and phase transformation during the precipitation of calcium carbonate minerals from intermediate ionic solution at 25°C. *Geochimica et Cosmochimica Acta* **65**, 3219–3231.

Jaffrés J. B. D., Shields G. A., and Wallmann K. (2007) The oxygen isotope evolution of seawater: A critical review of a long-standing controversy and an improved geological water cycle model for the past 3.4 billion years. *Earth-Science Reviews* **83**, 83–122.

Kele S., Breitenbach S. F. M., Capezzuoli E., Meckler A. N., Ziegler M., Millan I. M., Kluge T., Deák J., Hanselmann K., John C. M., Yan H., Liu Z., and Bernasconi S. M. (in press) Temperature dependence of oxygen- and clumped isotope fractionation in carbonates: A study of travertines and tufas in the 6–95 °C temperature range. *Geochimica et Cosmochimica Acta*.

Kim S.-T. and O'Neil J. R. (1997) Equilibrium and nonequilibrium oxygen isotope effects in synthetic carbonates. *Geochimica et Cosmochimica Acta* **61**, 3461–3475.

Kim S.-T., Hillaire-Marcel C. and Mucci A. (2006) Mechanisms of equilibrium and kinetic oxygen isotope effects in synthetic aragonite at 25 °C. *Geochimica et Cosmochimica Acta* **70**, 5790–5801.

Lécuyer C. and Allemand P. (1999) Modelling of the oxygen isotope evolution of seawater: Implications for the climate interpretation of the δ^{18}O of marine sediments. *Geochimica et Cosmochimica Acta* **63**, 351–361.

McCrea J.M. (1950) On the isotopic chemistry of carbonates and a paleotemperature scale. *The Journal of Chemical Physics* **18**, 849–857.

McManus J. F., Oppo D. W. and Cullen J. L. (1999) A 0.5-million-year record of millennial-scale climate variability in the North Atlantic. *Science* **283**, 971–975.

Muehlenbachs K. and Clayton R. N. (1976) Oxygen isotope composition of the oceanic crust and its bearing on seawater. *Journal of Geophysical Research* ***81,*** 4365-4369.

Petrizzo D. A., Young E. D. and Runnegar B. N. (2014) Implications of high-precision measurements of ^{13}C-^{18}O bond ordering in CO_2 for thermometry in modern bivalve mollusc shells. *Geochimica et Cosmochimica Acta* **142**, 400–410.

Tang J., Dietzel M., Fernandez A., Tripati A. K. and Rosenheim B. E. (2014) Evaluation of kinetic effects on clumped isotope fractionation (Δ_{47}) during inorganic calcite precipitation. *Geochimica et Cosmochimica Acta* **134**, 120–136.

Thiagarajan N., Adkins J., Eiler J. (2011) Carbonate clumped isotope thermometry of deep-sea corals and implications for vital effects. *Geochimica et Cosmochimica Acta* **75**, 4416–4425.

Tripati A. K., Eagle R. A., Thiagarajan N., Gagnon, A. C., Bauch H., Halloran P. R., and Eiler J. M. (2010) ^{13}C-^{18}O isotope signatures and ‘clumped isotope’ thermometry in foraminifera and coccoliths. *Geochimica et Cosmochimica Acta* **74**, 5697–5717.

Urey H. C. (1947) The thermodynamic properties of isotopic substances. *Journal of the Chemical Society (Resumed)*, 562–581.

Veizer J. (1992) Depositional and diagenetic history of limestones: Stable and radiogenic isotopes. *In N. Clauer and S Chaudhuri (ed.), Isotopic Signatures and Sedimentary Rocks*, Springer-Verlag, Berlin, 13–48.

Wacker U., Fiebig J., Tödter J., Schöne B. R., Bahr, A., Friedrich O., Tütken T., Gischler E., and Joachimski M. M. (2014) Empirical calibration of the clumped isotope paleothermometer using calcites of various origins. *Geochimica et Cosmochimica Acta* **141**, 127–144.

Wadleigh M. A. and Veizer J. (1992) $^{18}O/^{16}O$ and $^{13}C/^{12}C$ in lower Paleozoic articulate brachiopods: Implications for the isotopic composition of seawater. *Geochimica et Cosmochimica Acta* **56**, 431–443.

Zaarur S., Affek H. P. and Brandon M. T. (2013) A revised calibration of the clumped isotope thermometer. *Earth and Planetary Science Letters* **382**, 47–57.

Adkins J. F., McIntyre K. and Schrag D. P. (2002) The salinity, temperature, and $\delta^{18}O$ of the glacial deep ocean. *Science* **298**, 1769–1773.

Chacko T. and Deines P. (2008) Theoretical calculation of oxygen isotope fractionation factors in carbonate systems. *Geochimica et Cosmochimica Acta* **72**, 3642–3660.

Clark I. D., Fontes J.-C., and Fritz P. (1992) Stable isotope disequilibria in travertine from high pH waters: Laboratory investigations and field observations from Oman. *Geochimica et Cosmochimica Acta* **56**, 2041–2050.

Clark I. D. and Lauriol B. (1992) Kinetic enrichment of stable isotopes in cryogenic calcites. *Chemical Geology* **102,** 217–228.

Coplen T. B. (2007) Calibration of the calcite-water oxygen-isotope geothermometer at Devils Hole, Nevada, a natural laboratory. *Geochimica et Cosmochimica Acta* **71**, 3948–3957.

Defliese W. F., Hren M. T. and Lohmann K. C. (2015) Compositional and temperature effects of phosphoric acid fractionation on Δ_{47} analysis and implications for discrepant calibrations. *Chemical Geology* **396**, 51–60.

Demény A., Kele S., and Siklósy Z. (2010) Empirical equations for the temperature dependence of calcite-water oxygen isotope fractionation from 10 to 70 °C. *Rapid Communications in Mass Spectrometry* **24**, 3521–3526.

Dennis K. J. and Schrag D. P. (2010) Clumped isotope thermometry of carbonatites as an indicator of diagenetic alteration. *Geochimica et Cosmochimica Acta* **74**, 4110–4122.

Dietzel M., Tang J., Leis A. and Köhler S. J. (2009) Oxygen isotope fractionation during inorganic calcite precipitation – Effects of temperature, precipitation rate and pH. *Chemical Geology* **268**, 107–115.

Eagle R.A., Eiler J.M., Tripati A.K., Ries J.B., Freitas P.S., Hiebenthal C., Wanamaker Jr. A. D., Taviana M., Elliot M., Marenssi S., Nakamura K., Ramirez P., and Roy K. (2013) The influence of temperature and seawater carbonate saturation state on ^{13}C-^{18}O bond ordering in bivalve mollusks. *Biogeosciences* **10**, 4591–4606.

Eiler J. M. and Schauble E. (2004) ^{18}O^{13}C^{16}O in Earth's atmosphere. *Geochimica et Cosmochimica Acta* **68**, 4767–4777.

Epstein S., Buchsbaum R., Lowenstam H., and Urey H. C. (1951) Carbonate-water isotopic temperature scale. *Bulletin of the Geological Society of America* **62**, 417–425.

Fernandez A., Tang J. and Rosenheim B. E. (2014) Siderite 'clumped' isotope thermometry: A new paleoclimate proxy for humid continental environments. *Geochimica et Cosmochimica Acta* **126**, 411–421.

Garzione C. N., Hoke G. D., Libarkin J. C., Withers S., Macfadden B., Eiler J., Ghosh P. and Mulch A. (2008) Rise of the Andes. *Science* **320**, 1304–1307.

Ghosh P., Adkins J., Affek H., Balta B., Guo W., Schauble E. A., Schrag D. and Eiler J. M. (2006) ^{13}C–^{18}O bonds in carbonate minerals: A new kind of paleothermometer. *Geochimica et Cosmochimica Acta* **70**, 1439–1456.

Ghosh P., Eiler J., Campana S. E., and Feeney R. F. (2007) Calibration of the carbonate 'clumped isotope' paleothermometer for otoliths. *Geochimica et Cosmochimica Acta* **71**, 2736–2744.

Grauel A.-L., Schmid T. W., Hu B., Bergami C., Capotondi L., Zhou L. and Bernasconi S. M. (2013) Calibration and application of the 'clumped isotope' thermometer to foraminifera for high-resolution climate reconstructions. *Geochimica et Cosmochimica Acta* **108**, 125–140.

Guo W., Mosenfelder J. L., Goddard III W. A. and Eiler J. M. (2009) Isotopic fractionations associated with phosphoric acid digestion of carbonate minerals:

Insights from first-principles theoretical modeling and clumped isotope measurements. *Geochimica et Cosmochimica Acta* **73**, 7203–7225.

Henkes G. A., Passey B. H., Wanamaker Jr., A. D., Grossman E. L., Ambrose Jr. W. G., and Carroll M. L. (2013) Carbonate clumped isotope compositions of modern marine mollusk and brachiopod shells. *Geochimica et Cosmochimica Acta* **106**, 307–325.

Henkes G. A., Passey B. H., Grossman E. L., Shenton B. J., Pérez-Huerta A., and Yancy T. E. (2014) Temperature limits for preservation of primary calcite clumped isotope paleotemperatures. *Geochimica et Cosmochimica Acta* **139**, 362–382.

Hill P. S., Schauble E. A. and Tripati A. K. (2014) Theoretical constraints on the effects of pH, salinity, and temperature on clumped isotope signatures of dissolved inorganic carbon species and precipitating carbonate minerals. *Geochimica et Cosmochimica Acta* **125**, 610–652.

Horita J. and Clayton R. N. (2007) Comment on the studies of oxygen isotope fractionation between calcium carbonates and water at low temperatures by Zhou and Zheng (2003; 2005). *Geochimica et Cosmochimica Acta* **71**, 3131–3135.

Jiménez-López C., Cabellero E., Huertas F. J. and Romanek C. S. (2001) Chemical, mineralogical and isotope behavior, and phase transformation during the precipitation of calcium carbonate minerals from intermediate ionic solution at 25°C. *Geochimica et Cosmochimica Acta* **65**, 3219–3231.

Jaffrés J. B. D., Shields G. A., and Wallmann K. (2007) The oxygen isotope evolution of seawater: A critical review of a long-standing controversy and an improved geological water cycle model for the past 3.4 billion years. *Earth-Science Reviews* **83**, 83–122.

Kele S., Breitenbach S. F. M., Capezzuoli E., Meckler A. N., Ziegler M., Millan I. M., Kluge T., Deák J., Hanselmann K., John C. M., Yan H., Liu Z., and Bernasconi S. M. (in press) Temperature dependence of oxygen- and clumped isotope fractionation in carbonates: A study of travertines and tufas in the 6–95 °C temperature range. *Geochimica et Cosmochimica Acta*.

Kim S.-T. and O'Neil J. R. (1997) Equilibrium and nonequilibrium oxygen isotope effects in synthetic carbonates. *Geochimica et Cosmochimica Acta* **61**, 3461–3475.

Kim S.-T., Hillaire-Marcel C. and Mucci A. (2006) Mechanisms of equilibrium and kinetic oxygen isotope effects in synthetic aragonite at 25 °C. *Geochimica et Cosmochimica Acta* **70**, 5790–5801.

Lécuyer C. and Allemand P. (1999) Modelling of the oxygen isotope evolution of seawater: Implications for the climate interpretation of the δ^{18}O of marine sediments. *Geochimica et Cosmochimica Acta* **63**, 351–361.

McCrea J.M. (1950) On the isotopic chemistry of carbonates and a paleotemperature scale. *The Journal of Chemical Physics* **18**, 849–857.

McManus J. F., Oppo D. W. and Cullen J. L. (1999) A 0.5-million-year record of millennial-scale climate variability in the North Atlantic. *Science* **283**, 971–975.

Muehlenbachs K. and Clayton R. N. (1976) Oxygen isotope composition of the oceanic crust and its bearing on seawater. *Journal of Geophysical Research* ***81,*** 4365-4369.

Petrizzo D. A., Young E. D. and Runnegar B. N. (2014) Implications of high-precision measurements of ^{13}C-^{18}O bond ordering in CO_2 for thermometry in modern bivalve mollusc shells. *Geochimica et Cosmochimica Acta* **142**, 400–410.

Tang J., Dietzel M., Fernandez A., Tripati A. K. and Rosenheim B. E. (2014) Evaluation of kinetic effects on clumped isotope fractionation (Δ_{47}) during inorganic calcite precipitation. *Geochimica et Cosmochimica Acta* **134**, 120–136.

Thiagarajan N., Adkins J., Eiler J. (2011) Carbonate clumped isotope thermometry of deep-sea corals and implications for vital effects. *Geochimica et Cosmochimica Acta* **75**, 4416–4425.

Tripati A. K., Eagle R. A., Thiagarajan N., Gagnon, A. C., Bauch H., Halloran P. R., and Eiler J. M. (2010) ^{13}C-^{18}O isotope signatures and 'clumped isotope' thermometry in foraminifera and coccoliths. *Geochimica et Cosmochimica Acta* **74**, 5697–5717.

Urey H. C. (1947) The thermodynamic properties of isotopic substances. *Journal of the Chemical Society (Resumed)*, 562–581.

Veizer J. (1992) Depositional and diagenetic history of limestones: Stable and radiogenic isotopes. *In N. Clauer and S Chaudhuri (ed.), Isotopic Signatures and Sedimentary Rocks*, Springer-Verlag, Berlin, 13–48.

Wacker U., Fiebig J., Tödter J., Schöne B. R., Bahr, A., Friedrich O., Tütken T., Gischler E., and Joachimski M. M. (2014) Empirical calibration of the clumped isotope paleothermometer using calcites of various origins. *Geochimica et Cosmochimica Acta* **141**, 127–144.

Wadleigh M. A. and Veizer J. (1992) ^{18}O/^{16}O and ^{13}C/^{12}C in lower Paleozoic articulate brachiopods: Implications for the isotopic composition of seawater. *Geochimica et Cosmochimica Acta* **56**, 431–443.

Zaarur S., Affek H. P. and Brandon M. T. (2013) A revised calibration of the clumped isotope thermometer. *Earth and Planetary Science Letters* **382**, 47–57.

CHAPTER 2:

Carbonate clumped isotope paleothermometry: A review of recent advances in CO_2 gas evolution, purification, measurement and standardization techniques

Published in Geosciences Journal,
Re-printed with permission from Springer Science+Business Media LLC

License number: 3673140689289

Christopher Spencer

and

Sang-Tae Kim

Reference

Spencer, C. and Kim, S.-T. (2015) Carbonate clumped isotope paleothermometry: A review of recent advances in CO_2 gas evolution, purification, measurement and standardization techniques. *Geosciences Journal*. **19(2),** 357–374.

2.1 Abstract

Carbonate clumped isotope paleothermometry is based upon the principle that the formation temperature of carbonates is proportional to the relative abundance of $^{13}C^{18}O^{16}O$ in CO_2 produced through carbonate acid digestion. Furthermore, the relative abundance of $^{13}C^{18}O^{16}O$ is independent of the $\delta^{18}O$ value of parent water, providing a viable alternative to the classic oxygen isotope carbonate-water paleothermometer. The temperature resolution of this newly developed paleothermometer primarily relies on the analytical techniques required to determine the clumped isotope composition of a carbonate mineral. These analytical techniques involve: (1) CO_2 gas evolution, in which carbonate is reacted with phosphoric acid, yielding CO_2 with a clumped isotope composition proportional to the carbonate formation temperature; (2) CO_2 purification, in which a rigorous purification of acid-liberated CO_2 is achieved by removing contaminants; (3) clumped isotope measurement, in which a customized gas-source isotope ratio mass spectrometer quantifies the raw clumped isotope composition (Δ_{47}) of the purified CO_2 gas; and (4) inter-laboratory standardization, in which raw Δ_{47} values are normalized with respect to a community-accepted reference frame. This review provides an overview and comparison of the analytical techniques currently utilized in stable isotope laboratories for Δ_{47} measurements, specifically discussing carbonate pre-treatment techniques, phosphoric acid digestion systems, isotope and temperature effects during carbonate phosphoric acid digestion, CO_2 purification processes, and the challenges associated with the measurement and standardization of the Δ_{47} value. Continued refinement of these analytical techniques will aid in reducing sample size, increasing

sample throughput, and improving Δ_{47} external precision and associated paleotemperature resolution. Furthermore, these advances may assist in elucidating the source of discrepancies in slope between two groups of reported carbonate clumped isotope thermometer calibrations.

2.2. Introduction

The discovery of a correlation between stable isotopic variations in ancient carbonate deposits and certain environmental parameters has enabled researchers to reconstruct past environmental changes over substantial periods of Earth's history. Perhaps most significantly, the oxygen isotope carbonate-water paleothermometer, reported by McCrea (1950), allows for the determination of climate fluctuations based upon the variation between the oxygen isotope composition of ancient carbonate minerals and their parent waters. Suitable continental and marine carbonate records include speleothems (e.g., Gascoyne et al., 1980; van Breukelen et al., 2008), marine and fresh water mollusk shells (e.g., Buchardt, 1978; Yu and Eicher, 1998), foraminifera (e.g., Miller et al., 1987), and corals (e.g., Dunbar et al., 1994; Cole et al., 2000). Although significant marine carbonate reservoirs exist extending up to ~180 Ma, precise paleotemperature reconstructions using these carbonates are often hampered by the fact that the oxygen isotope composition of parent-water is poorly constrained (Grossman, 2012).

Recent advances in gas-source isotope ratio mass spectrometry have allowed researchers to examine the relative abundance of chemically identical molecules of varying isotopic composition – commonly referred to as isotopologues – of CO_2 gas (Eiler and Schauble, 2004). Interestingly, the relative abundance of multiply-substituted isotopologues or 'clumped isotopes' (isotopologues containing multiple heavy isotopes) of CO_3^{2-} in certain carbonate minerals is thermodynamically controlled and preserved during molecular formation at isotopic equilibrium (Schauble et al., 2006). Furthermore, experimental studies have revealed a proportional relationship between the relative abundance of clumped isotopes of CO_3^{2-} in certain carbonate minerals and the relative abundance of clumped isotopes in acid-liberated CO_2 produced by the traditional temperature-controlled phosphoric acid digestion of carbonate (e.g., Ghosh et al., 2006; Dennis and Schrag, 2010; Zaarur et al., 2013; Fernandez et al., 2014). The precise determination of the clumped isotope composition of acid-liberated CO_2 provides a viable proxy for the formation temperature of parent-carbonate, forming the basis of the carbonate clumped isotope paleothermometer. Beneficially, this paleothermometer is solely dependent on the availability of carbonate minerals formed in isotopic equilibrium, disregarding the necessity of the oxygen isotope composition of the parent-water body required by the classic oxygen isotope carbonate-water paleothermometer.

However, due to the extremely low abundance of multiply-substituted CO_2 isotopologues (e.g., ~45 ppm for $^{13}C^{18}O^{16}O$; Fig. 1), a stringent analytical technique is required, as follows, to produce viable carbonate temperature resolution: (1) CO_2 evolution, in which a specific amount of carbonate mineral is subjected to a temperature-controlled phosphoric acid digestion to liberate CO_2; (2) CO_2 purification, where potential contaminants are isolated and removed from the acid-liberated CO_2 gas; (3) CO_2 clumped isotope measurement, in which a gas-source isotope ratio mass spectrometer determines the raw clumped isotope composition of the purified CO_2 gas, and (4) inter-laboratory standardization of the raw clumped isotope composition to a community-accepted reference frame produced through measurement of a suite of laboratory standards of known conventional and clumped isotope composition. Refinement of the aforementioned analytical technique is intrinsically linked to improvements in clumped isotope measurement external precision and carbonate paleotemperature resolution.

This review aims to provide an overview of the classic oxygen isotope carbonate-water paleothermometer, the recently developed carbonate clumped isotope paleothermometer, and current clumped isotope CO_2 evolution, purification, measurement and standardization procedures. For a more detailed review of clumped isotope geochemistry and its applications, refer to Affek (2012), Eiler (2007, 2011), and Huntington et al. (2009).

2.3. The Classic Oxygen Isotope Carbonate-Water Paleothermometer

Stable isotope geochemistry has focused on assessing the ratio (R) of heavy isotopes in comparison to their lighter counterparts (e.g., R = $^{18}O/^{16}O$ or $^{13}C/^{12}C$). The stable isotope ratio of a sample is reported using delta (δ) notation typically in units of permil (‰) on a reference scale commonly anchored with two international reference materials (e.g., $\delta^{18}O$ and $\delta^{13}C$ values are reported on the VSMOW-SLAP and VPDB-LSVEC scale, respectively). The isotopic ratio of two chemically distinct substances (A, B) at equilibrium defines a stable isotope fractionation factor ($\alpha_{A\text{-}B}$) and its value is primarily temperature dependent (Eq. 1).

$$\alpha_{A-B} = \frac{R_A}{R_B} = \frac{1000+\delta_A}{1000+\delta_B}. \tag{1}$$

The theoretical development of the classic oxygen isotope carbonate-water paleothermometer began with Urey's (1947) proposition of a temperature-dependent equilibrium oxygen isotope fractionation factor between $CaCO_3$ and water ($\alpha_{\text{CaCO3-water}}$). This fractionation factor is essentially a reflection of the equilibrium constant for the following heterogeneous oxygen isotope exchange reaction:

$$\frac{1}{3}CaC^{16}O_3 + H_2{}^{18}O \rightleftarrows \frac{1}{3}CaC^{18}O_3 + H_2{}^{16}O. \tag{2}$$

This temperature-dependent oxygen isotope fractionation was initially validated through empirical assessment of marine carbonates grown at known temperatures by McCrea (1950). Since then, the classic carbonate-water oxygen isotope paleothermometer has been continually refined to encompass (1) various carbonate minerals including calcite and aragonite; (2) species-specific isotope effects – referred to as 'vital' effects – of certain biogenic carbonates; and (3) the effects of environmental parameters, such as pH, salinity, and precipitation rate, on the isotopic compositions of carbonates (McCrea, 1950; Epstein et al., 1951; O'Neil et al. 1969; Carothers et al., 1988; Kim and O'Neil, 1997; Bemis et al., 1998; Zheng, 1999; Chacko et al., 2001; White et al., 2001; Kim et al., 2006, 2007b, 2014; Dietzel et al., 2009).

$$1000ln\alpha_{(Calcite-H_2O)} = 18.03(10^3/T) - 32.42. \tag{3}$$

The usage of this carbonate-water paleothermometer (e.g., Eq. 3 from Kim and O'Neil (1997)) requires analytical techniques that enable researchers to quantify the oxygen isotope composition of $CaCO_3$ and water. The δ^{18}O value of $CaCO_3$ is generally determined using the phosphoric acid digestion technique developed by McCrea (1950), in which $CaCO_3$ is reacted with ~100 % phosphoric acid to produce CO_2 at a known reaction temperature (Eq. 4). This acid-liberated CO_2 is subsequently isolated from reaction byproducts, such as water, prior to its stable isotopic analysis. To calculate the δ^{18}O value of the carbonate, a mineral-specific and temperature-dependent phosphoric acid fractionation factor is applied to the measured δ^{18}O value of the acid-liberated CO_2 (Sharma and Clayton, 1965; Kim et al., 2007a).

$$CaCO_3 + H_3PO_4 \rightleftarrows CaHPO_4 + CO_2 + H_2O. \tag{4}$$

To determine the oxygen isotope composition of water, a small amount of CO_2 is allowed to equilibrate isotopically with a proportionally larger amount of water at a specific temperature (Eq. 5). Upon reaching isotopic equilibrium, this isotope exchange reaction enables the δ^{18}O value of CO_2 to be dictated by the δ^{18}O value of water. A correction factor is then applied to the measured δ^{18}O value of CO_2 to account for the oxygen isotope fractionation between CO_2 and water at the given reaction temperature (e.g., O'Neil et al., 1975).

$$\frac{1}{2}C^{16}O_2 + H_2{}^{18}O \rightleftarrows \frac{1}{2}C^{18}O_2 + H_2{}^{16}O. \tag{5}$$

The resolution of this paleothermometer is a reflection of the combined external precision associated with determining the δ^{18}O of $CaCO_3$ and water relative to a common reference scale (e.g., the VSMOW-SLAP scale). This resolution may worsen if carbonate samples are not prescreened for potential isotopic alteration caused by either diagenesis and/or metamorphism (Engel et al., 1958; Dickson and Coleman, 1980). Non-equilibrium isotope effects induced by increased precipitation rate (Dietzel et al., 2009) and varying pH (Spero et al., 1997; Zeebe, 2005) may further complicate temperature determinations.

2.4. The New Clumped Isotope Paleothermometer

2.4.1. The natural distribution of clumped isotopes

Within isotopically-exchanging molecules, the substitution from a light to a heavy stable isotope of the same element increases the mass of the isotopologue, while reducing the vibrational frequency of its chemical bond, thus lowering the overall zero-point energy of the molecule (Urey, 1947). This isotopic exchange alters the reaction kinetics and physicochemical properties of the isotopologue.

Bigeleisen (1955) initially presumed that the difference in zero-point energy between a non-substituted and a doubly-substituted isotopologue was double that between a non-substituted and a singly-substituted isotopologue of the same chemical species (i.e., the difference in bond energy between H-H and D-D is double that of H-H and H-D; see Fig. 1 of Eiler (2007)), implying no energetic advantage to either isotopic configuration. This theory, referred to as the ‘rule of the geometric mean’, would imply a random (commonly referred to as stochastic) distribution of all potential isotopologues. However, this theory represents a simplified approximation of the variance in bond energy between isotopologues of differing mass and only remains valid at the high temperature limit (Eiler, 2007). At typical Earth surface temperatures, a slight energetic advantage exists within multiply-substituted isotopologues, favoring their formation (represented in Eq. 6 by the preferential formation of D_2). The relative abundance of a preferentially formed multiply-substituted isotopologue is controlled by the temperature-dependent equilibrium constant of its representative homogeneous isotope exchange reaction.

$$HD + HD \rightleftarrows H_2 + D_2. \tag{6}$$

This temperature-dependent relationship provides a potential thermometer that is based upon the relative abundance of isotopologues in a single phase.

2.4.2. Definition of Δ_{47} and δ^{47}

At the time of molecular formation of CO_2, Eiler and Schauble (2004) concluded that the relative abundance of $^{13}C^{18}O^{16}O$ (the most abundant multiply-substituted isotopologue of CO_2; Fig. 1), is primarily temperature dependent. If in a state of isotopic equilibrium, the relative abundance of the $^{13}C^{18}O^{16}O$ isotopologue is a function of the temperature-dependent equilibrium constant of the following homogeneous isotope exchange reaction:

$$^{13}C^{16}O_2 + {}^{12}C^{18}O^{16}O \rightleftarrows {}^{12}C^{16}O_2 + {}^{13}C^{18}O^{16}O. \tag{7}$$

Eiler and Schauble (2004) introduced the term Δ_{47} to represent the deviation of the relative abundance of mass 47 isotopologues (primarily $^{13}C^{18}O^{16}O$; Fig. 1) of a sample CO_2 gas from the theoretical stochastic distribution of a CO_2 gas of identical bulk isotopic composition (Eq. 8). The term δ^{47} was also introduced to represent the isotope ratio R_{47} of sample CO_2 gas (SG) relative to a working gas (WG; Eq. 9). This δ^{47} value is related to the bulk isotopic composition of a sample CO_2 (i.e., $\delta^{47} \approx \delta^{45} + \delta^{46}$; Huntington et al., 2009). It is important to note that if two CO_2 gases of different δ^{47} are isotopically equilibrated at 1000 °C, they should theoretically possess identical Δ_{47}. In practice, a systematic non-linearity may exist between the raw Δ_{47} and δ^{47} values of these two CO_2 gases (Eiler and Schauble, 2004; Huntington et al., 2009). This non-linearity may be largely minimized and corrected through certain Δ_{47} data correction and standardization protocols (see section 2.4.9.3 and 2.4.10; Dennis et al., 2011; He et al., 2012; Bernasconi et al., 2013), or non-existent depending on mass spectrometer design (see section 2.4.8).

Normalized Δ_{47} and δ^{47} values are reported in units of permil (‰) with external precision typically reported as the standard error (1σ/√n) of the mean of repeated measurements (e.g., $\Delta_{47} = 0.410‰ \pm 0.007$ SE, $n = 10$; $\delta^{47} = 11.26‰ \pm 0.09$ SE, $n = 10$).

$$\Delta_{47} = \left[\left(\frac{R^{47}}{R^{47^*}} - 1\right) - \left(\frac{R^{46}}{R^{46^*}} - 1\right) - \left(\frac{R^{45}}{R^{45^*}} - 1\right)\right] \times 1000. \tag{8}$$

$$\delta^{47}_{(SG\ vs.\ WG)} = \left(\frac{R^{47}_{SG}}{R^{47}_{WG}} - 1\right) \times 1000. \tag{9}$$

R^{47}, R^{46}, and R^{45} represent the measured mass ratios 47/44, 46/44, and 45/44, respectively, while R^{47*}, R^{46*}, and R^{45*} represent the corresponding mass ratios occurring if the measured sample had a stochastic distribution and are defined as follows:

$$R^{47*} = 2 \times R^{13} \times R^{18} + 2 \times R^{17} \times R^{18} + R^{13} \times (R^{17})^2, \tag{10}$$

$$R^{46*} = 2 \times R^{18} + 2 \times R^{13} \times R^{17} + (R^{17})^2, \tag{11}$$

$$R^{45*} = R^{13} + 2 \times R^{17}, \tag{12}$$

where R^{13}, R^{17}, and R^{18} represent the isotopic ratio of $^{13}C/^{12}C$, $^{17}O/^{16}O$, and $^{18}O/^{16}O$, respectively. The $^{13}C/^{12}C$ and $^{18}O/^{16}O$ ratios are calculated on the basis of the conventional measurement of $\delta^{13}C_{VPDB\text{-}LSVEC}$ and $\delta^{18}O_{VSMOW\text{-}SLAP}$ of sample CO_2 gas whilst $^{17}O/^{16}O$ is estimated based upon the mass-dependent relationship (Eq. 13), a typical assumption for the vast majority of terrestrial samples. Furthermore, while the major contributor to the *m/z* 47 ion beam is $^{13}C^{18}O^{16}O$, relatively small contributions from $^{13}C^{17}O_2$ and $^{12}C^{18}O^{17}O$ exist. Nonetheless, these two isotopologues of CO_2 are deemed insignificant due to their relatively low abundance (Fig. 1).

$$\ln(R^{17}/R^{17}_{VSMOW}) = {\sim}0.516 \ln(R^{18}/R^{18}_{VSMOW}) \tag{13}$$

2.4.3. The carbonate clumped isotope paleothermometer

The initial research conducted by Eiler and Schauble (2004) was later adapted to assess the formation temperature of $CaCO_3$ (calcite and aragonite) – titled the carbonate clumped isotope paleothermometer – with the discovery of a proportional relationship between the relative abundance of $^{13}C^{18}O^{16}O_2^{2-}$ preserved in $CaCO_3$ (represented by Δ_{63}; a term similarly defined to Δ_{47}) and the relative abundance of $^{13}C^{18}O^{16}O$ in acid-liberated CO_2 produced by the conventional phosphoric acid digestion of $CaCO_3$ (Eq. 4; Ghosh et al., 2006; Schauble et al, 2006).

Theoretical, experimental, and empirical calibrations of the carbonate clumped isotope paleothermometer have defined the relationship between the normalized Δ_{47} value of acid-liberated CO_2 and carbonate formation temperature, as well as identified potential species-specific and/or non-equilibrium isotope effects (Table 1; e.g., Ghosh et al., 2006; Guo et al., 2009; Dennis and Schrag, 2010; Tripati et al., 2010; Thiagarajan et al., 2011; Saenger et al., 2012; Eagle et al., 2013; Grauel et al., 2013; Henkes et al., 2013; Yoshida et al., 2013; Zaarur et al., 2013; Tang et al., 2014; Wacker et al., 2014; Defliese et al., 2015). To date, these calibration studies have enabled paleotemperature determinations using a variety of carbonates, such as benthic foraminifera, coccoliths, mollusks, brachiopods, deep-sea corals, speleothems, carbonate concretions, paleosol carbonates, and carbonate phases from Martian meteorites as well as vertebrate bioapatite (notably including Jurassic sauropods) (e.g., Eagle et al., 2010, 2011; Tripati et al., 2010; Daëron et al., 2011; Helevy et al., 2011; Thiagarajan et al., 2011; Henkes et al., 2013; Dale et al., 2014; Fernandez et al., 2014; Hough et al., 2014).

Given the common practice of using standard error ($1\sigma/\sqrt{n}$), instead of standard deviation, to reflect Δ_{47} measurement precision, temperature resolution is most easily improved through increasing carbonate subsample measurement repetition. For example, substantial repeated analyses of biogenic carbonates (*n* = 20 to 26) has yielded maximum paleotemperature resolutions of ± 0.5 °C (Thiagarajan et al., 2014; Tripati et al., 2014). However, in cases where sample mass is limited, the reduced potential for replicate analyses may impede the resultant paleotemperature resolution. Improvement of CO_2 evolution and purification, along with Δ_{47} measurement and correction procedures are necessary to improve the external precision of Δ_{47} measurements, minimize required sample size, and ultimately achieve comparable or greater temperature resolution to that of alternative paleothermometers.

2.5. Analytical Techniques for the Carbonate Clumped Isotope Paleothermometer

2.5.1. Sample carbonate and reference CO_2 requirements

The determination of the normalized Δ_{47} value of carbonates necessitates a rigorous analytical technique to produce viable acid-liberated CO_2 gas, mass spectrometer CO_2 reference gas and CO_2 gas of varying clumped isotope and bulk isotope composition for sample standardization to the absolute reference frame (Dennis et al., 2011). To date, acid-liberated CO_2 is typically extracted from carbonate minerals via phosphoric acid digestion. CO_2 reference gas for the gas-source isotope ratio mass spectrometer is either prepared in-house (e.g., Schmid and Bernasconi, 2010) or purchased from a specialty gas supplier, such as Oztech (Safford, AZ, USA) (e.g., Ghosh et al., 2006; Rosenheim et al., 2013; Wacker et al., 2013; Kluge et al., 2014). Production of reference frame CO_2 gas of varying clumped isotope composition is achieved by establishing clumped isotope equilibrium of CO_2 gases at specific temperatures (e.g., 10, 25, 40 and 1000 °C). A theoretical Δ_{47} value reflective of the CO_2 equilibration temperature may then be assigned (Wang et al., 2004). Low temperature reference frame CO_2 gases (e.g., 10, 25, and 40 °C) are produced via CO_2-water equilibration. This process entails placing sealed Pyrex glass tubes containing water and CO_2 into a temperature-controlled water bath to allow efficient isotopic equilibration through the reversible hydration of CO_2 (Eq. 5). High temperature reference frame CO_2 gases (e.g., 1000 °C) are prepared by collecting a known volume of CO_2 in a quartz tube using a conventional vacuum line extraction system. This quartz tube is then baked in a muffle furnace for $\geq$ 2 hours, followed by rapid quenching to room temperature to avoid any potential isotopic re-equilibration. Lastly, all of these CO_2 gases are then purified using either a manual or automated vacuum line extraction system coupled to a packed divinyl benzene polymer gas chromatograph (GC) column or U-trap to remove potential contaminants, and are finally analyzed for their raw Δ_{47} value using a gas-source stable isotope mass spectrometer.

2.5.2. Carbonate pre-treatment techniques

Pre-treatment of carbonate samples, including foraminifera, coccoliths, fish otoliths, shells, organic sediments, bioapatite, and siderite nodules, is occasionally required to remove potential organic contaminants and may involve a combination of the following cleaning procedures: slicing and crushing, sonication, centrifugation, bleaching with 1 – 10% H_2O_2, treatments with methanol or purified water, and 50 – 70 °C oven drying cycles (Ghosh et al., 2007; Eagle et al., 2010; Tripati et al., 2010; Zaarur et al., 2011; Grauel et al., 2013; Fernandez et al., 2014; Henkes et al., 2014). Typically, slicing, cracking, and crushing of $CaCO_3$ samples with internal chambers adequately exposes internal organic tissue and/or sediments to further treatment (Ghosh et al., 2007; Zaarur et al., 2011; Grauel et al., 2013). Upon contaminant exposure, treatment of carbonate with 1 – 10% H_2O_2 for 15 – 720 minutes and/or 0.1M acetic acid (pH 2.8 – 4.6) removes the majority of organic materials (Ghosh et al., 2007; Eagle et al., 2010; Tripati et al., 2010; Suarez and Passey, 2014). However, as discovered by Grauel et al. (2013), 10 % H_2O_2 treatment may potentially lead to partial dissolution and re-precipitation of carbonate crystals, altering their Δ_{47} value. The safe usage of the H_2O_2 treatment likely requires sample-specific testing to determine optimal concentration, reaction temperature, and exposure time necessary to minimize Δ_{47} alteration. For example, Suarez and Passey (2014) have refined the pre-treatment of bioapatite to entail exposure to 3 % H_2O_2 for 24 hours followed by overnight exposure to 0.1 M Na-acetate acetic acid solution (pH 4.6). This procedure is based upon the findings of Eagle et al. (2010) in which bioapatite was reacted with H_2O_2 and acetic acid solutions of varying concentration and pH up to 24 hours to assess Δ_{47} alteration.

Alternatively, certain pre-treatment protocols withhold usage of H_2O_2 in favor of sonication of carbonate samples with de-ionized water (Zaarur et al., 2011; Henkes et al., 2014). This approach produces negligible alteration of the Δ_{47} value while adequately removing organic contaminants as well as adhered surface particles from carbonate samples in preparation for phosphoric acid digestion. Prior to acid-digestion, samples may be stored in a low temperature oven or desiccator to minimize isotopic exchange with atmospheric water vapor (Suarez and Passey, 2014; Defliese et al., 2015).

2.5.3. CO_2 evolution from carbonates: Types of phosphoric acid digestion systems

The three most common phosphoric acid digestion systems used in CO_2 evolution include the original McCrea-style reaction vessel method; the common acid bath method; and the acid drip method, used in the Kiel-IV Carbonate Device (Thermo Electron GmbH, Bremen, Germany) (Figs. 2a–c).

2.5.3.1. McCrea-style reaction vessel method

Initially developed by McCrea (1950) to assess the δ^{18}O value of carbonates, the manually-operated McCrea-style reaction vessel reacts a carbonate subsample with ≥ 100% phosphoric acid in a sealed vessel for a set period of time prior to the evolution of acid-liberated CO_2 (Fig. 2a). This method is likely the most simplistic approach to accomplish carbonate phosphoric acid digestion. Typical acid digestion reaction time, reaction temperature, and carbonate subsample size for a single Δ_{47} measurement is 12 – 20 hr, 25 °C, and 5 – 15 mg, respectively (Ghosh et al., 2006; Wacker et al., 2013). Given the necessity of replicate analyses for precise Δ_{47} measurements (e.g., $n = 3 – 4$), a minimum carbonate sample size of 15 - 60 mg is required.

Recent modifications to the McCrea-style reaction vessel have increased the reaction temperatures to 100 °C through submersion in boiling water, and have enabled the immediate collection of acid-liberated CO_2 in an attached liquid nitrogen trap while carbonate is reacting with the phosphoric acid (Rosenheim et al., 2013; Fernandez et al., 2014; Tang et al., 2014).

2.5.3.2. Common acid bath method

First utilized by Dennis and Schrag (2010) and Passey et al. (2010) in clumped isotope geochemistry, the common acid bath method digests carbonate subsamples into a shared ≥ 100% phosphoric acid reservoir while acid-liberated CO_2 is immediately collected in a liquid nitrogen trap (Figs. 2a and b). A magnetic stirrer within the phosphoric acid reservoir accelerates the removal rate of CO_2. If paired with an auto-sampler, this method may be incorporated into fully automated CO_2 evolution, purification, and Δ_{47} measurement systems (Fig. 2b; Passey et al., 2010; Henkes et al., 2013; Petersen and Schrag, 2014; Tripati et al., 2014). Typical acid digestion reaction time, temperature, and carbonate subsample size is 10 – 30 min, 90 °C, and > 1 mg, respectively (Dennis and Schrag, 2010; Passey et al., 2010; Wacker et al., 2013; Petersen and Schrag, 2014). The elevated acid digestion reaction temperature drastically increases the reaction rate of the carbonate acid digestion, maximizing sample throughput. Modification of the mass spectrometer dual-inlet system to include two gas reservoirs with a smaller volume than the typical bellow for the sample and a reference side has enabled the usage of < 1 mg carbonates (Petersen and Schrag, 2014). If unmodified, typical carbonate sample size is similar to the McCrea-style reaction vessel method.

The usage of a single acid reservoir for the digestion of multiple carbonate samples could produce slight memory effects similar to those witnessed with conventional $\delta^{18}O$ measurements by Swart et al. (1991). To the best of our knowledge, no assessments of potential Δ_{47} memory effects associated with the common acid bath method have been undertaken. Consequently, caution should still be given to consecutively measured carbonate samples of significantly different Δ_{47} values. In spite of this concern, the common acid bath method likely represents the most common method of carbonate phosphoric acid digestion for Δ_{47} measurements.

2.5.3.3. Acid drip method

First assessed by Schmid and Bernasconi (2010) for clumped isotope geochemistry, the acid drip method (Kiel-IV Carbonate Device) ‘drips’ a small volume of ≥ 100% phosphoric acid onto a carbonate subsample, while acid-liberated CO_2 is immediately collected in a liquid nitrogen micro-volume trap (Fig. 2c). This system is typically linked to a gas-source isotope ratio mass spectrometer, providing fully automated CO_2 evolution, purification, and Δ_{47} measurement of up to 46 carbonate subsamples with a total analysis time, acid reaction temperature, and carbonate subsample size of 30-35 min, 70 °C, and 0.150 – 0.200 mg, respectively (Schmid and Bernasconi, 2010; Meckler et al., 2014). In the past, slightly reduced Δ_{47} external precision specific to the acid drip method was hypothesized to be a result of atmospheric leakage in the reaction vessel, and/or carbonate heterogeneity more pronounced in ≤ 0.200 mg subsamples (Schmid and Bernasconi, 2010). However, recent measurement procedure and correction innovations (e.g., Hu et al., 2014; Meckler et al., 2014) have enabled similar Δ_{47} external precision to the McCrea-style reaction vessel and common acid bath methods while reducing total carbonate sample size to 1.5 – 2.0 mg (or less).

2.5.4. Isotope effects during CO_2 evolution from carbonates

Dependent on the phosphoric acid digestion temperature (T_{acid}), the acid digestion of carbonate produces a slight enrichment of the relative abundance of $^{13}C^{18}O^{16}O$ in acid-liberated CO_2 (Δ_{47}) in comparison to the relative abundance of $^{13}C^{18}O^{16}O_2^{2-}$ in carbonate (Δ_{63}) (Ghosh et al., 2006). This enrichment is defined by a clumped isotope acid fractionation factor (Δ^*_{47}) as shown in Equation (14). Theoretical modeling of this acid fractionation based upon classical transition state theory and *ab initio* calculations enables the estimation of Δ^*_{47} at a given T_{acid} (Eq. 15; Guo et al., 2009).

$$\Delta^*_{47} = \Delta_{47} - \Delta_{63}. \qquad (14)$$

$$\Delta^*_{47} = 0.189 \times 10^5 / T^2 + 0.0242. \qquad (15)$$

Initial experimental observations of Δ^*_{47} at 25 °C were attempted through the acid digestion and Δ_{47} measurement of calcite and aragonite subjected to high temperature re-crystallization, effectively producing a stochastic distribution of carbonate ion isotopologues prior to acid digestion (i.e., carbonate $\Delta_{63} = 0$, as a result its acid-liberated CO_2 $\Delta_{47} = \Delta^*_{47}$; Ghosh et al., 2006; Guo et al., 2009). Ghosh et al. (2006) determined the Δ^*_{47} at 25 °C to be ~ 0.2‰ while Guo et al. (2009) proposed a value of 0.232 ± 0.015‰. However, these values were determined prior to the wide-spread usage of the absolute reference frame complicating their comparison (see section 2.4.10.). Variation between these values may also result from the re-crystallization experiments unsuccessfully achieving a stochastic distribution of carbonate ion isotopologues and/or a theoretical generalization or misinterpretation of the clumped isotope systematics of carbonate acid digestion (Dennis et al., 2011). Beneficial to the understanding of carbonate clumped isotope systematics, the future precise definition of Δ^{*}_{47} would enable the exact quantification of Δ_{63}.

2.5.5. Acid digestion temperature correction for Δ_{47} measurements

To date, raw Δ_{47} measurements corrected to the absolute reference frame are presented relative to the T_{acid} of 25 °C originally utilized by Ghosh et al. (2006). To maintain compatibility of Δ_{47} measurements produced by laboratories using a differing T_{acid} (e.g., 75, 90 and 100 °C), a Δ^{*}_{47} correction factor ($\Delta^{*}_{25\text{-}T_{acid}}$) is applied. A theoretical quantification of $\Delta^{*}_{25\text{-}T_{acid}}$ may be determined using the Δ^{*}_{47} definition proposed by Guo et al. (2009) (Eq. 15). Alternatively, experimental measurements of $\Delta^{*}_{25\text{-}T_{acid}}$ have been accomplished through comparison of the Δ_{47} value of a carbonate digested at both 25 °C and a specific T_{acid} (Table 2; Passey et al., 2010).

Defliese et al. (2015) suggests that the Δ^{*}_{47} value is independent of carbonate mineralogy based upon their recent experimental assessment of Δ^{*}_{47} with a T_{acid} = 25, 50, 60, 75 and 90 °C for calcite, aragonite and dolomite minerals. They also observed similar $\Delta^{*}_{25\text{-}T_{acid}}$ in carbonates of widely varying Δ_{47}. Given these findings, variation in experimentally determined $\Delta^{*}_{25\text{-}T_{acid}}$ values (e.g., $\Delta^{*}_{25\text{-}90}$ = 0.066 to 0.092 ‰; Table 2) may relate to: (1) statistical uncertainty given the external precision of normalized Δ_{47} values utilized in these experiments; (2) a mineralogical or carbonate type effect not yet discernable given current Δ_{47} external precision (Dennis et al., 2013; Defliese et al., 2015); or (3) systematic Δ_{47} artifacts produced through usage of laboratory-specific carbonate acid digestion, purification, and measurement systems (Passey et al., 2010). This topic likely requires re-visiting to further the understanding of the clumped isotope dynamics occurring during carbonate phosphoric acid digestion.

2.5.6. Water effects during CO_2 evolution from carbonates

Phosphoric acid of ≥ 100 wt% (density ≥ 1.90 g/ml) inherently contains a minute abundance of water molecules produced via the reversible polymerization of phosphate species (Eqs. 16–18), and as a byproduct of the phosphoric acid digestion reaction (Eq. 4; Wachter and Hayes, 1985; Wacker et al., 2013). The vapor pressure of this H_2O reservoir increases relative to digestion temperature (Defliese et al., 2015). If in contact with acid-liberated CO_2, this water reservoir is potentially capable of isotopic exchange via the reversible hydration of CO_2 (Eq. 5). Prolonged isotopic exchange could effectively re-order the Δ_{47} value of the acid-liberated CO_2 to reflect the phosphoric acid digestion temperature (e.g., re-equilibrated CO_2 could reflect a Δ_{47} value of 0.651‰ when T_{acid} is 90 °C; this value is calculated using Eq. A2 of Dennis et al. (2011) and is based upon the theoretical thermodynamics of CO_2 clumped isotope equilibrium proposed by Wang et al (2004)).

$$2H_3PO_4 \rightleftarrows H_4P_2O_7 + H_2O. \tag{16}$$

$$H_4P_2O_7 + H_3PO_4 \rightleftarrows H_5P_3O_{10} + H_2O. \tag{17}$$

$$H_5P_3O_{10} + H_3PO_4 \rightleftarrows H_6P_4O_{13} + H_2O. \tag{18}$$

CO_2-H_2O re-equilibration may occur during the exsolution of acid-liberated CO_2 from the phosphoric acid reservoir or within the headspace of the reaction vessel (Wacker et al., 2013; Defliese et al., 2015). The extent of this effect is possibly controlled by certain laboratory-specific properties such as reaction vessel design, phosphoric acid concentration, digestion temperature, and the rate of CO_2 removal from the reaction vessel. For example, Wacker et al. (2013) attributed inconsistent positive enrichments in the Δ_{47} values of carbonate samples of <7 mg digested at 25 °C to CO_2-H_2O re-equilibration within the phosphoric acid solution prior to CO_2 exsolution. However, under similar conditions, Defliese et al. (2015) observed no enrichment. To minimize the potential for CO_2-H_2O re-equilibration, the majority of laboratories immediately remove and isolate acid-liberated CO_2 from the reaction vessel in a down-line liquid nitrogen trap (e.g., Dennis and Schrag, 2010; Schmid and Bernasconi, 2010; Fernandez et al., 2014).

2.5.7. CO_2 purification systems

CO_2 clumped isotope purification systems isolate and purify acid-liberated CO_2 gas in a series of traps capable of separating gaseous species and are, in some cases, connected directly to a mass spectrometer for direct on-line isotopic measurements (Fig. 2). These systems can also incorporate a packed trap containing a divinyl benzene polymer. This packed trap is typically in the form of either a gas chromatograph column, traditional U-trap, or linear trap (modified Kiel-IV system).

Current CO_2 purification systems may be separated into manually operated off-line systems and automated on-line systems. The usage of manually-operated off-line systems entails a researcher directly controlling each step of CO_2 purification, including the transfer of purified CO_2 to the mass spectrometer via a sealed glass sample vial or a reusable glass or metal container (Fig. 2a; e.g., Ghosh et al., 2006; Wacker et al., 2013). In contrast, automated on-line systems utilize software packages (e.g., NI-LabVIEW, National Instruments, Austin, USA) to control CO_2 evolution, purification, and transfer directly to the mass spectrometer (Figs. 2b and c; e.g., Passey et al., 2010; Schmid and Bernasconi, 2010). This automation likely increases sample purification efficiency and Δ_{47} external precision through improved operational consistency, reliability, and reduced supervision requirements.

These CO_2 purification systems are specifically designed to remove contaminants capable of inducing CO_2 re-equilibration and/or inhibiting precise Δ_{47} measurements. This includes water, non-condensable gases, and contaminants that upon ionization within the ion source produce an identical *m/z* to isotopologues of sample CO_2. Identified contaminants capable of producing isobaric interferences include chlorocarbons, halocarbons, hydrocarbons, nitrogen-bearing gases and sulfur compounds (Eiler and Schauble, 2004; Ghosh et al., 2006; Guo and Eiler, 2007; Huntington et al., 2009).

The majority of water and non-condensable gases, such as N_2 or O_2, can be cryogenically separated from CO_2 using the traditional cold U-traps. However, remaining contaminants – specifically halocarbons and hydrocarbons – may be isolated and removed using a divinyl benzene polymer trap (typically Porapak Q). This polymer is cooled to -10 to -30 °C and is either packed within a 1 – 2 m long GC column (e.g., Henkes et al., 2013; Petrizzo et al., 2014), a ~ 20 cm U-trap (e.g., Dennis and Schrag, 2010; Rosenheim et al., 2013), or specific to the modified Kiel-IV, a 2 cm linear stainless steel tube (Grauel et al., 2013). Packed GC columns typically utilize a helium carrier gas flowing at a rate of 2 – 25 ml/min to facilitate the transfer of sample CO_2 gas (e.g., Ghosh et al., 2006; Passey et al., 2010; Petrizzo et al., 2014). Alternatively, the modified Kiel-IV packed tube and certain packed U-traps transfer CO_2 across the polymer solely via pressure differential produced by a down-line liquid nitrogen trap (Grauel et al., 2013; Defliese et al., 2015). A silver wool getter may also be incorporated surrounding the packed trap to facilitate removal of sulfur-bearing contaminants (Henkes et al., 2013; Rosenheim et al., 2013; Meckler et al., 2014).

Upon contact with the divinyl benzene polymer, the flow rate of individual gases is regulated by volatility and temperature, with more volatile gases (e.g., CO_2) passing through the polymer faster than less volatile gases, such as halocarbons and hydrocarbons. Lower temperatures enhance separation at the expense of a longer total gas transfer time. As a result, temperatures of -10 to -30 °C are utilized to ensure isolation of acid-liberated CO_2 while maintaining purification efficiency.

Upon completion of CO_2 purification, heating of the GC packed column, U-trap or linear trap to 100 – 200 °C for 15 – 30 minutes promotes outgassing of residual contaminants adhered to the packing material (Ghosh et al., 2006; Passey et al., 2010; Wacker et al., 2013; Yoshida et al., 2013). The rate of outgassing is commonly enhanced by back-flushing helium through the divinyl benzene polymer trap.

Lechler et al. (2013) report similar Δ_{47} external precision between CO_2 gases prepared utilizing a packed GC column or packed U-trap. However, this comparison is limited to one laboratory's purification system. To the best of our knowledge, a comprehensive study of the effectiveness of current CO_2 clumped isotope purification systems has not yet been completed. However, some assumptions may be made regarding an optimized purification technique. For example, at the expense of high sample throughput, the cleaning potential of divinyl benzene polymer may be enhanced through increasing the residence time of sample gas within the trap and by improving decontamination of the polymer between samples. Residence time may be increased through a longer trap length, cooler trap temperature, lower helium flow rate (if applicable), and/or a compartmentalized expansion of CO_2 within the polymer prior to down-stream collection (e.g., Defliese et al., 2015). Decontamination between samples may be enhanced through usage of a helium back-flush to facilitate off-gassing of contaminants adhered to the polymer (e.g., Wacker et al., 2014).

2.5.8. Δ_{47} measurement

To date, the majority of raw Δ_{47} measurements have been made using a 10 kV MAT 253 dual-inlet isotope ratio mass spectrometer (Thermo Fisher Scientific, Bremen, Germany) configured for *m/z* 44 – 49. Typical Faraday cup configuration for this machine includes a 3×10^8, 3×10^{10} and 1×10^{11} Ω resistor for major ion beams *m/z* 44, 45 and 46, respectively; while multiply-substituted isotopologue ion beams (*m/z* 47 – 49) are measured by 1×10^{12} Ω resistors (e.g., Huntington et al., 2009; He et al., 2012; Wacker et al., 2013). To achieve reliable *m/z* 47 – 49 peak intensities, analyte pressure within the ion source is typically adjusted to produce a peak intensity of 16 –20 V for *m/z* 44 (e.g., Huntington et al., 2009; Bernasconi et al., 2013). Alternative dual-inlet isotope ratio mass spectrometers capable of Δ_{47} measurements include the 3 kV Delta XP (Thermo Fisher Scientific, Bremen, Germany; Yoshida et al., 2013), the 5 kV compact Isoprime (Elementar Analysensysteme GmbH, Hanau, Germany; Rosenheim et al., 2013), and the 8 kV MIRA (University of East Anglia, Norwich, United Kingdom; Dennis and Vinen, 2009). These mass spectrometers achieve a precision of 10^{-6} (thousandths per mil) to determine the raw Δ_{47} value of CO_2 (Eiler, 2007).

In comparison to traditional δ^{18}O and δ^{13}C, a rigorous measurement protocol is required to define the raw Δ_{47} value of CO_2. For example, the protocol proposed by He et al. (2012) entails 7 – 10 acquisitions each containing a peak-centering, pressure adjustment, background scan and 8 - 15 cycles (off-peak and on-peak), in which sample and reference gases are alternatively ionized to measure their respective *m/z* 44 – 49 ion beam intensities. On-peak cycles measure the peak-centered CO_2 beam intensities while off-peak cycles slightly offset CO_2 ion beam trajectories to establish Faraday cup residual background noise (He et al., 2012). Total measurement time is generally 3 – 4 hours per sample. This protocol enables raw Δ_{47} measurements to be made in either bellows or micro-volume mode with a typical internal precision of ± 0.006 – 0.008 ‰, and ± 0.010 – 0.012 ‰, respectively (He et al., 2012).

In most cases, bellows mode is optimal for > 50 μmol of CO_2 typically produced by either the McCrea-style reaction vessel or common acid bath method. This mode balances analyte peak intensities at initiation of each acquisition through pressure adjustment of the bellows. Alternatively, micro-volume mode is required for < 15 μmol of CO_2 typically produced by the acid-drip method or the recent on-line common acid bath method proposed by Petersen and Schrag (2014). Low sample gas volume complicates bellows pressure adjustment between acquisitions as the sample bellows is nearly compressed to achieve a suitable gas pressure (e.g., 16 V, *m/z* 44). Alternatively, sample and reference CO_2 can be stored within individual micro-volumes before the change-over valves (Fig. 3; e.g., He et al., 2012; Petersen and Schrag, 2014). Acid-liberated CO_2 is directly transferred from the purification system into the sample micro-volume while reference CO_2 is re-filled from the reference bellow. Prior to measurement, the peak intensity of the reference gas is balanced with the sample gas through compression of the reference bellows. During measurement, micro-volume gas pressure is unable to be adjusted, resulting in an equal decrease of analyte CO_2 peak intensities over time.

2.5.8.1. Alternative Δ_{47} measurement protocols

Recently, two new Δ_{47} measurement protocols have been proposed. First, the long-integration dual-inlet (LIDI) protocol which is optimized for micro-volume mode (Hu et al., 2014), and second, the 'multi-collector peak hopping' protocol, in which raw Δ_{47} measurements are achieved using only the 3 Faraday cups corresponding to *m/z* 44, 45, and 46 (Petrizzo and Young, 2014). Traditionally, dual-inlet measurement protocols waste up to ~70% of sample CO_2 gas through the initial analyte pressure-balancing period, as well as the constant flow of CO_2 sample gas to an exhaust pump during reference measurement (Hu et al., 2014). The LIDI protocol was developed to maximize the efficient usage of available sample CO_2. This is particularly beneficial for low-volume CO_2 samples prepared by the Kiel-IV device.

This protocol consists of a single sample measurement followed by a single reference measurement of ~ 600 seconds each (Hu et al., 2014). This process negates the requirement of an initial pressure balancing phase as well as the constant flow of sample CO_2 gas to the exhaust pump, effectively enabling the measurement of the bulk of the available sample CO_2 gas. The raw Δ_{47} value is subsequently determined based upon the comparison of sample and reference beam ratios at points of equal peak intensity. In comparison to previous micro-volume measurement protocols (e.g., Schmid and Bernasconi, 2010), the LIDI protocol obtains an improved internal precision of ± 0.006 – 0.008 ‰ ($n = 4 – 6$), while requiring a total carbonate sample size of ~ 1 – 2 mg to produce comparable Δ_{47} external precision (Hu et al., 2014). Although the usage of this protocol is currently limited to a single laboratory, its applicability to acid-liberated CO_2 produced by a Kiel-IV device is promising.

The ‘multi-collector peak hopping’ protocol enables the measurement of *m/*z 44, 45, 46, and 47 on a mass spectrometer with 3 Faraday cups configured for *m/z* 44, 45, and 46. This protocol may potentially enable raw Δ_{47} measurement utilizing mass spectrometers previously only capable of measuring $\delta^{18}O$ and $\delta^{13}C$ of CO_2. Measurement of *m/z* 46 and 47 is achieved by slightly altering the magnet current and the ion beam accelerating voltage to redirect the ion beams corresponding to *m/z* 46 and 47 to the Faraday cups used to measure *m/z* 44 and 45. To date, the usage of this measurement protocol is limited, and has only been accomplished on a single mass spectrometer

(Petrizzo et al., 2014; Petrizzo and Young, 2014). Although this measurement protocol is capable of attaining comparable external precision (~ ± 0.020 ‰; Petrizzo and Young, 2014), its effectiveness on alternative mass spectrometer models has not yet been established.

2.5.9. Δ_{47} measurement complications

The precise measurement of raw Δ_{47} is complex, and relies on multiple components of analysis, including: (1) purity and isotopic composition of the CO_2 sample and mass spectrometer reference gas; (2) mass spectrometer isotope effects, including isotopic re-distribution within capillaries and Δ_{47} scale compression caused by ion fragmentation and re-combination within the ion source (Passey et al., 2010; He et al., 2012); and (3) mass spectrometer Δ_{47} vs. δ^{47} non-linearity produced by the incorrect determination of Faraday cup pressure baselines (He et al., 2012; Bernasconi et al., 2013; Rosenheim et al., 2013).

2.5.9.1. Sample and reference CO_2 gas precautions

If stringent cleaning procedures are adhered to for the preparation of CO_2 sample and mass spectrometer reference gases, the likelihood of contamination is minimized. However, if assessing acid-liberated CO_2 from natural carbonates, inadequate removal of contamination capable of producing isobaric interferences with the *m/z* 44 - 49 Faraday cups may occur. For example, if a significant abundance of the chlorocarbon derivative

$^{12}C^{35}Cl^+$ (*m/z* = 47) is present within the CO_2 sample, raw Δ_{47} may appear abnormally elevated.

The presence of isobaric contamination may be detected through the paired measurement of sample Δ_{48} and Δ_{49}; terms calculated similarly to the Δ_{47} value (Eqs. 19 and 20; Huntington et al., 2009). Given the low abundance of mass 48 and 49 CO_2 isotopologues (Fig. 1), the measurement of Δ_{48} and Δ_{49} values for the determination of carbonate formation temperature is currently impractical. Furthermore, Huntington et al. (2009) report a significant correlation between Δ_{49} and pressure imbalances between analyte gases flowing into the ion source, further complicating Δ_{49} measurement.

However, if the Δ_{48} or Δ_{49} value of an individual CO_2 measurement is sporadically elevated in comparison to typical sample measurements, the presence of isobaric contamination is plausible (Eiler and Schauble, 2004; Huntington et al., 2009). Although isobaric contaminants could potentially elevate the *m/z* 48 and 49 beams while the *m/*z 47 beam remains unaltered, abnormal Δ_{48} and/or Δ_{49} reduce the reliability of Δ_{47} measurements (Huntington et al., 2009).

$$\Delta_{48}=\left[\left(\frac{R^{48}}{R^{48^*}}-1\right)-2\left(\frac{R^{46}}{R^{46^*}}-1\right)\right]\times 1000. \tag{19}$$

$$\Delta_{49}=\left[\left(\frac{R^{49}}{R^{49^*}}-1\right)-2\left(\frac{R^{46}}{R^{46^*}}-1\right)-\left(\frac{R^{45}}{R^{45^*}}-1\right)\right]\times 1000. \tag{20}$$

Where:

$$R^{48*} = (R^{18})^2 + 2R^{13}\times R^{17}\times R^{18}, \tag{21}$$

$$R^{49*} = R^{13}\times(R^{18})^2. \tag{22}$$

The clumped isotope composition of the CO_2 sample and mass spectrometer reference gas is also of concern. During storage, the clumped isotope composition of sample CO_2 gas may shift towards a state of isotopic equilibrium with respect to the ambient temperature, suggesting the period between CO_2 sample purification and measurement should be minimized. However, this concern may be minor, as Dennis et al. (2011) observed no observable shift in Δ_{47} when CO_2 was stored for several months. In contrast, CO_2 mass spectrometer reference gas should be given adequate time to reach a state of clumped isotope equilibrium with the ambient temperature of the laboratory. If not in equilibrium, a long-term systematic shift in measured raw Δ_{47} may be observed until the reference gas clumped isotope composition stabilizes.

2.5.9.2. Isotope effects during Δ_{47} measurement

Prior to the measurement of CO_2 ion beam intensity by the Faraday cups, various isotope effects may either fragment or re-order the CO_2 isotopologues, altering the resultant measured raw Δ_{47} (Fig. 3). First, in some cases, certain stock stainless steel capillaries have been found to encourage isotopic redistribution and exchange (Passey et al., 2010). This effect is potentially due to the capillaries being catalytically active, and/or due to the stainless steel internal capillary surface promoting adherence of water molecules capable of isotopic exchange with CO_2 (Passey et al., 2010). To minimize isotopic redistribution, these stock stainless steel capillaries have been replaced by either electroformed nickel (EFNi) capillaries (e.g., Passey et al., 2010; Wacker et al., 2013; Cui and Wang, 2014; Petrizzo and Young, 2014) or deactivated fused-silica capillaries (e.g., Dennis and Schrag, 2010).

Second, isotopic fragmentation and recombination of CO_2 isotopologues within the ion source – referred to as Δ_{47} scale compression – shifts analyte isotopologues towards a stochastic distribution (Fig. 3a; Huntington et al., 2009). Reducing scale compression may be achieved by decreasing the gas pressure and residence time of analyte CO_2 within the ion source (Huntington et al., 2009). On the MAT 253, increasing the ‘extraction potential’ value is reported to reduce analyte residence time (Cui and Wang, 2014). Alternatively, residence time may also be reduced by setting the Variable Ion Source Conductance (commonly referred to as the sulfur window) to ‘open’ (Huntington et al., 2009). Opening the sulfur window increases ion source pumping efficiency, reducing analyte residence time. These methods reduce Δ_{47} scale compression at the expense of Δ_{47} internal precision due to lower ion beam intensities (Huntington et al., 2009; Cui and Wang, 2014). Therefore, as proposed by Huntington et al. (2009), maintaining high Δ_{47} internal precision is preferable, so long as Δ_{47} scale compression can be systematically corrected through implementation of a reference frame. Ideally, a future alteration of ion source design and functioning may aid in significantly minimizing this effect.

2.5.9.3. Reduction of Δ_{47} vs. δ^{47} non-linearity

Initial clumped isotope research utilizing the MAT 253 mass spectrometer identified a systematic Δ_{47} vs. δ^{47} non-linearity between sample CO_2 gases of widely-varying bulk isotopic composition (Eiler and Schauble, 2004). Problematically, the extent of this dependence varies with time, and must be continuously characterized to maintain Δ_{47} precision (Huntington et al., 2009; Dennis et al., 2011). Reported Δ_{47} vs. δ^{47} non-linearity is typically characterized by a slope of 0.005 – 0.015 (e.g., Dennis et al., 2011; Petrizzo and Young, 2014). Interestingly, non-linearity varies between mass spectrometers, and has not been observed on the 3 kV Delta XP, suggesting it is a product of individual machine function and design (Huntington et al., 2009; Yoshida et al., 2013).

In fact, the primary cause of this non-linearity is now understood to originate from the method of determining the pressure baseline (PBL) of certain Faraday cups (He et al., 2012; Bernasconi et al., 2013; Rosenheim et al., 2013; Meckler et al., 2014). Previously, CO_2 *m/z* 44 – 49 ion beam intensities were computed relative to the background PBL (i.e., the residual background noise when analyte gas is not entering the ion source). However, dependent on mass spectrometer design, the true PBL (i.e., residual background noise during CO_2 ionization) of the *m/z* 47 – 49 Faraday cups may be negatively offset by the production of secondary electrons (Fig. 3b; Bernasconi et al., 2013; He et al., 2012; Meckler et al., 2014). The abundance of secondary electrons primarily relies on the beam intensity and focus of the *m/z* 44 ion beam (He et al., 2012). These secondary electrons are believed to originate from collisions of the *m/z* 44 ion beam within the flight tube of certain mass spectrometers (He et al., 2012). A smaller positive deviation (a few mV) possibly occurs from the scattering and coulomb repulsion of *m/z* 44 ions inadvertently entering the *m/z* 47 – 49 Faraday cups (Fig. 3; He et al., 2012). The collection of secondary electrons and divergent *m/z* 44 ions by the *m/z* 47 Faraday cup may impede the precise quantification of *m/z* 47 peak intensity.

Short-term PBL shifts occur between acquisitions due to analyte peak intensity adjustment, and in some cases, during a single acquisition as analyte peak intensity decreases (He et al., 2012; Fernandez et al., 2014). Long-term shifts may occur as the focus of the *m/z* 44 ion beam widens due to deterioration of the filament and/or accumulated contamination in the ion source (He et al., 2012). Finally, erratic PBL shifts may occur after filament replacement, venting or mass spectrometer baking (Meckler et al., 2014; Petrizzo and Young, 2014).

Shifts in the *m/z* 47 PBL may be corrected through incorporation of a modified sample acquisition structure (e.g., He et al., 2012; Bernasconi et al., 2013; Petrizzo and Young, 2014). Currently, the *m/z* 47 PBL correction (bellows and micro-volume mode) proposed by He et al. (2012) is most widely utilized. During a bellows mode acquisition, *m/z* 47 PBL is linearly interpolated by measuring the off-peak PBL before and after a set of on-peak analyte cycles. During a micro-volume mode acquisition, *m/z* 47 PBL is scaled from the *m/z* 49 PBL. The *m/z* 49 PBL is determined by subtracting the estimated *m/z* 49 ion beam contribution from the measured *m/z* 49 ion beam intensity to isolate the *m/z* 49 PBL offset. Application of the PBL correction typically reduces the Δ_{47} vs. δ^{47} non-linearity slope by an order of magnitude or more (e.g., He et al., 2012; Fernandez et al., 2014; Meckler et al., 2014; Petrizzo and Young, 2014). Oddly, certain PBL corrections appear to overcompensate, producing a slightly negative Δ_{47} vs. δ^{47} non-linearity slope (e.g., He et al., 2012). Despite this slight overcompensation, the usage of the PBL correction enables a significant improvement in Δ_{47} measurement precision due to the minimization of short- and long-term shifts in the PBL of the Faraday cups, and a reduced reliance of raw Δ_{47} on the δ^{47} value.

2.5.10. Standardization of Δ_{47} measurements

For the sake of data compatibility among laboratories, Δ_{47} values are most commonly reported in the 'absolute reference frame' proposed by Dennis et al. (2011). This reference frame defines the absolute Δ_{47} of CO_2 sample gas based upon two or more CO_2 reference gases of widely varying δ^{47} that have been isotopically equilibrated at multiple temperatures (e.g., 10, 25, 40, and 1000 °C). Equilibration at multiple temperatures produces a substantial isotopologue distribution and accounts for mass spectrometer Δ_{47} scale compression. CO_2 reference gases of varying δ^{47} are utilized to assess machine-specific Δ_{47} vs. δ^{47} non-linearity and define a common non-linearity correction relationship applicable to all CO_2 gases. If a PBL correction has already been applied, this non-linearity correction may be minimal.

Upon application of the non-linearity correction, the Δ_{47} of CO_2 reference gases is effectively independent of δ^{47}. The 'true' Δ_{47} value of CO_2 reference gases is defined on the basis of equilibration temperature and the established theoretical thermodynamics of CO_2 proposed by Wang et al. (2004). The relationship between the Δ_{47} of CO_2 references corrected for non-linearity and the theoretically defined 'true' Δ_{47} values is titled the 'empirical transfer function' (Dennis et al., 2011). The 'true' Δ_{47} values of sample CO_2 gases may therefore be determined by (1) projecting raw Δ_{47} values to the absolute reference frame using the established non-linearity correction and empirical transfer function (Dennis et al., 2011); and (2) applying the appropriate $\Delta^{*}_{25\text{-}T_{acid}}$ value (if applicable).

To account for shifts in Δ_{47} vs. δ^{47} non-linearity and Δ_{47} scale compression, Dennis et al. (2011) proposed a ‘secondary reference frame’. This secondary reference frame requires routine measurement of carbonate standards of known Δ_{47} to monitor the existing empirical transfer function. Finally, if raw Δ_{47} values were previously corrected to the heated gas reference frame (Eiler and Schauble, 2004), the ‘tertiary reference frame’ provides a practical method of re-correcting Δ_{47} values to the absolute reference frame (Dennis et al., 2011).

Improvement in the inter-laboratory precision of carbonate Δ_{47} projected to the absolute reference frame would likely benefit from the distribution and widespread usage of homogeneous, well-defined clumped isotope carbonate standards. To suit this requirement, multiple carbonates have undergone inter-laboratory assessment to establish clumped isotope composition, homogeneity, and facilitate in the precise application of the absolute reference frame. For example, NBS 19 (distributed by the IAEA) was assessed as a clumped isotope carbonate standard (Dennis et al., 2011). However, sizable intra and inter-laboratory Δ_{47} heterogeneity was observed between distributed bottles impeding its applicability as an inter-laboratory standard (Dennis et al., 2011). Alternatively, laboratories have begun distributing and testing alternative carbonate standards (e.g., ETH 1 - 4 by ETH Zurich; Bernasconi et al., 2014). Widespread acceptance of such a standard would also facilitate long-term monitoring of mass spectrometer function and provide a comparative tool for assessing the typical external precision of Δ_{47} associated with individual laboratories analytical techniques.

2.6. Discrepancy among Paleothermometer Calibrations

Current calibrations of the carbonate clumped isotope paleothermometer are commonly categorized by those exhibiting a steep slope, similar to the original calibration by Ghosh et al. (2006) (Fig. 4; e.g., Tripati et al., 2010; Thiagarajan et al., 2011; Zaarur et al., 2013) and those with a shallow slope similar to the theoretical calibration by Guo et al. (2009) (Fig. 4; e.g., Dennis and Schrag, 2010; Eagle et al., 2013; Henkes et al., 2013; Fernandez et al., 2014; Petrizzo et al., 2014; Tang et al., 2014; Wacker et al., 2014; Defliese et al., 2015). To date, a conclusive explanation for this discrepancy has not been discovered. However, various carbonate precipitation mechanisms and/or Δ_{47} artifacts specific to the previously discussed analytical techniques may provide a partial explanation.

For example, Eagle et al. (2013) suggested certain empirical calibration discrepancies are possibly related to Δ_{47} ‘vital effects’, in which the shell calcification mechanisms of bivalves, corals, and foraminifera alter the Δ_{47} of the precipitated carbonate. Alternatively, DIC-H_2O disequilibrium most pronounced in high pH and low temperature solutions may result in disequilibrium Δ_{47} of precipitated carbonates, altering the resultant calibration slope (Henkes et al., 2013). However, Tang et al. (2014) assessed the experimental design of ‘steep slope’ precipitation experiments and concluded carbonates were unlikely to have precipitated in disequilibrium. Tang et al. (2014)

alternatively suggest an unknown aspect of the laboratory-specific analytical procedure is most likely responsible for discrepant calibrations.

Hypotheses related to analytical aspects of the Δ_{47} determination of acid-liberated CO_2 include (1) different acid-digestion temperature and associated $\Delta^{*}_{25\text{-}T_{acid}}$ values between laboratories (Eagle et al., 2013; Fernandez et al., 2014; Tang et al., 2014; Wacker et al., 2014); (2) analytical variation in H_2O removal during carbonate digestion and/or purification (Wacker et al., 2014; Defliese et al., 2015); and (3) poor inter-laboratory calibration of the absolute reference frame or secondary projections (Wacker et al., 2014).

Assessment of the clumped isotope systematics during phosphoric acid digestion by Defliese et al. (2015) concluded that acid-digestion temperature, carbonate mineralogy and/or Δ_{47} scaling are all improbable sources of the calibration discrepancy. Instead, it is proposed that laboratory-specific variation in H_2O and contaminant removal during acid-digestion and purification may instead promote Δ_{47} alteration and/or partial re-equilibration (Wacker et al., 2013; Defliese et al., 2015). Dependent on the specific phosphoric acid digestion system, this H_2O-CO_2 interaction may be elevated in carbonates between 4 – 7 mg and/or with higher T_{acid} due to increased H_2O vapor pressure (see section 2.4.6; Wacker et al., 2013; Defliese et al., 2015). Finally, if inter-laboratory standards were incorrectly defined during application of the secondary or tertiary reference frame, resultant Δ_{47} may be imprecise. For example, the calibration proposed by Ghosh et al. (2006) was originally projected in the ‘heated gas reference frame’ and may only be re-projected to the absolute reference frame for comparison based upon published

Δ_{47} NBS 19 values. This re-projection may pose concern given the presumed Δ_{47} heterogeneity of NBS 19 observed by Dennis et al. (2011). However, as concluded by Wacker et al. (2014), the maximum extent of this re-projection imprecision could only partially account for the calibration discrepancies.

The source of these discrepancies remains elusive; however, continued refinement of the analytical techniques specific to carbonate clumped isotope paleothermometry may provide clues to its source. Prior to the understanding of this discrepancy, the conservative usage of calibrations produced under identical analytical conditions to carbonate samples may benefit paleotemperature determinations.

2.7. Conclusion

Advances in the analytical techniques specific to clumped isotope geochemistry have solidified the usage of the carbonate clumped isotope paleothermometer as a viable method of paleotemperature reconstruction. Recent developments in the analytical procedures required for carbonate Δ_{47} determinations include (1) refined carbonate pre-treatment protocols (e.g., Zaarur et al., 2011; Henkes et al., 2014); (2) characterization of the clumped isotope mineralogical and temperature effects associated with phosphoric acid digestion (e.g., Wacker et al., 2013; Defliese et al., 2015); (3) the establishment of on-line automated CO_2 evolution, purification, and Δ_{47} measurement systems that are capable of increased throughput and reduced sample size (e.g., Petersen and Schrag, 2014; Meckler et al., 2014); (4) adapted Δ_{47} measurement protocols accounting for Faraday cup pressure baseline shifts, reduced sample size, and mass spectrometers without dedicated *m/z* 47 – 49 Faraday cups (e.g., He et al., 2012; Hu et al., 2014; Meckler et al., 2014; Petrizzo and Young, 2014); and finally, (5) wide-spread usage of the absolute reference frame, facilitating in precise inter-laboratory comparison of Δ_{47} measurements (Dennis et al., 2011).

Future improvements to paleotemperature precision and the resolution of calibration discrepancies may potentially be achieved through the continued refinement of the analytical techniques responsible for carbonate acid-digestion, CO_2 purification, Δ_{47} measurement and reference frame standardization. These improvements will likely necessitate the investigation of the following predominant analytical issues:

(1) Disagreement among proposed Δ^{*}_{47} values limits the direct determination of the clumped isotope composition of carbonates (Δ_{63}), potentially due to an inability to achieve a stochastic distribution of carbonate ion isotopologues through current experimental re-crystallization protocols, and/or a limited theoretical understanding of the clumped isotope systematics of the carbonate acid digestion reaction.

(2) Variability among proposed $\Delta^{*}_{25\text{-}T_{acid}}$ values possibly due to variable mineralogy, carbonate types, and/or systematic fractionation offsets indiscernible given the current external precision of Δ_{47} measurements.

(3) Ongoing assessment of the cleaning effectiveness, optimal transfer temperature, length, and potential isotopic fractionation associated with the usage of divinyl benzene polymers as a cleaning agent when housed within packed GC columns, U-traps, or the linear trap specific to the Kiel-IV Carbonate Device.

(4) Limitations on the internal precision of clumped isotope measurements due to mass spectrometer design and functioning (e.g., enhanced isotopic exchange within certain stainless steel capillaries, fragmentation and re-combination within the ion source, production of secondary electrons within the flight tube, and partial diversion of the *m/z* 44 ion beam due to possible scattering and coulomb repulsion).

(5) Current limited distribution of clumped isotope carbonate standards with a homogeneous, well-defined Δ_{47} (preferably with formation temperatures similar to typical carbonate samples) to facilitate in an inter-laboratory comparison of the analytical techniques associated with carbonate Δ_{47} determinations.

2.8. Figures

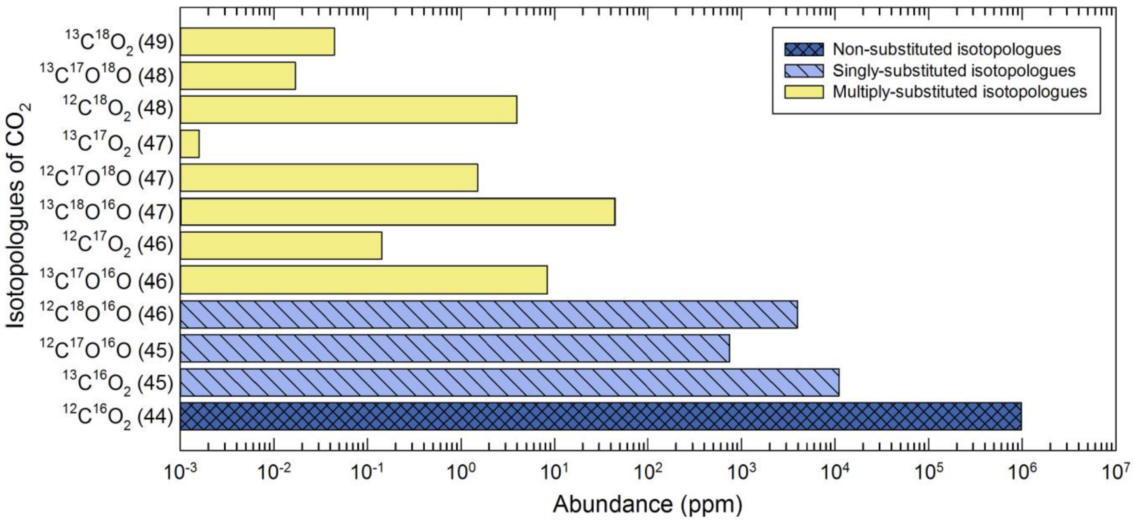

Figure 1: Abundances of the non-substituted, singly-substituted and multiply-substituted stable isotopologues of CO_2 given a stochastic distribution of all potential CO_2 isotopologues.

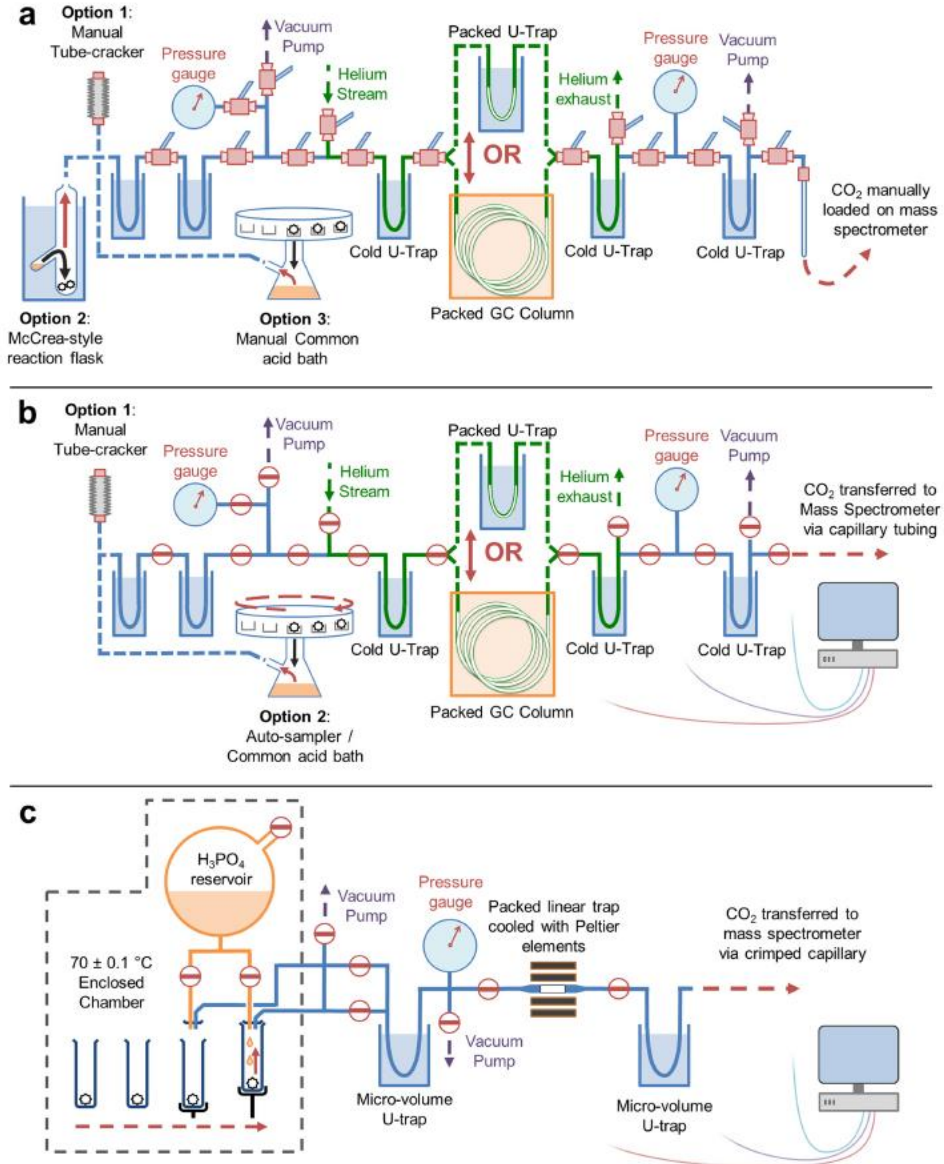

Figure 2: Generalized schematics of CO_2 clumped isotope evolution and purification systems. Black arrows indicate carbonate-acid mixing direction. Red arrows indicate the flow direction of acid-liberated CO_2 gas. Purple arrows indicate the flow direction of waste gases. Green arrows indicate the flow direction of helium. Three operational configurations are presented: (a) manual system design, commonly incorporating either the McCrea-style reaction vessel or the common acid bath phosphoric acid digestion CO_2 evolution system, and either divinyl benzene polymer packed U-trap or packed GC column; (b) automated system design commonly incorporating either the packed U-trap or packed GC column; (c) automated acid drip system (Kiel-IV Carbonate Device) incorporating a divinyl benzene polymer linear trap.

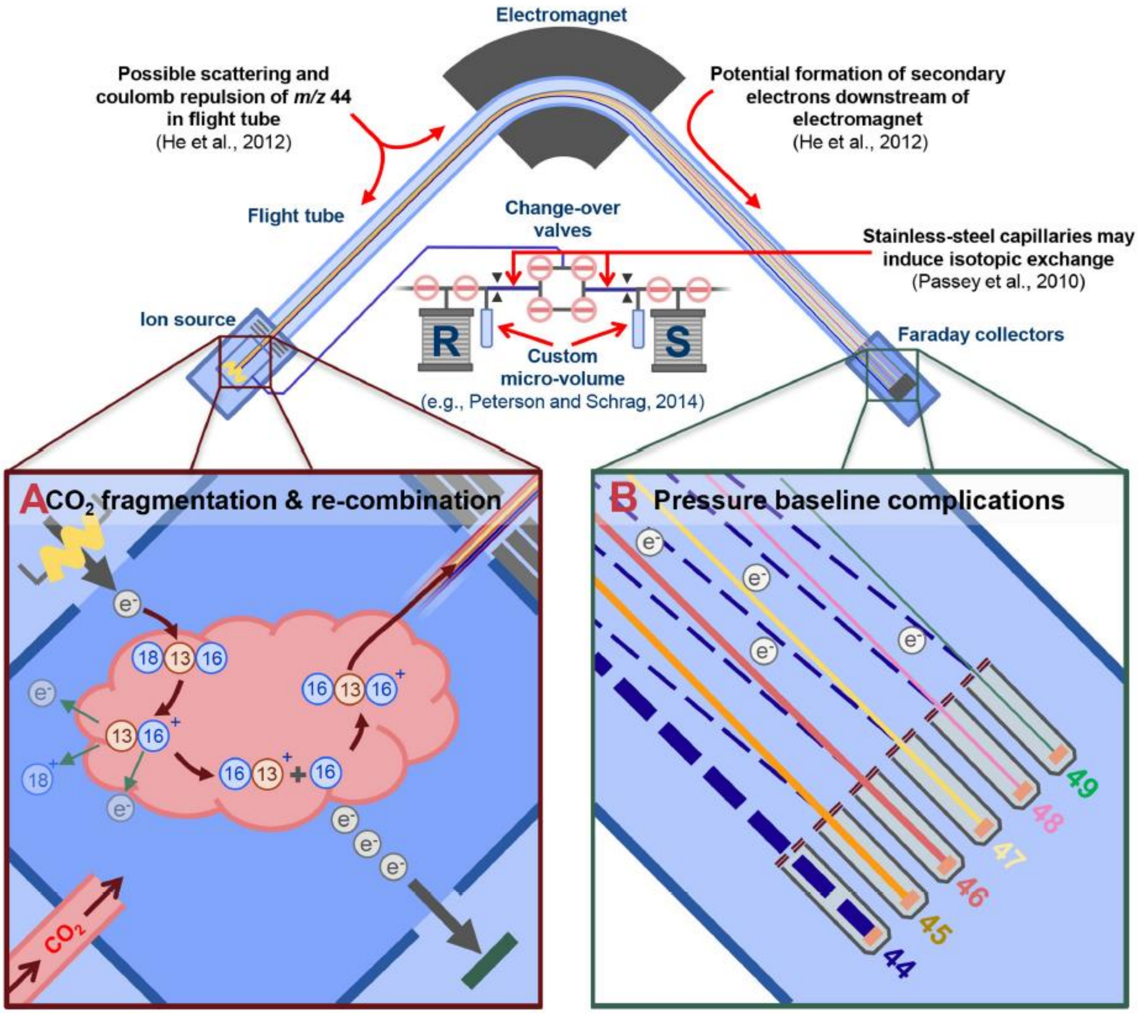

Figure 3: Simplified dual-inlet gas source mass spectrometer schematic illustrating current Δ_{47} measurement complications: (a) CO_2 fragmentation and re-combination within the ion source forces CO_2 isotopologues towards a stochastic distribution, dependent on ion source gas pressure and residence time; (b) formation of secondary electrons from collision of the *m/z* 44 ion beam with the flight tube and possible scattering and/or coulomb repulsion of the *m/z* 44 ion beam inadvertently altering the PBL of *m/z* 45, 47, 48 and 49 Faraday collectors.

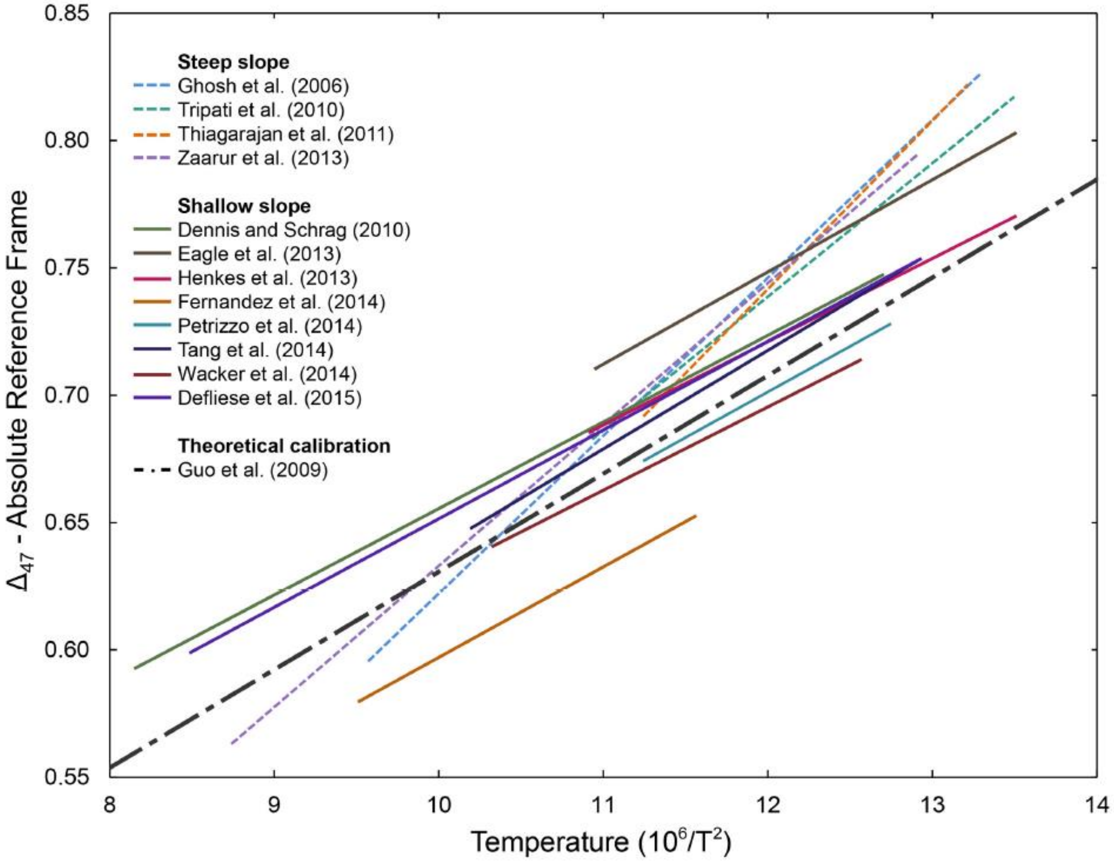

Figure 4: A comparison of carbonate clumped isotope paleothermometer calibrations categorized by 'steep' slope (e.g., Ghosh et al., 2006), 'shallow' slope (e.g., Dennis and Schrag, 2010) and the theoretical calcite calibration proposed by Guo et al. (2009). For calibrations in which an acid digestion temperature other than 25 °C was used, the published $\Delta^*_{25\text{-}T_{acid}}$ correction was applied. As the siderite calibration of Fernandez et al. (2014) was published without a correction, a $\Delta^*_{25\text{-}100}$ of 0.077 ‰ was applied (calculated using Eq. 23 of Guo et al. (2009)).

2.9. Tables

Table 1. Carbonate clumped isotope paleothermometer calibrations projected in the absolute reference frame proposed by Dennis et al. (2011)

Reference	Regression line ($\Delta_{47} = m(10^6/T^2) + b$) where T is in kelvins					
	Temperature range (°C)	Slope (*m*)	Slope SE	Intercept (*b*)	Intercept 1se	R^2
Empirical calibrations						
Tripati et al. (2010)[a]	-0.9 − 29.2	0.0524	0.0026	0.1099	0.0312	0.9068
Thiagarajan et al. (2011)[a]	2 − 25	0.0661	0.0053	-0.0515	0.0659	0.8703
Eagle et al. (2013)[b]	-1 − 29	0.0362	0.0044	0.3140	0.0527	0.7258
Henkes et al. (2013)[b]	-1 − 29.5	0.0327	0.0022	0.3286	0.0278	0.84
Petrizzo et al. (2014)[b]	7 − 25	0.0358	0.0060	0.2717	0.0734	0.856
Wacker et al. (2014)[b]	9 − 38	0.0327	0.0026	0.3030	0.0308	0.9915
Experimental calibrations						
Ghosh et al. (2006)[c]	1 − 50	0.0620	0.0099	0.0021	0.1095	0.8877
Dennis and Schrag (2010)[c]	7.5 − 77	0.0340	0.0038	0.3155	0.0408	0.8600
Zaarur et al. (2013) [b]	5 − 65	0.0555	0.0027	0.0780	0.0298	0.93
Fernandez et al. (2014)[b]	21 − 51	0.0356	0.0018	0.172	0.019	0.997
Tang et al. (2014)[b]	5 − 40	0.0387	0.0072	0.2532	0.0829	0.9998
Defliese et al. (2015)[b]	5 – 70	0.03484	0.00229	0.3031	0.0244	0.8778
Theoretical calibration						
Guo et al. (2009) (calcite)	$\Delta_{47} = -3.33040 \times 10^9/T^4 + 2.32415 \times 10^7/T^3 - 2.91282 \times 10^3/T^2 - 5.54042/T + 0.23252$					

[a] Calibration has been re-projected into the absolute reference frame by Wacker et al. (2014) using a 2-point transfer function.

[b] Calibration is presented as originally published, including (if applicable) the original $\Delta^*_{25\text{-}T acid}$ correction.

[c] Calibration has been re-projected into the absolute reference frame by Eagle et al. (2013) using a 2-point transfer function.

Table 2. Comparison of experimental and theoretical $\Delta^*_{25\text{-}T_{acid}}$ derivations and associated acid digestion attributes

Reference	$\Delta^*_{25\text{-}T_{acid}}$ (‰)	Carbonate mineralogy	Carbonate type	System information
T_{acid} = 25 and 75 °C				
Guo et al. (2009) (Theoretical)	0.057[a]	All carbonates	n/a	n/a
Lechler et al. (2013)[b]	0.0670	Calcite	n/a	n/a
T_{acid} = 25 and 90 °C				
Guo et al. (2009) (Theoretical)	0.069[a]	All carbonates	n/a	n/a
Defliese et al. (2015)	0.074	Calcite	Carrara marble	Common manual extraction line and mass spectrometer
Defliese et al. (2015)	0.088	Calcite	Antarctic scallop	Common manual extraction line and mass spectrometer
Passey et al. (2010)	0.081[c]	Calcite	NBS-19 and speleothem	Multiple extraction lines and mass spectrometers
Wacker et al. (2013)	0.075	Calcite	NBS-19	Common manual extraction line and mass spectrometer
Defliese et al. (2015)	0.089	Aragonite	Joulters Cay ooids	Common manual extraction line and mass spectrometer
Henkes et al. (2013)	0.092	Aragonite	Mollusk shells	Common automated extraction line and mass spectrometer
Wacker et al. (2013)	0.066	Aragonite	Bivalve shells	Common manual extraction line and mass spectrometer
Defliese et al. (2015)	0.079	Dolomite	SRM 88b	Common automated extraction line and mass spectrometer

In all cases, the off-line manual McCrea-style reaction vessel (sealed for the duration of reaction) was utilized for T_{acid} = 25 °C, while the on-line or off-line common acid bath (immediate removal) was utilized for T_{acid} = 75 and 90 °C.

[a] Value has been calculated using Eq. 23 of Guo et al. (2009).

[b] 25 °C carbonate acid digestion, purification, and measurement system not specified.

[c] Mean of NBS-19 and speleothem carbonate samples calculated from the results presented in Table S5, Passey et al. (2010).

2.10. References

Affek H. P. (2012) Clumped isotope paleothermometry: Principles, applications, and challenges. *The Paleontological Society Papers* **18**, 101–114.

Bemis B. E., Spero H. J., Bijma J., and Lea W. (1998) Reevaluation of the oxygen isotopic composition of planktonic foraminifera: Experimental results and revised paleotemperature Equations. *Paleoceanography* **13**, 150–160.

Bernasconi S. M., Hu B., Wacker U., Fiebig J., Breitenbach S. F. M., and Rutz T. (2013) Background effects on Faraday collectors in gas-source mass spectrometry and implications for clumped isotope measurements. *Rapid Communications in Mass Spectrometry* **27**, 603–612.

Bernasconi S., the ETH clumpy team and interlaboratory calibration test participants (2014) Interlaboratory comparison of clumped isotope measurements of 4 carbonate samples: Towards the establishment of carbonate standards for clumped isotope analysis. *4th International Workshop on Clumped Isotopes*, Zürich, Aug. 24–27, p. 35.

Bigeleisen J. (1955) Statistical Mechanics of Isotopic Systems with Small Quantum Corrections. I. General Considerations and the Rule of the Geometric Mean. *The Journal of Chemical Physics* **23**, 2264–2267.

Buchardt B. (1978) Oxygen isotope paleotemperatures from the Tertiary period in the North Sea area. *Nature* **275**, 121–123.

Carothers W. W., Adami L. H., and Rosenbauer R. J. (1988) Experimental oxygen isotope fractionation between siderite-water and phosphoric acid liberated CO_2-siderite. *Geochimica et Cosmochimica Acta* **52**, 2445–2450.

Chacko T., Cole D. R., and Horita J. (2001) Equilibrium oxygen, hydrogen and carbon isotope fractionation factors applicable to geologic systems. *Reviews in Mineralogy and Geochemistry* **43**, 1–81.

Cole J. E., Dunbar R. B., McClanahan T. R., and Muthiga N. A. (2000) Tropical pacific forcing of decadal SST variability in the Western Indian Ocean over the past two centuries. *Science* **287**, 617–619.

Cui L. and Wang X. (2014) Determination of clumped isotopes in carbonate using isotope ratio mass spectrometer: Effects of extraction potential and long-term stability. *International Journal of Mass Spectrometry* **372**, 46–50.

Daëron M., Guo W., Eiler J., Genty D., Blamart D., Boch R., Drysdale R., Maire R., Wainer K., and Zanchetta G. (2011) $^{13}C^{18}O$ clumping in speleothems: Observations from natural caves and precipitation experiments. *Geochimica et Cosmochimica Acta* **75**, 3303-3317.

Dale A., John C. M., Mozley P. S., Smalley P. C., and Muggeridge A. H. (2014) Time-capsule concretions: Unlocking burial diagenetic processes in the Mancos Shale using carbonate clumped isotopes. *Earth and Planetary Science Letters* **394**, 30–37.

Defliese W. F., Hren M. T., and Lohmann K. C. (2015) Compositional and temperature effects of phosphoric acid fractionation on Δ_{47} analysis and implications for discrepant calibrations, *Chemical Geology* **396**, 51–60.

Dennis K. J., Affek H. P., Passey B. H., Schrag D. P., and Eiler J. M. (2011) Defining an absolute reference frame for 'clumped' isotope studies of CO_2. *Geochimica et Cosmochimica Acta* **75**, 7117–7131.

Dennis K. J., Cochran J. K., Landman N. H., and Schrag D. P. (2013) The climate of the Late Cretaceous: New insights from the application of the carbonate clumped isotope thermometer to Western Interior Seaway macrofossil. *Earth and Planetary Science Letters* **362**, 51–65.

Dennis K. J. and Schrag D. P. (2010) Clumped isotope thermometry of carbonatites as an indicator of diagenetic alteration. *Geochimica et Cosmochimica Acta* **74**, 4110–4122.

Dennis P. F. and Vinen S. J. (2009) MIRA: A new approach to measuring Δ47 in carbonates and geothermometry of MVT type deposits. *European Geosciences Union General Assembly Conference (Abstract),* Vienna, Apr. 19–24, p. 5540.

Dickson J. A. D. and Coleman M. L. (1980) Changes in carbon and oxygen isotope composition during limestone diagenesis. *Sedimentology* **27**, 107–118.

Dietzel M., Tang J., Leis A. and Köhler S. J. (2009) Oxygen isotope fractionation during inorganic calcite precipitation – Effects of temperature, precipitation rate and pH. *Chemical Geology* **268**, 107–115.

Dunbar R. B., Wellington G. M., Colgan M. W., and Glynn P. W. (1994) Eastern Pacific sea surface temperature since 1600 A.D.: The δ^{18}O record of climate variability in Galápagos corals. *Paleoceanography* **9**, 291–315.

Eagle R. A., Schauble E. A., Tripati A. K., Tütken T., Hulbert R. C., and Eiler J. M. (2010) Body temperatures of modern and extinct vertebrates from ^{13}C-^{18}O bond abundances in bioapatite. *Proceedings of the National Academy of Sciences of the United States of America* **107**, 10377–10382.

Eagle R. A., Tütken T., Martin T. S., Tripati A. K., Fricke H. C., Connely M., Cifelli R. L., and Eiler J. M. (2011) Dinosaur body temperatures determined from isotopic (^{13}C-^{18}O) ordering in fossil biominerals. *Science* **333**, 443–445.

Eagle R. A., Eiler J. M., Tripati A. K., Ries J. B., Freitas P. S., Hiebenthal C., Wanamaker Jr. A. D., Taviana M., Elliot M., Marenssi S., Nakamura K., Ramirez P., and Roy K. (2013) The influence of temperature and seawater carbonate saturation state on ^{13}C-^{18}O bond ordering in bivalve mollusks. *Biogeosciences* **10**, 4591–4606.

Eiler J. M. (2007) “Clumped-isotope” geochemistry–The study of naturally-occurring, multiply-substituted isotopologues. *Earth and Planetary Science Letters* **262**, 309–327.

Eiler J. M. (2011) Paleoclimate reconstruction using carbonate clumped isotope thermometry. *Quaternary Science Reviews* **30**, 3575–3588.

Eiler J. M. and Schauble E. (2004) ^{18}O^{13}C^{16}O in Earth’s atmosphere. *Geochimica et Cosmochimica Acta* **68**, 4767–4777.

Engel A. E. J., Clayton R. N., and Epstein S. (1958) Variations in isotopic composition of oxygen and carbon in Leadville limestone (Mississippian, Colorado) and in its hydrothermal and metamorphic phases. *The Journal of Geology* **66**, 374–393.

Epstein S., Buchsbaum R., Lowenstam H., and Urey H.C. (1951) Carbonate-water isotopic temperature scale. *Bulletin of the Geological Society of America* **62**, 417–426.

Fernandez A., Tang J. and Rosenheim B. E. (2014) Siderite ‘clumped’ isotope thermometry: A new paleoclimate proxy for humid continental environments. *Geochimica et Cosmochimica Acta* **126**, 411–421.

Gascoyne, M., Schwarcz, H. P. and Ford, D. C. (1980) A paleotemperature record for the mid-Wisconsin in Vancouver Island. *Nature* **285**, 474-476.

Ghosh P., Adkins J., Affek H., Balta B., Guo W., Schauble E. A., Schrag D. and Eiler J. M. (2006) ^{13}C–^{18}O bonds in carbonate minerals: A new kind of paleothermometer. *Geochimica et Cosmochimica Acta* **70**, 1439–1456.

Ghosh P., Eiler, J., Campana S.E., and Feeney R.F. (2007) Calibration of the carbonate ‘clumped isotope’ paleothermometer for otoliths. *Geochimica et Cosmochimica Acta* **71**, 2736–2744.

Grauel A.-L., Schmid T. W., Hu B., Bergami C., Capotondi L., Zhou L., and Bernasconi S. M. (2013) Calibration and application of the ‘clumped isotope’ thermometer to foraminifera for high-resolution climate reconstructions. *Geochimica et Cosmochimica Acta* **108**, 125–140.

Grossman E. (2012) Applying oxygen isotope paleothermometry in deep time. *The Paleontological Society Papers* **18**, 39–67.

Guo W. and Eiler J.M. (2007) Temperatures of aqueous alteration and evidence for methane generation on the parent bodies of the CM chondrites. *Geochimica et Cosmochimica Acta* **71**, 5565–5575.

Guo W., Mosenfelder J. L., Goddard III W. A. and Eiler J. M. (2009) Isotopic fractionations associated with phosphoric acid digestion of carbonate minerals: Insights from first-principles theoretical modeling and clumped isotope measurements. *Geochimica et Cosmochimica Acta* **73**, 7203–7225.

Halevy I., Fischer W. W., and Eiler J. M. (2011) Carbonates in the Martian meteorite Allan Hills 84001 formed at 18 ± 4 °C in a near-surface aqueous environment.

Proceedings of the National Academy of Sciences of the United States of America **108**, 16895–16899.

He B., Olack G. A., and Colman A. S. (2012) Pressure baseline correction and high-precision CO_2 clumped-isotope (Δ_{47}) measurements in bellows and micro-volume modes. *Rapid Communications in Mass Spectrometry* **26**, 2837–2853.

Henkes G. A., Passey B. H., Grossman E. L., Shenton B. J., Pérez-Huerta A., and Yancey T.E. (2014) Temperature limits for preservation of primary calcite clumped isotope paleotemperatures. *Geochimica et Cosmochimica Acta* **139**, 362–382.

Henkes G. A., Passey B. H., Wanamaker Jr. A. D., Grossman E. L., Ambrose Jr. W. G., and Carroll, M. L. (2013) Carbonate clumped isotope compositions of modern marine mollusk and brachiopod shells. *Geochimica et Cosmochimica Acta* **106**, 307–325.

Hough B. G., Fan M., and Passey B. H. (2014) Calibration of the clumped isotope geothermometer in soil carbonate in Wyoming and Nebraska, USA: Implications for paleoelevation and paleoclimate reconstruction. *Earth and Planetary Science Letters* **391**, 110–120.

Hu B., Radke J., Schlüter H.-J., Heine F. T., Zhou L., and Bernasconi S. M. (2014) A modified procedure for gas-source isotope ratio mass spectrometry: the long-integration dual-inlet (LIDI) methodology and implications for clumped isotope measurements. *Rapid Communications in Mass Spectrometry* **28**, 1413–1425.

Huntington K.W., Eiler J.M., Affek H.P., Guo W., Bonifacie M., Yeung L.Y., Thiagarajan N., Passey B., Tripati A., Daëron M., and Came R. (2009) Methods and limitations of 'clumped' CO_2 isotope (Δ_{47}) analysis by gas-source isotope ratio mass spectrometry. *Journal of Mass Spectrometry* **44**, 1318–1329.

Kim S.-T. and O'Neil J. R. (1997) Equilibrium and nonequilibrium oxygen isotope effects in synthetic carbonates. *Geochimica et Cosmochimica Acta* **61**, 3461–3475.

Kim S.-T., Hillaire-Marcel C. and Mucci A. (2006) Mechanisms of equilibrium and kinetic oxygen isotope effects in synthetic aragonite at 25 °C. *Geochimica et Cosmochimica Acta* **70**, 5790–5801.

Kim S.-T., Mucci A., and Taylor B.E. (2007a) Phosphoric acid fractionation factors for calcite and aragonite between 25 and 75 °C: Revisited. *Chemical Geology* **246**, 135–146.

Kim S.-T., O'Neil J. R., Hillaire-Marcel C. and Mucci A. (2007b) Oxygen isotope fractionation between synthetic aragonite and water: Influence of temperature and Mg^{2+} concentration. *Geochimica et Cosmochimica Acta* **71**, 4704–4715.

Kim S.-T., Gebbinck C. K., Mucci A. and Coplen T. B. (2014) Oxygen isotope systematics in the aragonite-CO_2-H_2O-NaCl system up to 0.7 mol/kg ionic strength at 25 °C. *Geochimica et Cosmochimica Acta* **137**, 147–158.

Kluge T., Affek H. P., Zhang Y. G., Dublyansky Y., Spötl C., Immenhauser A., and Richter D. K. (2014) Clumped isotope thermometry of cryogenic cave carbonates. *Geochimica et Cosmochimica Acta* **126**, 541–554.

Lechler A. R., Niemi N. A., Hren M. T., and Lohmann K. C. (2013) Paleoelevation estimates for the northern and central proto-Basin and Range from carbonate clumped isotope thermometry. *Tectonics* **32**, 295–316.

McCrea J. M. (1950) On the isotopic chemistry of carbonates and a paleotemperature scale. *The Journal of Chemical Physics* **18**, 849–857.

Meckler A. N., Ziegler M., Millán M. I., Breitenbach S. F. M., and Bernasconi S. M. (2014) Long-term performance of the Kiel carbonate device with a correction scheme for clumped isotope measurements. *Rapid Communications in Mass Spectrometry* **28**, 1705–1715.

Miller K. G., Fairbanks R. G., and Mountain G. S. (1987) Tertiary oxygen isotope synthesis, sea level history, and continental margin erosion. *Paleoceanography* **2**, 1–19.

O'Neil J. R., Clayton R. N., and Mayeda T. K. (1969) Oxygen isotope fractionation in divalent metal carbonates. *The Journal of Chemical Physics* **51**, 5547–5558.

O'Neil J. R., Adami L. H., and Epstein S. (1975) Revised value for the O^{18} fractionation between CO_2 and H_2O at 25°C. *Journal of Research of the U.S. Geological Survey* **3**, 623–624.

Passey B. H., Levin N. E., Cerling T. E., Brown F. H., and Eiler J. M. (2010) High-temperature environments of human evolution in East Africa based on bond ordering in paleosol carbonates. *Proceedings of the National Academy of Sciences of the United States of America* **107**, 11245–11249.

Petersen S. V. and Schrag D. P. (2014) Clumped isotope measurements of small carbonate samples using a high-efficiency dual-reservoir technique. *Rapid Communications in Mass Spectrometry* **28**, 2371–2381.

Petrizzo D. A. and Young E. D. (2014) High-precision determination of ^{13}C-^{18}O bonds in CO_2 using multicollector peak hopping. *Rapid Communications in Mass Spectrometry* **28**, 1185–1193.

Petrizzo D. A., Young E. D., and Runnegar B. N. (2014) Implications of high-precision measurements of ^{13}C-^{18}O bond ordering in CO_2 for thermometry in modern bivalve mollusk shells. *Geochimica et Cosmochimica Acta* **142**, 400–410.

Rosenheim B. E., Tang J., and Fernandez A. (2013) Measurement of multiply substituted isotopologues (’clumped isotopes') of CO_2 using a 5 kV compact isotope ratio mass spectrometer: Performance, reference frame, and carbonate paleothermometry. *Rapid Communications in Mass Spectrometry* **27**, 1847–1857.

Saenger C., Affek H. P., Felis T., Thiagarajan N., Lough J. M., and Holcomb M. (2012) Carbonate clumped isotope variability in shallow water corals: Temperature dependence and growth-related vital effects. *Geochimica et Cosmochimica Acta* **99**, 224–242.

Schauble E. A., Ghosh P., and Eiler J. M. (2006) Preferential formation of ^{13}C–^{18}O bonds in carbonate minerals, estimated using first-principles lattice dynamics. *Geochimica et Cosmochimica Acta* **70**, 2510–2529.

Schmid T. W. and Bernasconi S. M. (2010) An automated method for ‘clumped- isotope’ measurements on small carbonate samples. *Rapid Communications in Mass Spectrometry* **24**, 1955–1963.

Sharma T. and Clayton R. N. (1965) Measurement of O^{18}/O^{16} ratios of total oxygen of carbonates. *Geochimica et Cosmochimica Acta* **29**, 1347–1353.

Spero H. J., Bijma J., Lea D. W., and Bemis B. E. (1997) Effect of seawater carbonate concentration on foraminiferal carbon and oxygen isotopes. *Nature* **390**, 497–500.

Suarez M. B. and Passey B. H. (2014) Assessment of the clumped isotope composition of fossil bone carbonate as a recorder of subsurface temperatures. *Geochimica et Cosmochimica Acta* **140**, 142–159.

Swart P. K., Burns S. J., and Leder J. J. (1991) Fractionation of the stable isotopes of oxygen and carbon in carbon dioxide during the reaction of calcite with phosphoric acid as a function of temperature and technique. *Chemical Geology: Isotope Geoscience Section* **86**, 89–96.

Tang J., Dietzel M., Fernandez A., Tripati A. K. and Rosenheim B. E. (2014) Evaluation of kinetic effects on clumped isotope fractionation (Δ_{47}) during inorganic calcite precipitation. *Geochimica et Cosmochimica Acta* **134**, 120–136.

Thiagarajan N., Adkins J., and Eiler J. (2011) Carbonate clumped isotope thermometry of deep-sea corals and implications for vital effects. *Geochimica et Cosmochimica Acta* **75**, 4416–4425.

Thiagarajan N., Subhas A. V., Southon J. R., Eiler J. M., and Adkins J. F. (2014) Abrupt pre-Bølling-Allerød warming and circulation changes in the deep ocean. *Nature* **511**, 75–78.

Tripati A. K., Eagle R. A., Thiagarajan N., Gagnon A. C., Bauch H., Halloran P. R., and Eiler J. M. (2010) ^{13}C–^{18}O isotope signatures and ‘clumped isotope’ thermometry in foraminifera and coccoliths. *Geochimica et Cosmochimica Acta* **74**, 5697–5717.

Tripati A. K., Sahany S., Pittman D., Eagle R. A., Neelin J. D., Mitchell J. L., and Beaufort L. (2014) Modern and glacial tropical snowlines controlled by sea surface temperature and atmospheric mixing. *Nature Geoscience* **7**, 205–209.

Urey H.C. (1947) The thermodynamic properties of isotopic substances. *Journal of the Chemical Society*, 562–581.

van Breukelen M. R., Vonhof H. B., Hellstrom J. C., Wester W. C. G., and Kroon D. (2008) Fossil dripwater in stalagmites reveals Holocene temperature and rainfall variation in Amazonia. *Earth and Planetary Science Letters* **275**, 54–60.

Wachter E. A. and Hayes J. M. (1985) Exchange of oxygen isotopes in carbon dioxide-phosphoric acid systems. *Chemical Geology: Isotope Geoscience Section* **52**, 365–374.

Wacker U., Fiebig J. and Schoene B. R. (2013) Clumped isotope analysis of carbonates: comparison of two different acid digestion techniques. *Rapid Communications in Mass Spectrometry* **27**, 1631–1642.

Wacker U., Fiebig J., Tödter J., Schöne B. R., Bahr A., Friedrich O., Tütken T., Gischler E., and Joachimski M. M. (2014) Empirical calibration of the clumped isotope paleothermometer using calcites of various origins. *Geochimica et Cosmochimica Acta* **141**, 127–144.

White T., González L., Ludvigson G., and Poulsen C. (2001) Middle Cretaceous greenhouse hydrologic cycle of North America. *Geology* **29**, 363–366.

Wang Z., Schauble E. A. and Eiler J. M. (2004) Equilibrium thermodynamics of multiply substituted isotopologues of molecular gases. *Geochimica et Cosmochimica Acta* **68**, 4779–4797.

Yoshida N., Vasilev M., Ghosh P., Abe O., Yamada K., and Morimoto M. (2013) Precision and long-term stability of clumped-isotope analysis of CO_2 using a small-sector isotope ratio mass spectrometer. *Rapid communications in mass spectrometry* **27**, 207–215.

Yu Z. and Eicher U. (1998) Abrupt climate oscillations during the last deglaciation in central North America. *Science* **282**, 2235–2238.

Zaarur S., Olack G., and Affek H. P. (2011) Paleo-environmental implication of clumped isotopes in land snail shells. *Geochimica et Cosmochimica Acta* **75**, 6859–6869.

Zaarur S., Affek H. P. and Brandon M. T. (2013) A revised calibration of the clumped isotope thermometer. *Earth and Planetary Science Letters* **382**, 47–57.

Zeebe R. E. (2005) Reply to the comment by P.Deines on "An explanation of the effect of seawater carbonate concentration on foraminiferal oxygen isotopes," by R. E. Zeebe 1999. *Geochimica et Cosmochimica Acta* **69**, 989–790.

Zheng Y.-F. (1999) Oxygen isotope fractionation in carbonate and sulfate minerals. *Geochemical Journal* **33**, 109–126.

CHAPTER 3:

Deciphering clumped and oxygen isotope effects in the low temperature calcite-water system

Christopher Spencer[a]

spenccj@mcmaster.ca

and

Sang-Tae Kim[a]

sangtae@mcmaster.ca

[a]School of Geography and Earth Sciences, McMaster University, 1280 Main Street West,
Hamilton, ON, L8S 4K1, Canada

To be submitted to *Geochimica et Cosmochimica Acta*

3.1 Abstract

Carbonate clumped isotope geochemistry relies upon the measurable temperature dependence of ^{13}C-^{18}O bonds within the carbonate crystal lattice. This geochemical relationship provides a viable proxy for carbonate formation temperatures without knowledge of the oxygen isotope composition of the parent water. Experimental calibrations of this clumped isotope paleothermometer are commonly categorized by those that report a *'steep'* or *'shallow'* slope. For low temperature carbonates, this discrepancy can account for variation in estimated formation temperatures of up to 10 – 20 °C. To resolve this discrepancy, calcites were precipitated using the new upgraded constant addition method between 15 – 40 °C. This method enabled slow precipitation of calcite while providing control of both the oxygen and carbon isotope composition of the parent solution. Precipitated calcites yield the following clumped isotope temperature dependence relationship ($r^2 = 0.96$):

$$\Delta_{47\text{-RF}} = 0.0351\ (\pm\ 0.0021) \times 10^6/T^2 + 0.2982\ (\pm\ 0.0233)$$

All calcites were confirmed to have precipitated in oxygen isotope equilibrium with their parent water. Our clumped isotope calibration is indistinguishable from other experimental *'shallow'* slope calibrations, yet differs dramatically from *'steep'* slope calibrations. A source for this observed discrepancy between our calcites and *'steep'* slope calibrations could relate to precipitation method, where all 'steep' slope calibrations used the forced CO_2 degassing method. Several studies have now confirmed that non-

equilibrium isotope effects associated with both CO_2 hydration/hydroxylation and HCO_3^- dehydration/dehydroxylation can produce disequilibrium clumped and oxygen isotope compositions in $CaCO_3$. This study investigates the possibility of similar unidentified non-equilibrium isotope effects as a source for the calibration discrepancy.

3.2. Introduction

The recent expansion of clumped isotope geochemistry has provided researchers an alternative geochemical proxy for assessing the formation temperature of carbonate minerals. This technique – commonly referred to as the carbonate clumped isotope paleothermometer – relies upon the inverse relationship between carbonate formation temperature and the relative abundance of ^{13}C-^{18}O bonds preserved in the carbonate crystal as $Ca^{13}C^{18}O^{16}O^{16}O$ when $CaCO_3$ precipitates in isotopic equilibrium (Eiler and Schauble, 2004; Ghosh et al., 2006). The relative abundance of $Ca^{13}C^{18}O^{16}O^{16}O$ can be described by the following thermodynamically controlled homogenous isotope exchange reaction (Eq. 1).

$$Ca^{\mathbf{13}}C^{16}O^{16}O^{16}O + Ca^{12}C^{\mathbf{18}}O^{16}O^{16}O \leftrightarrow Ca^{\mathbf{13}}C^{\mathbf{18}}O^{16}O^{16}O + Ca^{12}C^{16}O^{16}O^{16}O \tag{1}$$

Unfortunately, current generation mass spectrometers preclude the direct determination of the relative abundance of the $Ca^{13}C^{18}O^{16}O^{16}O$ isotopologue preserved within the carbonate crystal lattice. Instead, a comparable temperature dependence of ^{13}C-^{18}O clumping can be observed within CO_2 produced through phosphoric acid digestion of carbonate minerals (Ghosh et al., 2006; Dennis and Schrag, 2010). This relationship is shown by the Δ_{47} value of acid-liberated CO_2; defined as the measured abundance of *m/z* 47 isotopologues of the CO_2 (primarily $^{13}C^{18}O^{16}O$) in comparison to the estimated abundance of *m/z* 47 isotopologues when ^{13}C and ^{18}O isotopes reflect a stochastic distribution among all CO_2 isotopologues (Eq. 2; Eiler and Schauble, 2004). The estimated stochastic distribution (represented by the R_{47}^*, R_{46}^*, and R_{45}^* values in Eq. 2) is determined based upon conventional $\delta^{13}C_{VPDB}$ and $\delta^{18}O_{VSMOW-SLAP}$ measurements of the acid-liberated CO_2 gas from a carbonate mineral. Measured $\Delta_{47-[SGvsWG]}$ values are commonly normalized to the Absolute Reference Frame (hereafter ARF) proposed by Dennis et al. (2011).

$$\Delta_{47} = \left[\left(\frac{R_{47}}{R_{47}{}^*} - 1\right) - \left(\frac{R_{46}}{R_{46}{}^*} - 1\right) - \left(\frac{R_{45}}{R_{45}{}^*} - 1\right)\right] \times 1000 \qquad (2)$$

Similar to conventional oxygen isotope systematics investigated by McCrea (1950), Beck et al.(2005), and Kim et al.(2006), dissolved inorganic carbon (DIC) species, such as HCO_3^- and CO_3^{2-}, exhibit a unique equilibrium Δ_{47-RF} value relative to $CaCO_3$ (Tripati et al., 2015). This would imply that CO_3^{2-} ions entrapped to the carbonate crystal surface must undergo some degree of isotopic exchange to attain clumped and oxygen isotope equilibrium. Tripati et al. (2015) recently proposed a conceptual interfacial model, which suggests that non-equilibrium clumped and oxygen isotope effects can be induced by the chemical composition of the parent water, precipitation rate, and the chemical and isotope exchange reactions occurring in the carbonate interfacial region (i.e., exchange amongst entrapped CO_3^{2-}, interfacial DIC, and water). This model agrees well with previous studies which observed similar physicochemical properties controlling the extent of non-equilibrium isotope effects in $CaCO_3$ (Clark et al., 1992; Kim and O'Neil, 1997; Kim et al., 2006; Dietzel et al., 2009; Affek and Zaarur, 2014; Tang et al., 2014; Tripati et al., 2015). To a lesser extent, solid-state diffusion of carbon and oxygen could also promote clumped isotope exchange amongst isotopologues within the crystal lattice (Watson et al., 2004).

In systems where interfacial DIC is in extensive isotopic disequilibrium (e.g., due to $CO_{2(aq)}$ hydration/hydroxylation or HCO_3^- dehydration/dehydroxylation), entrapped carbonate ions may inherit an anomalous $\Delta_{47\text{-RF}}$ and/or $\delta^{18}O$ signature (McConnaughey, 2003; Guo, 2008; Daëron et al., 2011; Affek and Zaarur, 2014; Tang et al., 2014). For example, Affek and Zaarur (2014) associated disequilibrium $\Delta_{47\text{-RF}}$ and $\delta^{18}O$ values in calcite precipitated at the surface of a parent solution to CO_2 degassing (i.e., dehydration/dehydroxylation of HCO_3^-) at the solution-atmosphere interface. In comparison, Tang et al. (2014) observed opposing deviations of disequilibrium $\Delta_{47\text{-RF}}$ and $\delta^{18}O$ values in calcites from a high pH solution at 5 °C using the CO_2-diffusion method and attributed these observations to $CO_{2(aq)}$ hydration/hydroxylation reactions. This poses a concern in $CaCO_3$ synthesis methods widely used in the calibration studies of the carbonate clumped isotope thermometer, where similar disequilibrium in DIC could remain unidentified. In these cases, $\Delta_{47\text{-RF}}$ and $\delta^{18}O$ values of $CaCO_3$ reflecting non-equilibrium isotope effects could be misinterpreted to have precipitated in isotopic equilibrium.

Interestingly, a discrepancy exists among experimental calibrations of the carbonate clumped isotope paleothermometer. These calibrations separate into two groups: shallow slope with high intercept (e.g., Dennis and Schrag, 2010; Tang et al., 2014; Defliese et al., 2015) and steep slope with low intercept (e.g., Ghosh et al., 2006; Zaarur et al., 2013; Kluge et al., 2015; Tripati et al., 2015). To identify the sources of discrepancies among the existing experimental calibrations of the carbonate clumped isotope thermometer, this study assesses the relationship between clumped isotope and conventional oxygen isotope compositions of calcites precipitated in apparent oxygen and clumped isotope equilibrium.

Inorganic calcite was slowly precipitated from aqueous solutions of pH = 7.83 - 8.46 between 15 – 40 °C utilizing an upgraded version of the constant addition method employed in Kim et al. (2006, 2007). This improved carbonate synthesis method ensures the precipitation of calcite from isotopically homogenous solutions (both δ^{13}C of DIC species and δ^{18}O of H_2O) by minimizing the rate of CO_2 degassing while replenishing consumed calcium ions and DIC species. Sustained stable isotope consistency of the parent solution provides an ideal environment for precipitating calcites of homogenous carbon and oxygen isotope compositions over periods of 1 – 2 weeks, a requirement for avoiding potential non-linear mixing effects during the calculation of the $\Delta_{47\text{-RF}}$ value (Defliese and Lohmann, 2015). We also explored potential cases of disequilibrium $\Delta_{47\text{-RF}}$ and δ^{18}O values in calcite where either $CO_{2(aq)}$ hydration/hydroxylation or HCO_3^- dehydration/dehydroxylation can induce non-equilibrium isotope effects in DIC as well as precipitating calcite.

3.2. Experimental Methods

3.2.1. Preparation of solutions

Two sets of solutions (parent and titrant) were prepared for each carbonate precipitation experiment. First, parent solutions were produced through mixing of a predissolved DIC- and a calcium ion-containing solution. These constituent solutions were prepared through dissolution of either ACS-grade $NaHCO_3$ or $CaCl_2 \bullet H_2O$ in 500 ml of de-ionized water (NANOpure Diamond, ~18 MΩ cm). These constituent solutions were stored in HDPE bottles in either a temperature-controlled chamber (15.0 or 16.2 ± 0.1 °C) or a circulating water bath (25.00 or 40.00 ± 0.01 °C) for a minimum of 24 hours in order to establish thermal and oxygen isotope equilibrium between DIC species and water (Beck et al., 2005). Mixing of the constituent solutions yielded the parent solution, which was stored in a closed 1000 ml HDPE reaction vessel for an additional 24 hours. Our preliminary tests revealed that combined 48-hour storage of the parent solutions yielded negligible precipitation of carbonates. For all experiments, the initial concentration of $NaHCO_3$ in the parent solution was 10 mM. However, the calcium ion concentration was varied dependent on precipitation temperature (e.g., 15.0, 16.2, 25.00, and 40.00 °C) to maintain an initial saturation index (SI) of 0.98 – 1.29 with respect to calcite (SI values determined using Geochemists Workbench 10.0, Aqueous Solutions LLC, USA).

Second, two types of titrant solutions were prepared through dissolution of ACS grade 29.5 mM $NaHCO_3$ or 2.4 – 3.4 mM $CaCl_2 \bullet H_2O$ in de-ionized water, respectively. For 15.0 and 16.2 °C precipitation experiments, titrants were stored within the temperature-controlled chamber at either 15.0 or 16.2 ± 0.1 °C for 48 or more hours to ensure thermal and isotopic equilibrium prior to injection. For 25.00 and 40.00 °C experiments, titrants were stored for 48 or more hours at room temperature. However, thermal and isotopic equilibrium of the two titrants at a given temperature was established before their use (see section 3.2.2 for details). Table 1 details the chemical compositions of the parent and titrant solutions used in this study.

3.2.2. Upgraded constant addition method

This study utilized an upgraded version of the constant addition method described by Kim et al. (2006). After the initial 48-hour thermal and isotopic equilibration phase, injection of both DIC- and calcium ion-containing titrants into a 1L parent solution was initiated at a constant rate of 0.25 – 0.5 ml/hr using a dual-syringe pump (Table 1). Parent solution was stored in a 1L HDPE reaction vessel that incorporated a flexible nitrile membrane separating the parent solution from atmosphere (Figure 1). This membrane conformed to the parent solution, maintaining negligible headspace within the reaction vessel and moderated the rate of CO_2 loss to atmosphere. Chemical homogeneity of the parent solution was achieved using a 60 rpm floating stirrer bar.

For 15.0 and 16.2 °C experiments, both the parent solution and the titrant solutions were placed within a temperature-controlled growth chamber. For precipitation experiments conducted at 25.00 and 40.00 °C, temperature of the parent solution was controlled by housing the reaction vessel within an insulated double-walled chamber linked to a temperature-controlled circulator. Although titrant solutions remained at room temperature, our unique design of the temperature-regulated reaction chamber enabled the DIC-containing titrant solution to achieve thermal and isotopic equilibrium prior to its injection into the parent solution (see Figure 1). The temperatures of the parent solutions were held at either 15 ± 0.1, 16.2 ± 0.1, 25 ± 0.05 or 40 ± 0.05 °C (Table 1).

Constant addition of titrants slightly increased the parent solution volume, compressing the nitrile membrane. Daily removal of 12 – 24 ml of parent solution through a septum enabled the nitrile membrane to decompress, and provided a source of parent solution for pH and isotopic analyses. This method of parent solution removal ensured the reaction vessel remained sealed for the duration of each precipitation experiment. Upon completion, a rubber policeman was used to harvest $CaCO_3$ primarily from the sides and bottom of the HDPE reaction vessel. A small amount of precipitate was also collected from the Teflon-coated titrant tubes as well as the internal surface of the nitrile membrane. Precipitates were vacuum-filtered, rinsed with DI-water and then 100 % methanol and dried at 70 °C overnight prior to storage in sealed containers. All re-usable system components were washed in a 1% HCL acid bath for $\geq$ 24 hours between experiments. XRD analyses confirmed the mineralogy of all $CaCO_3$ precipitates is calcite. Trace amounts of Teflon were discovered in samples from several experiments (see Table 1). This is likely a result of rigorous scrubbing of the Teflon-coated titrant tubes during precipitate collection. Given the non-reactivity of Teflon with phosphoric acid, it is unlikely that stable isotope compositions of the calcite precipitates were altered.

3.2.3. Isotopic analysis: Measurement and normalization

3.2.3.1 $\delta^{13}C_{VPDB}$, $\delta^{18}O_{VSMOW}$, and $\Delta_{47\text{-}RF}$ values of calcite

4-5 mg carbonate samples were reacted for 15 minutes with 5 ml of 104 wt.% H_3PO_4 in a 90 °C common acid bath to liberate CO_2. CO_2 gases were then purified using a custom-designed automated $CaCO_3$-CO_2 purification system at the McMaster Research

Group for Stable Isotopologues (MRSI) laboratory. The common acid bath was replaced after the analyses of 4-5 carbonate samples. CO_2 gases for the ARF were also introduced into the automated purification system through a tube cracker. All CO_2 gases were subsequently passed through four double-looped cryogenic U-traps as well as a -20 °C 15cm × 4mm (length x I.D.) U-trap containing Porapak™-Q (mesh size 50/80; Supelco, Bellefonte, USA). Finally, purified CO_2 gases were sealed in Pyrex® breakseals prior to measurement. CO_2 gases measured for their isotopic compositions within 24 hours to minimize the potential for isotopic re-equilibration during storage.

The isotopic composition of CO_2 gases were determined relative to MRSI's CO_2 reference gas ($\delta^{13}C_{VPDB}$ = 5.62 ‰ and $\delta^{18}O_{VSMOW}$ = -25.05 ‰; OzTech, Safford, USA) on a Thermo Scientific MAT 253 DI-IRMS. Sample CO_2 gases were screened for possible isobaric contamination based on irregular *m/z* 48 offsets (i.e., $\Delta_{48} >> 1$; Eiler and Schauble, 2004; Huntington et al., 2009). To minimize observed Δ_{47} vs. δ^{47} non-linearity, measurement protocol incorporated the pressure baseline correction provided by He et al. (2012). Typical measurement protocol included 6 acquisitions, each containing 15 on-peak cycles with a 6 s integration time.

$\delta^{13}C$ and $\delta^{18}O$ values were normalized to the recommended isotopic compositions of NBS 18 and NBS 19, following the protocol proposed by Kim et al. (2015). They are reported on the VPDB and VSMOW-SLAP scale, respectively. $\Delta_{47[SGvs.WG]}$ values of CO_2 were normalized using a 64-point ARF, comprising replicates of three CO_2 gases of distinct bulk isotopic composition equilibrated at 25, 40, 70 and 1000 °C. An in-house Carrara marble standard (Carrara P74) and equilibrated CO_2 gases were measured over the course of the study period to assess machine-specific Δ_{47} scale compression and the $\Delta_{47[SGvs.WG]}$ vs. δ^{47} non-linearity relationship (Huntington et al., 2009; Dennis et al., 2011). Both monitoring protocols yielded negligible shifts in $\Delta_{47[SGvs.WG]}$ values. For carbonates digested at 90 °C, an acid fractionation factor (AFF; Δ^{*}_{25-90}) of 0.069 ‰ was applied to the normalized $\Delta_{47\text{-}RF}$ values (determined using Eq. 23; Guo et al., 2009a). This AFF enables comparison of carbonate $\Delta_{47\text{-}RF}$ values to those digested at 25 °C. When comparing carbonate $\Delta_{47\text{-}RF}$ values among published studies, the reported $\Delta_{47\text{-}RF}$ values from each study were used. Our $\Delta_{47\text{-}RF}$ values for NBS 19 and MRSI's Carrara marble standard are comparable to those reported from other studies, validating our calibration of the ARF (Table S2). This study also reports the first determination of the $\Delta_{47\text{-}RF}$ value of NBS 18 (Table S2).

3.2.3.2. $\delta^{13}C_{VPDB}$ and $\delta^{18}O_{VSMOW}$ values of parent solution

Both carbon and oxygen isotope analyses of parent solutions were performed using MRSI's Gas Bench II system coupled to a Thermo Scientific Delta plus XP CF-IRMS. The δ^{13}C values of DIC in the parent solutions ($\delta^{13}C_{DIC}$) were determined through reaction of DIC-containing solution sample with phosphoric acid at 25 °C to produce acid-liberated CO_2. The $\delta^{13}C_{DIC}$ values were normalized to carbon isotope compositions of NBS 18 and NBS 19. The δ^{18}O values of the solutions ($\delta^{18}O_{H2O}$) were determined utilizing the traditional CO_2-H_2O equilibration technique at 25 °C. The $\delta^{18}O_{H2O}$ values were normalized using two MRSI water standards calibrated against VSMOW and SLAP.

All $\delta^{13}C_{DIC}$ and $\delta^{18}O_{H2O}$ measurements were run in replicate (*n* = 2 – 3) and are reported on the VPDB and VSMOW-SLAP scale, respectively.

3.3. Results

3.3.1. Chemical and conventional isotopic compositions of parent solutions

The pH of parent solution slightly decreased with time due to the formation of $CaCO_3$ and the reduced rate of CO_2 degassing through the nitrile membrane. Starting pH of the parent solution was between 8.13 – 8.46, with a pH shift of ≤ 0.41 over the course of $CaCO_3$ precipitation, confirming HCO_3^- to be the dominant DIC species of the parent solution (Table 1). A common source for de-ionized water, reagent $NaHCO_3$ and $CaCl_2$•H_2O for the preparation of parent solution provided robust isotopic homogeneity across experiments (average initial $\delta^{18}O_{H2O}$ = -6.46 ± 0.04 ‰; $\delta^{13}C_{DIC}$ = -6.19 ± 0.17 ‰; 1σ). For all precipitation experiments, $\delta^{18}O_{H2O}$ drift between initial and final parent solutions was less than ± 0.09 ‰, similar to our external precision of $\delta^{18}O_{H2O}$ measurements (± 0.08 ‰). In comparison, $\delta^{13}C_{DIC}$ drift of the parent solution increased slightly at higher temperatures, 0.23 ± 0.15, 0.43 ± 0.23, and 0.43 ± 0.09 ‰ at 15, 25, and 40 °C, respectively. For reference, CO_2 peak intensity monitoring of DIC-containing parent solutions on the CF-IRMS showed negligible shifts in parent solution DIC concentration, confirming that the consumption of DIC was proportional to the injection rate of DIC titrant solution during the slow precipitation of $CaCO_3$. Furthermore, mass balance indicates collected precipitates from all experiments account for a consumption of less than 0.01 % of the available DIC reservoir from parent solution and injected DIC titrant.

To the best of our knowledge, our upgraded constant addition method enabled us to maintain unprecedented $\delta^{13}C_{DIC}$ and $\delta^{18}O_{H2O}$ stability of the parent solution, and thus to synthesize carbonates of near-homogenous $\delta^{13}C$ and $\delta^{18}O$ values, unlike alternative carbonate precipitation methods, minimizing the potential for $\Delta_{47\text{-}RF}$ non-linear mixing effects (Defliese and Lohmann, 2015).

3.3.2. Carbon and oxygen isotope compositions of calcite

The carbon and oxygen isotope compositions of precipitated calcite are presented in Table 2. Among all the precipitation experiments, the average $\delta^{13}C$ value of calcite was -5.55 ± 0.09 ‰ (1σ) and that of DIC-containing parent solution was -6.19 ± 0.17 ‰ (1σ). Carbon isotope fractionation between calcite and DIC yielded an average $1000\ln\alpha_{calcite\text{-}DIC}$ value of 0.68 ± 0.13, 0.65 ± 0.06, 0.35 ± 0.30, and 0.31 ± 0.12 (1σ) from 15, 16.2, 25, and 40 °C, respectively. Because HCO_3^- was the dominant DIC species in our parent solutions, carbon isotope fractionation between calcite and DIC would be similar to that between calcite and HCO_3^-. Therefore, our estimated $1000\ln\alpha_{calcite\text{-}HCO3\text{-}}$ value is 0.46 ± 0.24 (1σ). This value represents the combined average of all $1000\ln\alpha_{calcite\text{-}HCO3\text{-}}$ values from 15, 16.2, 25, and 40 °C. However, this fractionation factor ($1000\ln\alpha$) of 0.46 ± 0.24 (1σ) neither reflects our analytical uncertainty of $\delta^{13}C$ measurements for DIC (± 0.12 ‰; 1σ), nor considers the $\delta^{13}C_{DIC}$ drift of the parent solution that increases with temperature (see section 3.3.1.). Consequently, it is hard to judge whether our new measurement is indeed different from $1000\ln\alpha_{\text{Calcite-HCO3-}}$ values of 1.0 ± 0.2 (1σ) and 0.94 ± 0.06 (1σ) previously reported by Romanek et al. (1992) and Jiménez-López et al. (2001), respectively.

Dependent on formation temperature, average δ^{18}O values of calcite were 24.25 ± 0.08, 24.02 ± 0.00, 22.19 ± 0.08, and 19.20 ± 0.05 ‰ (1σ) for 15.0, 16.2, 25.00, and 40.00 °C, respectively. For all $1000\ln\alpha_{\text{calcite-water}}$ values reported in this study, an analytical uncertainty of ± 0.16 was estimated. This uncertainty approximately represents the combined maximum 1SD of δ^{18}O measurements for all water and calcite standards (± 0.08 and ± 0.08 ‰, respectively). Measured $1000\ln\alpha_{\text{calcite-water}}$ values range from 30.46 to 25.45 between 15 to 40 °C. All $1000\ln\alpha_{\text{calcite-water}}$ values lie within the analytical and experimental uncertainty of Kim and O'Neil (1997)'s calcite-water calibration curve (Figure 2).

3.3.3. Clumped isotope composition of calcite

$\Delta_{47\text{-RF}}$ values for calcites prepared in this study are presented in Table 3. Average $\Delta_{47\text{-RF}}$ values of calcite samples were 0.725 ± 0.001, 0.717 ± 0.002, 0.688 ± 0.003, and 0.659 ± 0.002 ‰ (1SE) for formation temperatures 15, 16.2, 25, and 40 °C, respectively. Measurement precision of individual $\Delta_{47\text{-RF}}$ values was ± 0.004 – 0.015 ‰ (1SE). Among the carbonate samples at each temperature ($n = 2 – 4$), reproducibility of $\Delta_{47\text{-RF}}$ values was between ± 0.001 to 0.003 ‰ (1SE). This reproducibility is among the best observed in experimental calcite clumped isotope calibration studies (see Table S1). Temperature dependence of $\Delta_{47\text{-RF}}$ based upon calcites precipitated from 15 to 40 °C yields (where T is in Kelvin; $r^2 = 0.96$):

$$\Delta_{47\text{-RF}} = 0.0351\ (\pm\ 0.0021) \times 10^6/T^2 + 0.2982\ (\pm\ 0.0233) \qquad (3)$$

3.4. Discussion

3.4.1. Test of calcite equilibrium precipitation: This study

McCrea (1950) first investigated the temperature dependence of oxygen isotope fractionation between $CaCO_3$ and water using carbonate precipitation methods similar to the passive and forced CO_2 degassing methods described in Kim et al. (2007). The latter method was later modified to better constrain the temperature dependence of oxygen isotope fractionation between calcite and water (e.g., O'Neil, 1969; Kim and O'Neil, 1997). The equilibrium oxygen isotope fractionation proposed by Kim and O'Neil (1997) has since been corroborated by various experimental observations (e.g., Jiménez-López et al., 2001) and theoretical calculations (e.g., Horita and Clayton, 2007; Chacko and Deines, 2008). This fractionation is commonly applied to assess paleo-oceanic temperatures as well as to constrain the oxygen isotope composition of terrestrial surface-waters (e.g., McManus et al., 1999; Adkins et al., 2002; Garzione et al., 2008).

In this study, we developed and employed an upgraded constant additional method (see section 3.2.2.) to precipitate equilibrium calcite samples for precise calibration of the calcite clumped isotope paleothermometer. The constant addition method has been successfully used to investigate oxygen isotope effects in the aragonite-water system

(Kim et al., 2006; Kim et al., 2007; Kim et al., 2014) and is proven to yield aragonite, a polymorph of $CaCO_3$, in apparent isotopic equilibrium with its parent water (Kim et al., 2006; Kim et al., 2007). Prior to this study, the constant addition method had not been used to determine oxygen isotope fractionation in the calcite-water system.

To test our calcites were in oxygen isotope equilibrium with their parent water, our $1000\ln\alpha_{calcite\text{-}water}$ values were compared to Kim and O'Neil (1997)'s equation for the temperature dependence of $1000\ln\alpha_{calcite\text{-}water}$ (See section 3.3.2.). Exceptional agreement between this study and Kim and O'Neil (1997) indicates the rate and duration of interfacial $CaCO_3$-DIC oxygen isotope exchange was sufficient in achieving oxygen isotope equilibrium between calcite and water in our precipitation experiments.

Given that our calcite samples are deemed to be in apparent oxygen isotope equilibrium with their parent water, we propose that our observed temperature dependence of $\Delta_{47\text{-}RF}$ values also represents clumped isotope equilibrium. Based on our calcite clumped isotope calibration and the well-established calcite-water oxygen isotope calibration of Kim and O'Neil (1997), this study examined the isotopic composition of calcites used in other calibration studies in order to identify non-equilibrium isotope effects in inorganic carbonates as well as to understand the discrepancy among the existing calcite clumped isotope thermometer calibrations.

3.4.2. Test of equilibrium precipitation of calcite: Previous studies

We defined non-equilibrium $1000\ln\alpha_{calcite\text{-}water}$ values (or disequilibrium carbonates) based upon offsets greater than 0.67 from Kim and O'Neil (1997)'s calcite-water calibration curve. This exclusion criterion is based upon maximum systematic discrepancies associated with laboratory-specific analytical protocols (e.g., the choice of $\alpha_{CO2(ACID)\text{-}calcite}$) and carbonate precipitation methods observed in Kim et al. (2007) (see the difference among the average 1000ln$\alpha_{aragonite\text{-}water}$ values from each group and the variation of 1000ln$\alpha_{aragonite\text{-}water}$ values within each group in Fig. 1 from Kim et al. (2007)).

1000ln$\alpha_{calcite\text{-}water}$ values are reported in some of the published calibration studies for the carbonate clumped isotope thermometer (i.e., Ghosh et al., 2006; Dennis and Schrag, 2010; Zaarur et al., 2013; Affek and Zaruur, 2014; Tang et al., 2014). However, among these studies, oxygen isotope equilibrium between calcite sample and parent solution is not always achieved (Figure 2). Based upon our exclusion criteria, most of Dennis and Schrag (2010)'s calcite samples achieved apparent oxygen isotope equilibrium (12 out of 15 experiments). Calcites from three high temperature experiments (two from 70 and one from 77 °C) are out of equilibrium, with 1000ln$\alpha_{calcite\text{-}H2O}$ values of + 1.01 to 1.75 from the apparent equilibrium value. Because the parent solution was stirred and open to atmosphere over the course of precipitation, evaporation of lighter water isotopologues at this temperature may be responsible for 1000ln$\alpha_{calcite\text{-}water}$ values higher than the expected equilibrium value. On the contrary, Figure 2 shows that 3 out of 7 and 4 out of 6 calcite samples used in the clumped isotope equilibrium calibrations of Ghosh et al. (2006) and Zaarur et al. (2013) were not in apparent oxygen isotope equilibrium with respect to their corresponding parent solutions. Furthermore, all carbonate samples from Ghosh et al. (2006) are ^{18}O depleted, while carbonates from

Zaarur et al. (2013) are all ^{18}O enriched with respect to Kim and O'Neil (1997)'s equilibrium value regardless of their magnitude. The source of these non-equilibrium oxygen isotope effects is unclear for lack of experimental details reported, given that both studies used the CO_2 degassing method with a common experimental protocol.

For studies assessing non-equilibrium oxygen and clumped isotope effects, 12 out of 19 calcites from Tang et al. (2014) were not in apparent oxygen isotope equilibrium. Affek and Zaarur (2014) ran two separate experiments for clumped and oxygen isotope studies. For studies designed to assess the oxygen isotope composition of $CaCO_3$, referred to as "short-period precipitation experiments", 14 out of 17 samples were not in apparent oxygen isotope equilibrium with respect to their parent water. For $CaCO_3$ samples used for clumped isotope study based upon their "long-period precipitation experiments", 10 out of 15 samples were out of oxygen isotope equilibrium. All of the disequilibrium carbonates from Tang et al. (2014) are ^{18}O depleted whereas all disequilibrium carbonates from Affect and Zaarur (2014)'s short-period precipitation experiments are ^{18}O enriched. Long-period precipitation experiments show inconsistent $CaCO_3$-water oxygen isotope fractionation. Affek and Zaarur (2014) attribute this to evaporation altering the oxygen isotope composition of the parent solution during precipitation. For this reason, this study only considers the short-period precipitation experiments for assessing $CaCO_3$-water oxygen isotope fractionation relationships.

3.4.3. Comparison of the clumped isotope composition of calcite

Between 15 – 40 °C, our calibration of the calcite clumped isotope thermometer is in good agreement with theoretical models of Guo et al.(2009a) and Hill et al.(2014) when the revised experimental AFF of 0.280 ‰ is applied for converting Δ_{63} values of calcite to Δ_{47} values (Figure 3a; Tripati et al., 2015). Furthermore, given the experimentally determined $\Delta_{47\text{-RF}}$ values of HCO_3^- and CO_3^{2-} by Tripati et al. (2015) at 25 °C, our calibration behaves as predicted because our $\Delta_{47\text{-RF}}$ values of calcite at 25 °C are located between the $\Delta_{47\text{-RF}}$ values of HCO_3^- and CO_3^{2-} (Hill et al., 2014).

Figures 3b and 3c show a 95% confidence interval of our experimental data vs. the combined 95% confidence interval of '*shallow*' and '*steep*' slope carbonates. '*Shallow*' slope carbonates were precipitated using the passive degassing method (Dennis and Schrag, 2010; Defliese et al., 2015) and the CO_2 diffusion method (Tang et al., 2014). In passive degassing experiments, parent solution was produced through slow mixing of a CaCl solution into a $NaHCO_3$ solution. Combining all '*shallow*' slope carbonates yields the following $\Delta_{47\text{-RF}}$ calibration ($r^2 = 0.89$), which is indistinguishable from our own:

$$\Delta_{47\text{-RF}} = 0.0356\ (\pm\ 0.0019) \times 10^6/T^2 + 0.2901\ (\pm\ 0.0209) \qquad (4)$$

When the individual $\Delta_{47\text{-RF}}$ temperature dependence of each study is compared, our slope of 0.0351 ± 0.0021 (1SE) is compatible to that of Dennis and Schrag (2010), Defliese et al. (2015), and Tang et al. (2015) which exhibit slopes of 0.0340 ± 0.0038, 0.03484 ± 0.00229 and 0.0387 ± 0.0072 (1SE), respectively. Either considered individually or combined, our calibration study, which only used calcite in oxygen isotope equilibrium, suggests that the passive degassing method and CO_2 diffusion method employed in these studies are capable of precipitating carbonates in apparent clumped isotope equilibrium without necessarily achieving conventional oxygen isotope equilibrium with parent water. It is important to note that the calibration proposed by Tang et al (2015) excluded two carbonates with abnormally elevated $\Delta_{47\text{-RF}}$ values that were prepared from high pH solutions at 5 °C.

We also note that the siderite calibration by Fernandez et al. (2014) exhibits a very similar slope (0.0356 ± 0.0018). However, direct comparison of mineral-specific $\Delta_{47\text{-RF}}$ values may not be possible until an AFF for siderite is determined (Guo et al., 2009a; Fernandez et al., 2014). Siderite was precipitated using the forced CO_2 degassing method with parent solution being prepared similar to Dennis and Schrag (2010) and Defliese et al. (2015), where a FeCl solution was slowly titrated into a $NaHCO_3$ solution.

All '*steep*' slope carbonates were also precipitated using the forced CO_2 degassing method. However, unlike the aforementioned passive degassing method and the forced CO_2 degassing method used for siderite, parent solution was created through dissolution of reagent $CaCO_3$ while bubbling CO_2 (Ghosh et al., 2006; Zaarur et al., 2013; Kluge et al., 2015; Tripati et al., 2015). Kluge et al. (2015) also precipitated carbonates from 25 – 250 °C in a pressurized reaction vessel; however, for this study we only compare carbonate precipitated at atmospheric pressure. Combining all '*steep*' slope carbonates yields the following $\Delta_{47\text{-RF}}$ temperature dependence ($r^2 = 0.94$):

$$\Delta_{47\text{-RF}} = 0.0475\ (\pm\ 0.0018) \times 10^6/T^2 + 0.1630\ (\pm\ 0.0190) \quad (5)$$

This combined calibration differs significantly from our own, where $\Delta_{47\text{-RF}}$ values are more negative at higher temperatures, and more positive at lower temperature, relative to our proposed equilibrium values. Intersection of both calibrations occurs at 29.7 °C where $\Delta_{47\text{-RF}}$ = 0.681 ‰. Disagreement is also observed when the temperature dependence of '*steep*' slope $\Delta_{47\text{-RF}}$ calibrations is considered individually. Compared to our slope of 0.0351 ± 0.0021 (1SE), Ghosh et al. (2006), Zaarur et al. (2013), Kluge et al. (2015), and Tripati et al. (2015) report slopes of 0.0620 ± 0.0099, 0.0555 ± 0.0027, 0.0464 ± 0.0020 and 0.0505 ± 0.0034 (1SE), respectively. These findings suggest that carbonates precipitated from $CaCO_3$ dissolved parent solution using the forced CO_2 degassing method have $\Delta_{47\text{-RF}}$ values partially reflecting non-equilibrium clumped isotope effects at temperatures above and below 29.7 °C.

Finally, co-variation between non-equilibrium $\Delta_{47\text{-RF}}$ and $\delta^{18}O$ values is reported by two studies (Figure 3d). Tang et al. (2014) reported higher $\Delta_{47\text{-RF}}$ and lower $\delta^{18}O$ values relative to equilibrium in two carbonates precipitated from high pH solutions at 5 °C where CO_2 diffused into the parent solution. These carbonates are believed to reflect non-equilibrium isotope effects associated with $CO_{2(aq)}$ hydration/hydroxylation. In addition, Affek and Zaarur (2014) observed lower $\Delta_{47\text{-RF}}$ and higher $\delta^{18}O$ values relative to equilibrium in carbonates precipitated at the surface of a passive CO_2 degassing solution. They proposed that HCO_3^- dehydration/dehydroxylation are responsible for the non-equilibrium isotope effects in their surface carbonates.

3.4.4. Sources of non-equilibrium oxygen and clumped isotope effects in inorganic calcite

Recent experimental studies indicate that the $\Delta_{47\text{-RF}}$ value of carbonates is largely insensitive to formation conditions that generally produce disequilibrium δ^{18}O values, such as solution chemistry, pH, and precipitation rate (Tang et al., 2014). Several exceptions exist, where δ^{18}O and $\Delta_{47\text{-RF}}$ values can simultaneously reflect non-equilibrium conditions. First, in cases of quasi-instantaneous carbonate precipitation and/or limited isotopic exchange of interfacial $CaCO_3$-DIC, δ^{18}O and $\Delta_{47\text{-RF}}$ values of precipitating carbonate can reflect the weighted isotopic composition of DIC species based upon their relative abundance at a given pH (Usdowksi et al., 1991; Zeebe, 2005; Kim et al., 2006; Hill et al., 2014; Tripati et al., 2015). To the best of our knowledge, this non-equilibrium clumped isotope effect has only been tested during quasi-instantaneous precipitation of inorganic witherite (Tripati et al., 2015). Second, in the $CaCO_3$-CO_2- H_2O systems with active CO_2 degassing, the isotopic composition of DIC can inherit non-equilibrium isotope effects associated with HCO_3^- dehydration/dehydroxylation (Daëron et al., 2011; Affek and Zaarur, 2014). Finally, in the $CaCO_3$-CO_2- H_2O systems where $CO_{2(aq)}$ is an abundant component of the DIC reservoir, non-equilibrium isotope effects caused by $CO_{2(aq)}$ hydration/hydroxylation can also influence the isotopic composition of DIC (McConnaughey, 1989; Saenger et al., 2012; Tang et al., 2014). This DIC disequilibrium can be reflected in the δ^{18}O and $\Delta_{47\text{-RF}}$ values of precipitating carbonates where the δ^{18}O and $\Delta_{47\text{-RF}}$ values are predicted to co-vary from their respective equilibrium values, dependent on the dominant non-equilibrium isotope effect pathway (e.g., $CO_{2(aq)}$ hydration vs. HCO_3^- dehydration; Guo, 2008; Guo et al., 2009b).

3.4.4.1 HCO_3^- dehydration/dehydroxylation

The HCO_3^- dehydration/dehydroxylation reaction deprotonates HCO_3^- to form $CO_{2(aq)}$, releasing an oxygen atom in the form of either water or a hydroxyl group (Eq. 6, 7). Rapid HCO_3^- dehydration/dehydroxylation results in preferential CO_2 degassing of lighter isotopologues (e.g., $^{12}C^{16}O^{16}O$), increasing the $\delta^{13}C$ and $\delta^{18}O$ values of the remaining HCO_3^- reservoir (Clark and Lauriol, 1992). Theoretical modeling predicts the increased $\delta^{13}C$ and $\delta^{18}O$ values of HCO_3^- will be paired to a decreased $\Delta_{47\text{-RF}}$ value of HCO_3^- (Guo, 2008). This decrease is primarily due to the non-linear relationship between $\delta^{13}C$ and $\delta^{18}O$ values of the HCO_3^-, and the relative abundance of isotopologues (e.g., $H^{13}C^{18}O^{16}O^{16}O^-$) within the HCO_3^- reservoir (Guo, 2008). The decrease in the $\Delta_{47\text{-RF}}$ value can also be accentuated by increased non-equilibrium carbon and oxygen isotope fractionation between $CO_{2(g)}$ and HCO_3^- (Guo, 2008).

For the non-equilibrium isotope effects of HCO_3^- dehydration/dehydroxylation to be inherited by precipitating $CaCO_3$, minimal isotopic exchange should occur between entrapped CO_3^{2-} and parent water. In nature, the rate of CO_2 degassing from a $CaCO_3$-saturated thin film is several orders of magnitude faster than isotopic exchange between DIC species and water (Dreybrodt and Scholz, 2011). In this case, the non-equilibrium isotope effects of HCO_3^- dehydration/dehydroxylation can be inherited by $CaCO_3$ precipitating in the thin film (Daëron et al., 2011).

At 25 °C, if HCO_3^- dehydration/dehydroxylation results in an irreversible chemical and isotope exchange reaction between $CO_{2(g)}$ and HCO_3^-, theoretical models predict that every 1 ‰ increase in the δ^{18}O of the HCO_3^- reservoir will coincide with an increase of 1.1 – 3.2 ‰ of the δ^{13}C and a decrease of 0.017 – 0.026 ‰ in the $\Delta_{47\text{-RF}}$ value (Guo, 2008). The exact increase/decrease of the δ^{13}C, δ^{18}O, and $\Delta_{47\text{-RF}}$ values is dependent on the proportion of HCO_3^- dehydration to dehydroxylation, and the rate of carbonate precipitation relative to CO_2 degassing (Guo, 2008).

$$HCO_3^- + H^+ \rightarrow CO_2\uparrow + H_2O \tag{6}$$

$$HCO_3^- \rightarrow CO_2\uparrow + OH^- \tag{7}$$

Affek and Zaarur (2014) observed similar non-equilibrium isotope effects in carbonates precipitated by the passive CO_2 degassing at the solution-atmosphere interface of a stagnant CaCO3-saturated solution. In short-period experiments, carbonate δ^{18}O values were elevated, while in long-period experiments the $\Delta_{47\text{-RF}}$ values are lower than their anticipated equilibrium value, respectively (Figure 4). Problematically, their short-period experiments did not yield sufficient $CaCO_3$ for $\Delta_{47\text{-RF}}$ analyses, and the long-period experiments sustained inconsistent evaporation of parent solution, complicating the interpretation of δ^{18}O values. Although co-variance in δ^{18}O and $\Delta_{47\text{-RF}}$ values of $CaCO_3$ from either short- or long- period precipitation experiments could not be tested, Figure 4 shows that the direction of δ^{18}O and $\Delta_{47\text{-RF}}$ non-equilibrium isotope effects are consistent with that predicted based upon HCO_3^- dehydration/dehydroxylation (Guo, 2008). $CaCO_3$-

water oxygen isotope fractionation values for long-period experiments are included for reference.

3.4.4.2. $CO_{2(aq)}$ hydration/hydroxylation

$CO_{2(aq)}$ hydration/hydroxylation occurs when $CO_{2(aq)}$ is protonated with an oxygen atom from either H_2O or OH^- to form HCO_3^- (opposite of Eqs. 6, 7). Non-equilibrium isotope effects associated with $CO_{2(aq)}$ hydration/hydroxylation can be proliferated during a rapid pH transition of a $CO_{2(aq)}$-dominated solution. For example, as CO_2 degasses from a $CO_{2(aq)}$-dominated solution, consumption of carbonic acid (H_2CO_3) decreases solution acidity (Eq. 8). This pH shift promotes the transition to a HCO_3^- and then CO_3^{2-} -dominated DIC reservoir. Therefore, remaining $CO_{2(aq)}$ is hydrated/hydroxylated to form HCO_3^-.

$$HCO_3^- + H^+ \rightarrow H_2CO_3 \rightarrow CO_2 \uparrow + H_2O \qquad (8)$$

Non-equilibrium isotope effects associated with $CO_{2(aq)}$ hydration/hydroxylation can also occur as CO_2 diffuses or dissolves into a high pH solution where the DIC reservoir is dominated by HCO_3^- or CO_3^{2-}. This is akin to biogenic calcification of corals, where $CO_{2(aq)}$ diffuses from skeletogenetic membrane into the calcifying layer, undergoing $CO_{2(aq)}$ hydration/hydroxylation, and is subsequently precipitated as $CaCO_3$ (McConnaughey, 1989; Saenger, 2012).

Non-equilibrium isotope effects associated with $CO_{2(aq)}$ hydration/hydroxylation are opposite in direction from those caused by HCO_3^- dehydration/dehydroxylation. Preliminary estimation of the co-variance of $\Delta_{47\text{-RF}}$ and $\delta^{18}O$ values in precipitating carbonates at 25 °C predicts a 0.01 to 0.05 ‰ increase in $\Delta_{47\text{-RF}}$ for every 1 ‰ decrease in $\delta^{18}O$ (i.e., $\Delta(\Delta_{47})/\Delta(\delta^{18}O) = -0.01$ to -0.05; Guo et al., 2009b). The decrease in $\delta^{18}O$ is largely dependent on the relative proportion of $CO_{2(aq)}$ hydration to hydroxylation. Hydroxylation is the dominant process in solutions with pH above 10 (Kern, 1960). Given that the $\delta^{18}O$ value of OH^- is approximately -40 ‰ relative to that of H_2O at 25 °C (Green and Taube, 1963), $CO_{2(aq)}$ hydroxylation produces HCO_3^- with lower $\delta^{18}O$ values compared to that formed by $CO_{2(aq)}$ hydration. Assuming no kinetic isotope effects associated with the $CO_{2(aq)}$ hydration/hydroxylation reaction, and insignificant HCO_3^--H_2O isotopic re-equilibration, the $\delta^{18}O$ value of protonated $CO_{2(aq)}$ can be estimated using an isotope mass balance equation (Eqs. 9, 10; McConnaughey, 2003).

$$\delta^{18}O_{HCO3-} = \tfrac{2}{3}[\delta^{18}O_{CO2}] + \tfrac{1}{3}[\delta^{18}O_{H2O}] \tag{9}$$

$$\delta^{18}O_{HCO3-} = \tfrac{2}{3}[\delta^{18}O_{CO2}] + \tfrac{1}{3}[\delta^{18}O_{OH-}] \tag{10}$$

Tang et al. (2014) observed non-equilibrium clumped and oxygen isotope effects similar in direction to $CO_{2(aq)}$ hydration/hydroxylation when precipitating calcite using the CO_2-diffusion method. This method induces CO_2 diffusion across a polyethylene membrane into a parent solution, where $CO_{2(aq)}$ undergoes hydration/hydroxylation prior to its precipitation as $CaCO_3$. In experiments C21 and C23 (conducted at 5 °C with a pH of either 10 or 10.5, respectively) from Tang et al. (2014), $\Delta_{47\text{-RF}}$ values were higher and δ^{18}O values were lower than their respective equilibrium values. For C21 and C23, δ^{18}O values were 4.33 and 2.89 ‰, and $\Delta_{47\text{-RF}}$ values were 0.962 and 1.065 ‰, respectively. Based upon the published δ^{18}O value of the parent solution (-9.59 ‰), the equilibrium δ^{18}O and $\Delta_{47\text{-RF}}$ values of the calcite would have been 23.03 ‰, and = 0.755 ‰, respectively. These values are calculated based upon the Kim and O'Neil (1997) calcite-water oxygen isotope calibration and our proposed calcite clumped isotope equilibrium. The calculated $\Delta(\Delta_{47})/\Delta(\delta^{18}\text{O})$ co-variance from equilibrium is -0.016 and -0.011 for C21 and C23, respectively, falling within the boundaries of the hydration/hydroxylation co-variance relationship proposed by Guo et al. (2009b).

Given the reasonable fit with Guo et al. (2009b), this would imply that the observed deviations of δ^{18}O and $\Delta_{47\text{-RF}}$ values could be a result of $CO_{2(aq)}$ hydration/hydroxylation after CO_2 is diffused across the polyethylene membrane. This finding suggests that HCO_3^- formed from CO_2 hydration/hydroxylation underwent limited isotopic re-equilibration with water prior or during $CaCO_3$ precipitation. However, Thiagarajan et al. (2011) predict similar non-equilibrium clumped and oxygen isotope effects during CO_2 diffusion across bi-lipid membranes. Although it is unclear how this biological isotope fractionation applies to the polyethylene membrane, it cannot be ruled out as a possible contributor to the non-equilibrium clumped and oxygen isotope effects observed in experiments C21 and C23.

3.4.5. Non-equilibrium isotope effects and the existing calibration discrepancy

Several analytical mechanisms associated with the measurement of the $\Delta_{47\text{-RF}}$ value have been proposed to account for the calibration discrepancy, including acid digestion temperature and associated clumped isotope AFF values ($\Delta_{25\text{-}Tacid}$), CO_2-H_2O isotope exchange during purification, and poor inter-laboratory calibration (e.g., Eagle et al., 2013; Fernandez et al., 2014; Wacker et al., 2014; Defliese et al., 2015). However, in all cases, these mechanisms are unable to account for the full extent of the shift between '*steep*' and '*shallow*' calibrations. Instead, we propose that improper usage of the forced CO_2 degassing method employed in '*steep*' slope calibration studies could cause non-equilibrium clumped isotope effects in precipitating carbonates.

The rate and extent of oxygen and clumped isotope exchange among parent water, interfacial DIC, and precipitating $CaCO_3$ depends on several factors, including temperature, DIC speciation, and the occurrence of non-equilibrium isotope effects such as the CO_2 hydration/hydroxylation or HCO_3^- dehydration/dehydroxylation reaction pathways. In $CaCO_3$ synthesis experiments, these factors can be controlled through the design of the precipitation method (i.e., passive or forced CO_2 degassing, CO_2 diffusion, or our upgraded constant addition method), as well as the experimental protocol (i.e., parent solution preparation). In the majority of precipitation experiments of Affek and Zaarur (2014) (see Figure 4) and two cases (i.e., C21 and C23) for Tang et al. (2014), it is likely that non-equilibrium isotope effects associated with HCO_3^- dehydration/dehydroxylation and $CO_{2(aq)}$ hydration/hydroxylation were at least partially responsible for observed disequilibrium $\delta^{18}O$ and $\Delta_{47\text{-RF}}$ values of $CaCO_3$.

3.4.5.1 'Shallow' slope calibrations

Our upgraded constant addition method minimizes these potential non-equilibrium isotope effects in order to ensure calcite precipitated in clumped and oxygen isotope equilibrium. This was achieved by the slow injection of CaCl- and $NaHCO_3$-bearing titrants into our HCO_3^--dominated parent solution prepared through mixing of a CaCl and a $NaHCO_3$ solution, and by limiting the rate of CO_2 degassing during precipitation.

The '*shallow*' slope calibrations of Dennis and Schrag (2010) and Defliese et al. (2015) precipitated $CaCO_3$ using a passive CO_2 degassing method. Although the rate of CO_2 degassing was not intrinsically controlled, it was presumably slow enough to minimize possible non-equilibrium clumped isotope effects caused by HCO_3^- dehydration/dehydroxylation, owing to the nature of the precipitation method. Our test of calcite oxygen isotope equilibrium precipitation for Dennis and Schrag (2010) also supports this hypothesis (see sections 3.4.1 and 3.4.2). Furthermore, their parent solutions were prepared through combination of a CaCl solution and a $NaHCO_3$ solution, presumably forming a HCO_3^- -dominated parent solution. As a result, given the low abundance of $CO_{2(aq)}$, it is likely that $CO_{2(aq)}$ hydration/hydroxylation was insignificant during $CaCO_3$ precipitation.

Excluding sample C21 and C23, Tang et al. (2014) also observed a *'shallow'* slope using the CO_2 diffusion method even though 12 out of 19 samples did not pass the equilibrium precipitation test (see section 3.4.2; Figure 2, 3b). Non-equilibrium oxygen isotope effects in these samples were attributed to either salinity and/or precipitation rate.

To explain how these calcites could reflect non-equilibrium oxygen isotope effects and still maintain clumped isotope equilibrium, Tang et al. (2014) suggest the $\Delta_{47\text{-RF}}$ value could be less sensitive to salinity and precipitation rate-related non-equilibrium isotope effects, possibly due to thermodynamic equilibrium being established more readily for clumped isotopes in precipitating calcite. It is also possible that the disequilibrium oxygen isotope compositions of these calcites are a reflection of large isotopic heterogeneities of the parent solution over the course of precipitation. In this case, $\Delta_{47\text{-RF}}$ values could still reflect equilibrium given the insubstantial effect of oxygen and carbon isotopic heterogeneities on the $\Delta_{47\text{-RF}}$ value (Defliese and Lohmann, 2015).

3.4.5.2. 'Steep' slope calibrations and the forced CO_2 degassing method

The forced CO_2 degassing method, employed by all '*steep*' slope calibration studies, precipitates $CaCO_3$ through continuous slow bubbling of N_2. Interestingly, all *'steep'* slope calibration studies employed an identical experimental protocol (Table 4) with the exception of Kluge et al. (2015) who used a slightly faster N_2 bubbling rate. When compared with the CO_2 degassing method used by Dennis and Schrag (2010) and Defliese et al. (2015), two primary differences are noted.

First, an identical parent solution was prepared for all temperatures through dissolution of a constant mass of reagent $CaCO_3$. Dissolution was mediated by CO_2 bubbling for 1 – 3 hrs. Given the duration of CO_2 bubbling, the most dominant DIC species of initial parent solution used in these studies is thought to be $CO_{2(aq)}$. For a $CO_{2(aq)}$-dominated system, the CO_2 hydration/hydroxylation reaction pathway is a necessary precursor to $CaCO_3$ precipitation. As previously discussed, non-equilibrium isotope effects of CO_2 hydration/hydroxylation can occur in systems undergoing rapid pH changes. In the forced CO_2 degassing method, initiation of N_2 bubbling can induce substantial pH changes in the parent solution as CO_2 degasses. For example, in the first 24 hours of N_2 bubbling, Kluge and John (2015) observed the initial pH of 5 to 6 increase to ~ 6.5 to 7.5 (see Figure 1; Kluge and John (2015)). Furthermore, they observed visible $CaCO_3$ precipitation over the course of the same time interval. This pH increase would induce rapid $CO_{2(aq)}$ hydration/hydroxylation while $CaCO_3$ precipitates depending on the temperature and solution chemistry. Second, the rate of CO_2 degassing is presumably faster in the forced CO_2 degassing method in comparison to the passive CO_2 degassing method. If the degassing rate was faster than anticipated, dependent on the availability of HCO_3^-in parent solution, non-equilibrium isotope effects associated with HCO_3^- dehydration/dehydroxylation could also occur.

3.5.4.3. Temperature-dependent isotopic inheritance of non-equilibrium isotope effects

It would appear that *'steep'* slope calibrations may result from a combination of both CO_2 hydration/hydroxylation and HCO_3^- dehydration/dehydroxylation, given that $\Delta_{47\text{-RF}}$ values are above our clumped isotope equilibrium value at lower temperatures, and below at higher temperatures (Figure 3c). The behavior of disequilibrium $\Delta_{47\text{-RF}}$ values could result from CO_2 hydration/hydroxylation dominating at low temperatures, whilst HCO_3^- dehydration/dehydroxylation dominates at higher temperatures, with equal or no contributions from either occurring at 29.7 °C intersection (see section 3.4.3.). At lower temperatures, non-equilibrium isotope effects associated with CO_2 hydration/hydroxylation are plausible due to the slower rate of isotopic re-equilibration between HCO_3-H_2O. At higher temperatures, non-equilibrium isotope effects associated with HCO_3^- dehydration/dehydroxylation could predominate for two reasons. First, increased temperature reduces the solubility of $CO_{2(aq)}$, amplifying the rate of CO_2 degassing. Second, given the common mass of dissolved $CaCO_3$ during preparation of the parent solution, the increased saturation state at higher temperatures could drive rapid precipitation of $CaCO_3$, disallowing adequate re-equilibration of $CaCO_3$-H_2O.

This interpretation is complexed by the oxygen isotope fractionation between calcite and water. Co-variance of the $\Delta_{47\text{-RF}}$ and $1000\ln\alpha_{\text{calcite-water}}$ values does not conform to the predictions for either CO_2 hydration/hydroxylation or HCO_3^- dehydration/dehydroxylation (Figure 5; Guo, 2008; Guo et al., 2009b). $1000\ln\alpha_{\text{calcite-water}}$ values from Zaarur et al. (2013) are either close or above the Kim and O'Neil's calibration curve whereas those reported from Ghosh et al. (2006) are either close or below the equilibrium value.

3.5.4.4. A simplified CO_2 hydration model for explaining uncorrelated oxygen and clumped isotope signatures in disequilibrium carbonates

Observation of the equilibrium oxygen isotope and clumped isotope signatures of $CO_{2(g)}$, $CO_{2(aq)}$, HCO_3^-, CO_3^{2-}, and calcite may provide a second explanation for *'steep'* slope oxygen and clumped isotope systematics. Oxygen isotope fractionation between calcite, $CO_{2(g)}$, $CO_{2(aq)}$, HCO_3^-, CO_3^{2-}, and water is well-defined (Brenninkmeijer et al., 1983; Kim and O'Neil, 1997; Beck et al., 2005). However, the clumped isotope compositions of $CO_{2(g)}$, HCO_3^-, CO_3^{2-} are solely based upon theoretical models (Wang et al., 2004; Hill et al., 2014). To the best of our knowledge, these theoretical models have not been validated at temperatures other than ~ 25 °C (Cao and Liu, 2012; Tripati et al., 2015). Furthermore, the clumped isotope composition of $CO_{2(aq)}$ has not yet been defined. For the sake of this interpretation, we will assume the theoretical temperature dependence of DIC clumped isotope compositions is realistic, and that $CO_{2(g)}$ and $CO_{2(aq)}$ share a similar clumped isotope temperature dependency.

Between 0 to 100 °C, conventional oxygen isotope fractionation among calcite, $CO_{2(g)}$, $CO_{2(aq)}$, HCO_3^-, CO_3^{2-}, and H_2O share a comparable temperature dependence (Figure 6a). If we apply the simplified CO_2 hydration model proposed by McConnaughey (2003) (Eq. 9), the calculated $1000\ln\alpha_{\text{calcite-water}}$ value of newly formed HCO_3^- is similar to equilibrium calcite between 0 – 100 °C. In this case, minimal re-equilibration between HCO_3^--H_2O may sufficiently minimize non-equilibrium oxygen isotope effects associated with CO_2 hydration.

In contrast, the temperature dependence of $\Delta_{47\text{-RF}}$ values for calcite, HCO_3^-, and CO_3^{2-} are notably shallower than that of $CO_{2(g)}$, and presumably $CO_{2(aq)}$ (Figure 6b). If $CO_{2(aq)}$ hydration/hydroxylation reactions do not substantially alter the original abundance of ^{13}C-^{18}O bonds in CO_2, and $CaCO_3$ precipitates prior to substantial clumped isotope re-equilibration, it is plausible that the clumped isotope signature of calcite may partially reflect that of $CO_{2(aq)}$. For example, between 0 – 100 °C, the $\Delta_{47\text{-RF}}$ temperature dependence of the Ghosh et al. (2006) calibration is comparable to $CO_{2(g)}$, and possibly

$CO_{2(aq)}$ (Figure 6b). This alternative explanation represents a simplified approach to the isotopic exchange pathways that occur during CO_2 hydration and $CaCO_3$ precipitation. However, it may provide partial explanation to the observed clumped and oxygen isotope systematics of $CaCO_3$ precipitated using the forced CO_2 degassing method.

3.5. Conclusion

This study presents a revised calibration of the calcite clumped isotope paleothermometer based upon inorganic calcites slowly precipitated at 15, 25, and 40 °C using an upgraded constant addition technique. This technique permitted excellent control of the oxygen and carbon isotope composition of parent solution, as well as various physicochemical properties of parent solution, such as pH, precipitation rate and the rate of CO_2 degassing. Given the similar isotopic exchange pathways for conventional oxygen and clumped isotope systematics, assessment of oxygen isotope equilibrium between calcite samples prepared in this study and their parent solution provided a conservative metric for ensuring calcite clumped isotope equilibrium. All calcites used in this calibration study conform to Kim and O'Neil (1997)'s calcite-water oxygen isotope equilibrium curve, and exhibit an indistinguishable temperature dependence. However, conformity to calcite-water oxygen isotope equilibrium is commonly not achieved in $CaCO_3$ used in other calibration studies of the $CaCO_3$ clumped isotope paleothermometer. This finding suggests that some previous calibration studies may have used $CaCO_3$ with unidentified non-equilibrium clumped isotope effects.

Our calibration of the calcite clumped isotope paleothermometer is indistinguishable from the *'shallow'* slope calibrations proposed by Dennis and Schrag (2010), Tang et al. (2014), and Defliese et al. (2015). In comparison, the *'steep'* slope calibrations proposed by Ghosh et al. (2006), Zaarur et al. (2013), Kluge et al. (2015), and Tripati et al. (2015) differ significantly. $CaCO_3$ samples, used in these *'steep'* slope calibrations, were precipitated by a consistent adaptation of the forced CO_2 degassing method and they might have been influenced by non-equilibrium isotope effects that could alter the slope of the carbonate clumped isotope thermometer. At lower temperatures, the clumped isotope composition of $CaCO_3$ is more heavily influenced by non-equilibrium isotope effects associated with CO_2 hydration/hydroxylation, as the $CO_{2(aq)}$ reservoir is precipitated prior to substantial isotope re-equilibration. At higher temperatures, rapid $CO_{2(aq)}$ degassing via HCO_3^- dehydration/dehydroxylation dominates, lowering the expected clumped isotope value. Given the limited conformity of oxygen isotope systematics to these proposed non-equilibrium isotope effects, we also propose a simplified CO_2 hydration pathway, where precipitating $CaCO_3$ can partially inherit the clumped and oxygen isotopic composition of $CO_{2(aq)}$. The clumped isotope composition for $CO_{2(g)}$, and presumably $CO_{2(aq)}$, shares a temperature dependence similar to *'steep'* slope calibrations. Alternatively, the predicted oxygen isotope composition of HCO_3^- formed through $CO_{2(aq)}$ hydration is similar to calcite precipitated in equilibrium. $CaCO_3$ inheriting both the clumped and oxygen isotope composition of HCO_3^- formed through $CO_{2(aq)}$ hydration could explain why the predicted co-variance of the oxygen and clumped isotope composition of disequilibrium $CaCO_3$ does not conform to predictions. Resolving the carbonate clumped isotope paleothermometer discrepancy is of primary importance for the accurate application of this paleotemperature proxy.

3.6. Figures

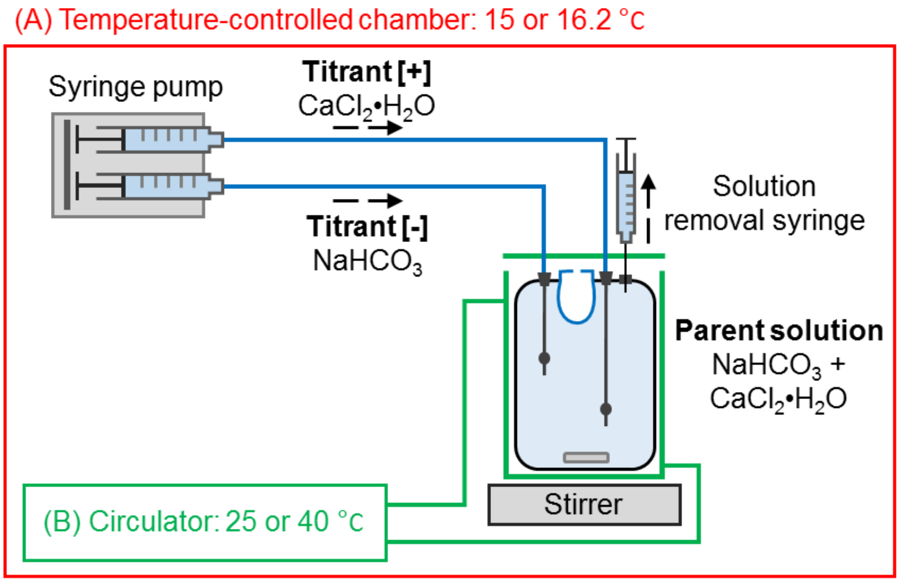

Figure 1: Schematic of the upgraded constant addition method. Titrant is first injected into an internal tubing and spherical reservoir prior to entering the parent solution. Given the slow injection speed, this ensured titrants were in thermal and isotopic equilibrium. **(a)** For experiments conducted at 15 and 16.2 °C, the parent solution and titrant syringes were stored within a temperature-controlled chamber. **(b)** For experiments conducted at 25 and 40 °C, parent solution was stored in a double-walled circulating water bath while titrant syringes were kept at room temperature.

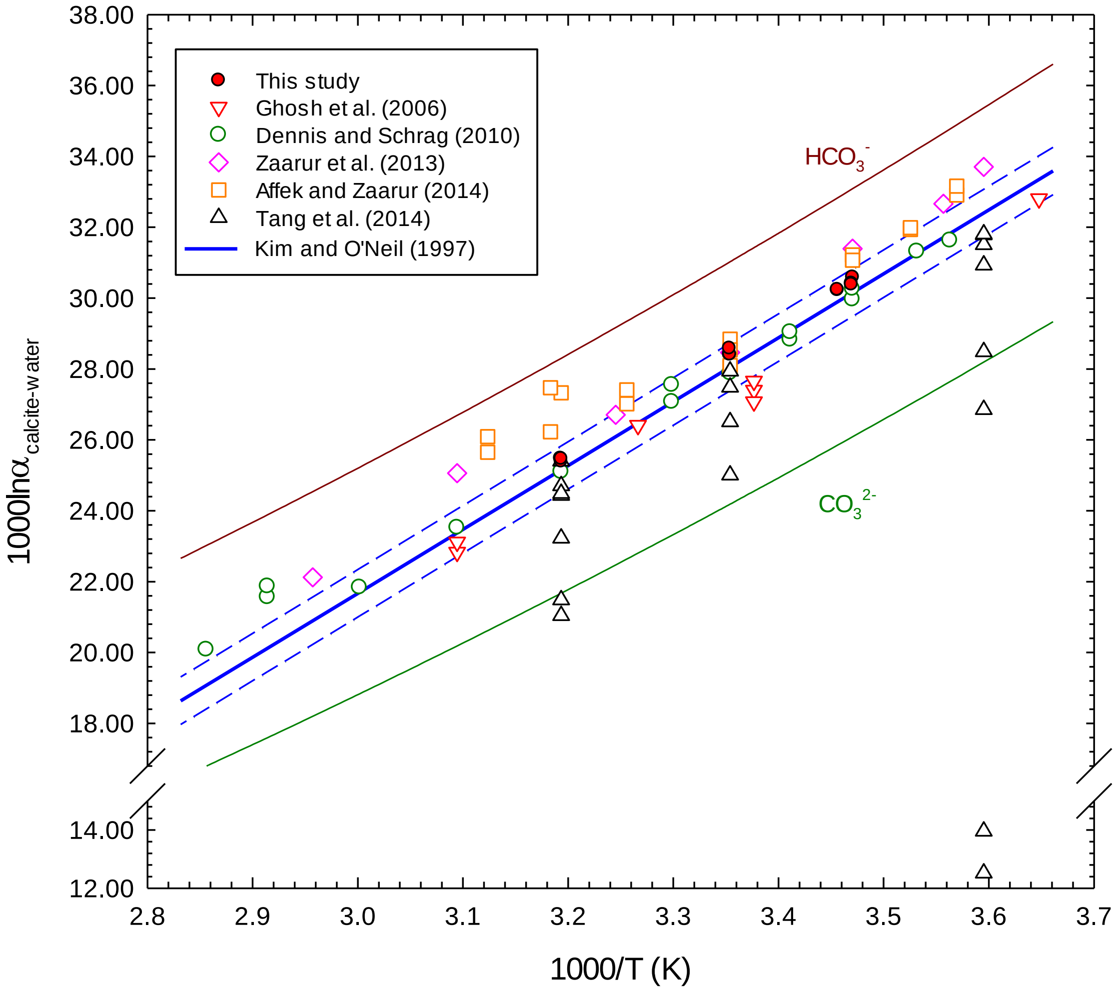

Figure 2: Comparison of the carbonate-water oxygen isotope fractionation among carbonate clumped isotope calibration studies. Only $CaCO_3$ samples whose mineralogy is predominantly calcite are considered. Values for Affek and Zaarur (2014) are from the short-period experiments, and were not measured for their clumped isotope composition. For this study, the associated error of $1000\ln\alpha_{calcite-water}$ is ± 0.16 ‰, and is smaller than the symbol. The error for $1000\ln\alpha_{calcite-water}$ of other studies is unpublished.

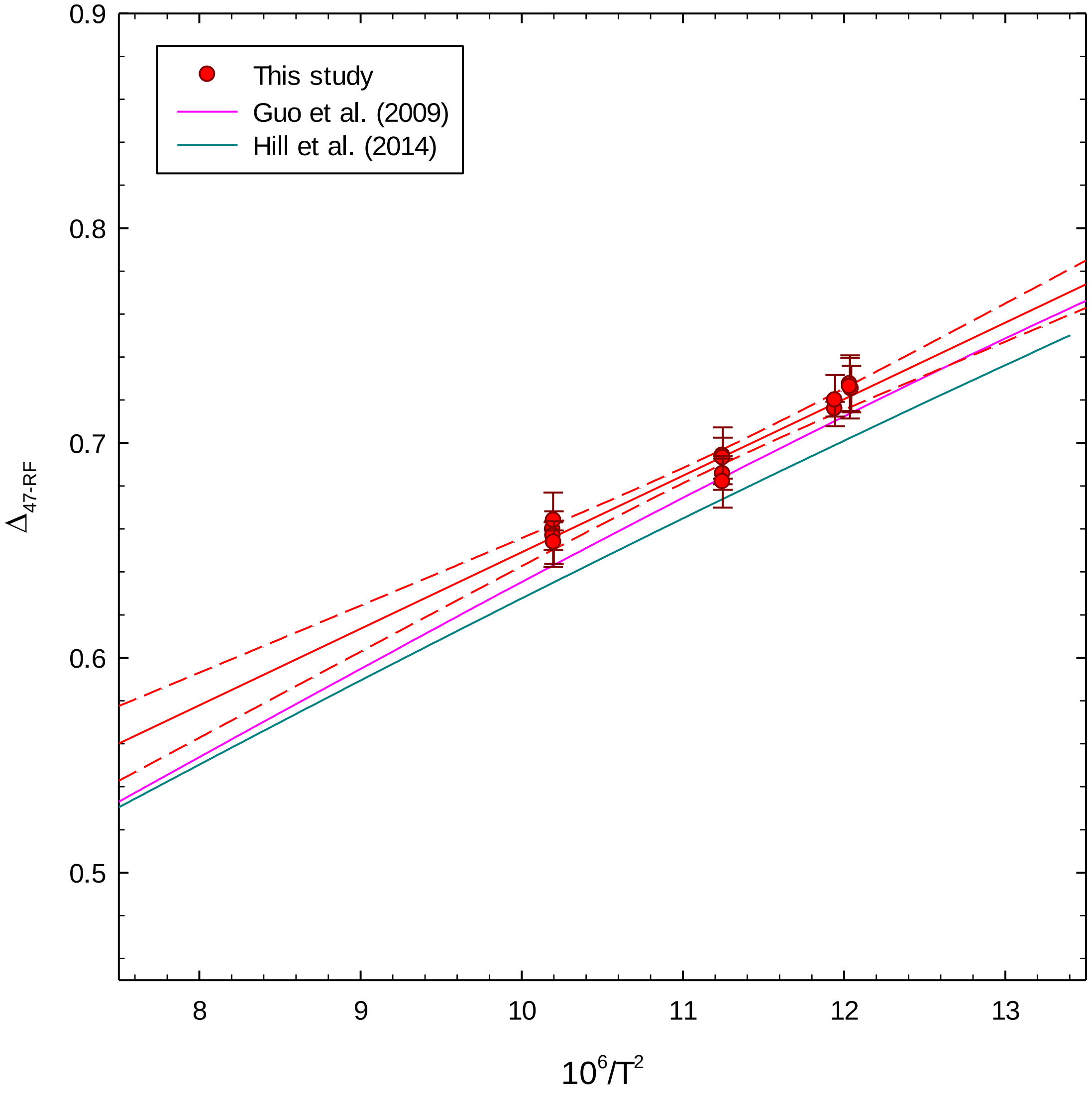

Figure 3a: Average $\Delta_{47\text{-RF}}$ values and calibration including 95% confidence intervals for this study's calcite experiments. Error bars represent 1SE. The theoretical calibrations of Guo et al. (2009) and Hill et al. (2014) are shown for comparison. Both theoretical calibrations have been corrected using the Δ_{63}-Δ_{47} AFF of 0.280 ‰ (Tripati et al., 2015).

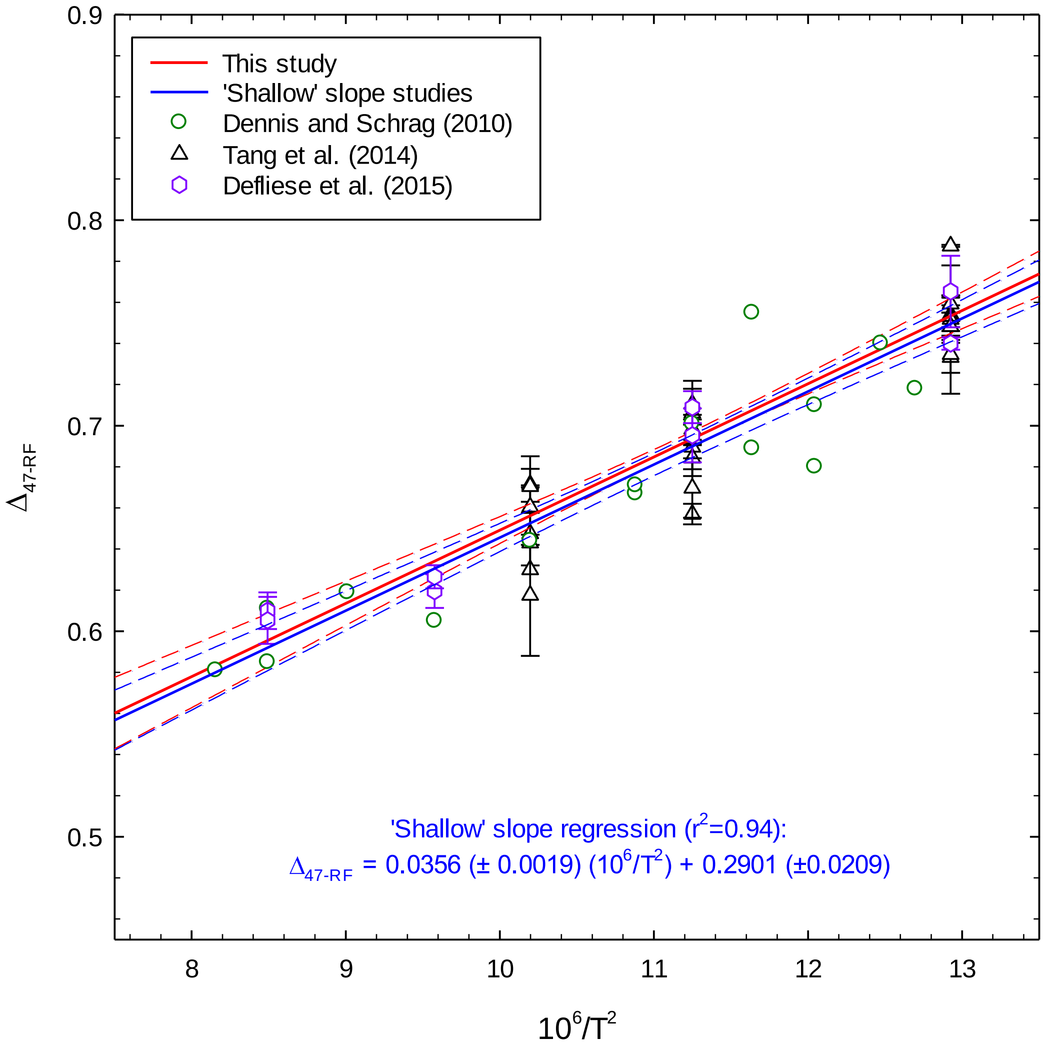

Figure 3b: This study's calcite clumped isotope calibration compared to the combined regression of all *'shallow'* slope calibrations. $\Delta_{47\text{-RF}}$ values for Dennis and Schrag (2010) have been re-projected to the ARF, thus 1SE error bars are not provided for these samples.

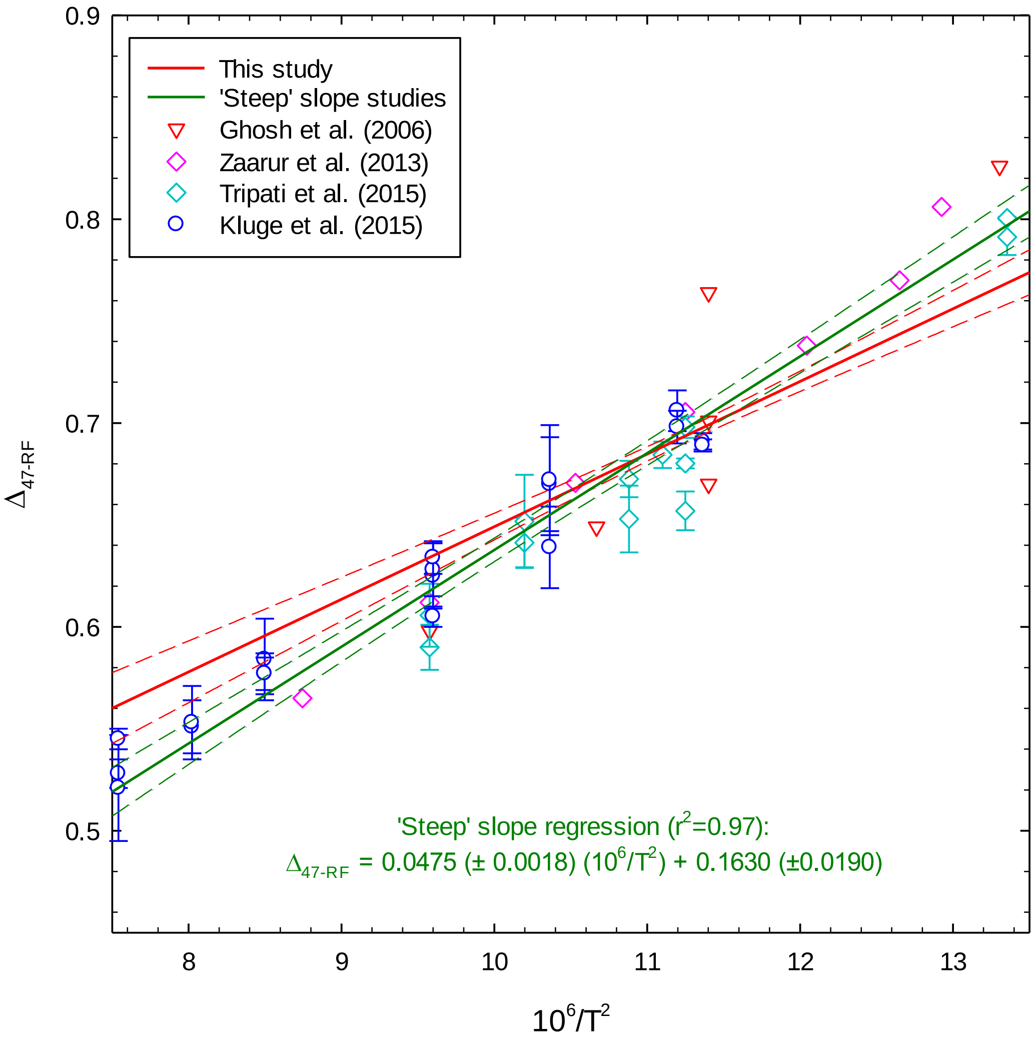

Figure 3c: This study's calcite clumped isotope calibration compared to the combined regression of all *'steep'* slope calibrations. Error bars represent 1SE. $\Delta_{47\text{-RF}}$ values for Ghosh et al. (2006) have been re-projected to the ARF, thus 1SE error bars are not provided for these samples.

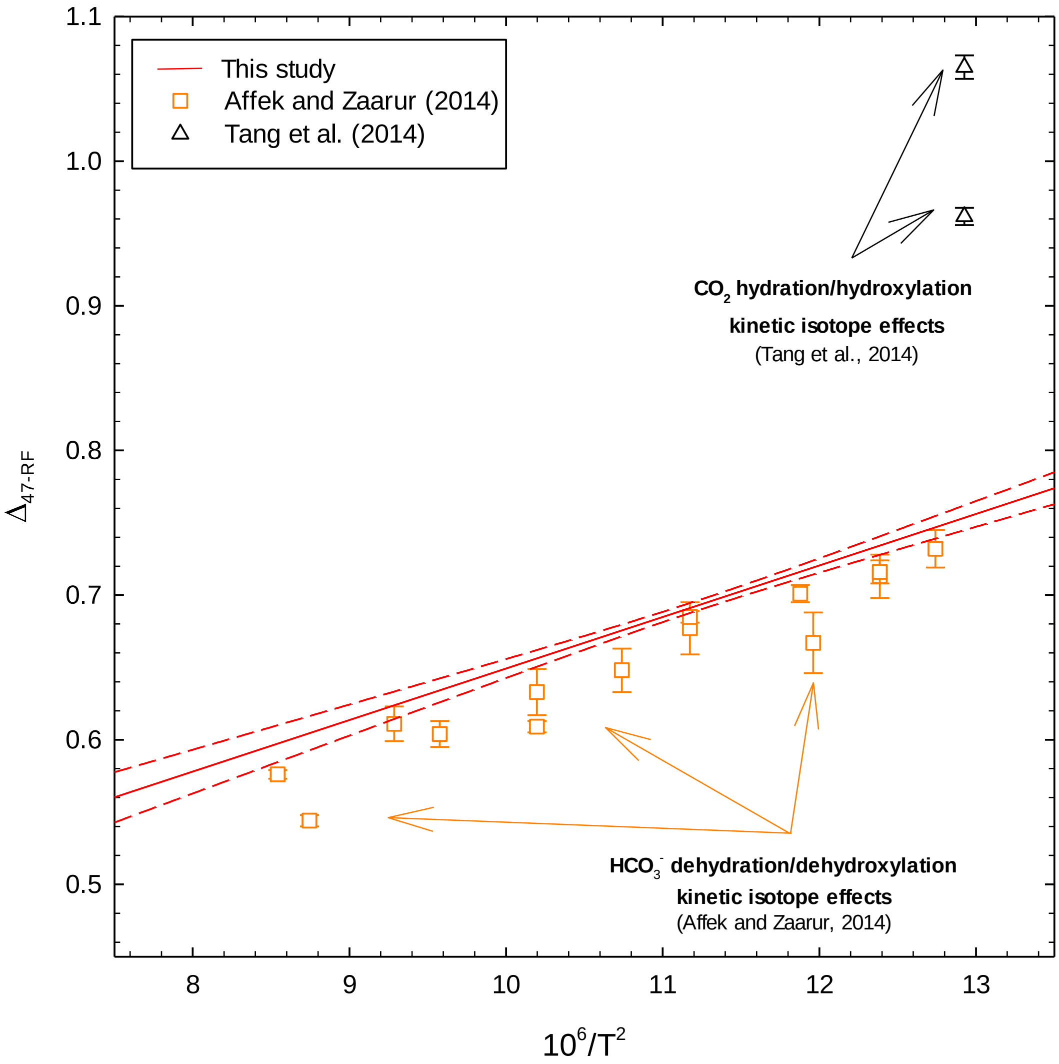

Figure 3d: This study's calcite clumped isotope calibration compared to the CO_2 hydration/hydroxylation and HCO_3^- dehydration/dehydroxylation non-equilibrium $\Delta_{47\text{-RF}}$ values of Tang et al. (2014) and Affek and Zaarur (2014), respectively. Error bars represent 1SE.

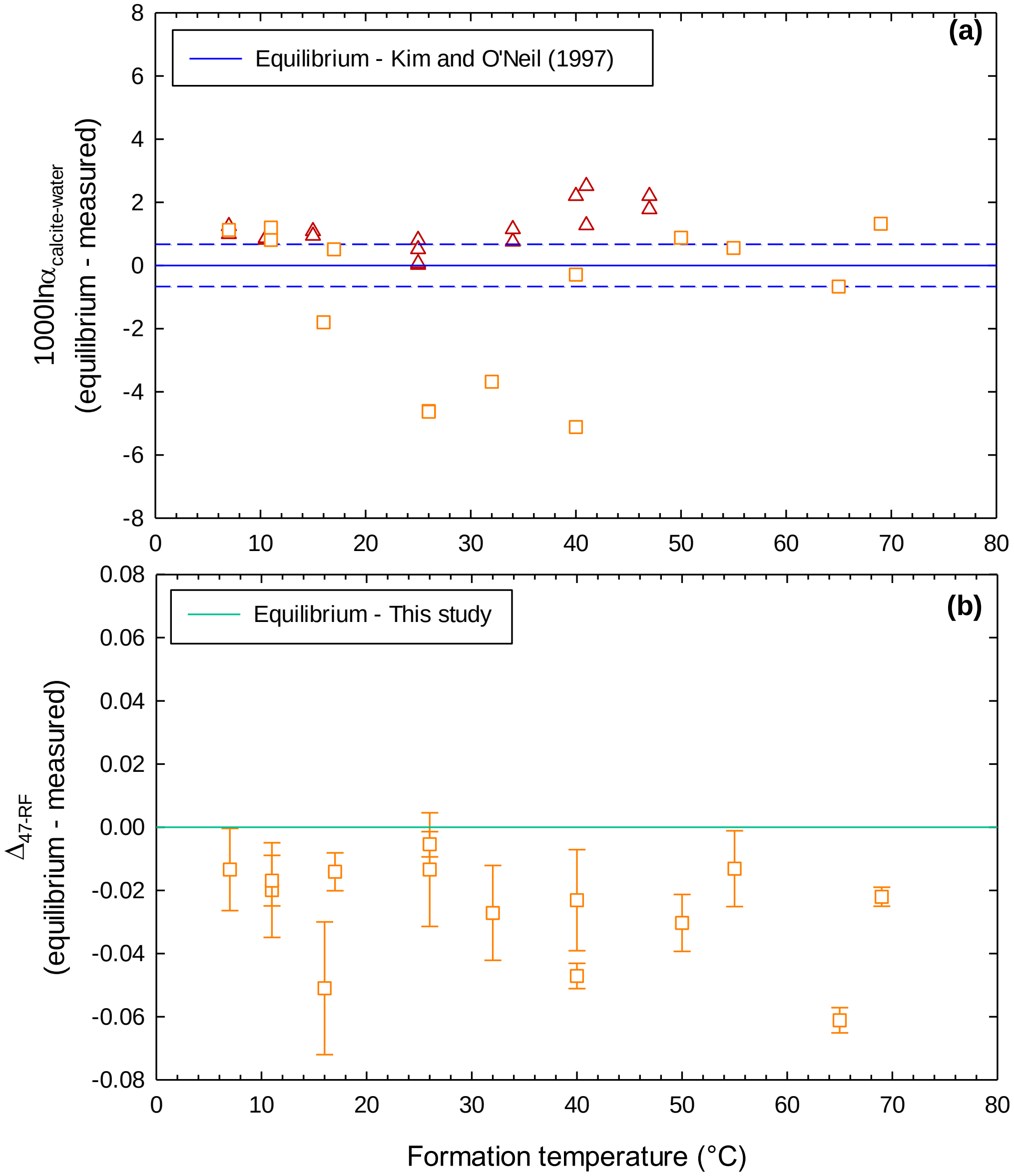

Figure 4: Combined evidence supporting non-equilibrium isotope effects associated with HCO_3^- dehydration/dehydroxylation in the short- and long-period passive degassing experiments of Affek and Zaarur (2014). **(a)** Deviations from the Kim and O'Neil (1997) calcite-water oxygen isotope equilibrium for short-period (red triangles) and long-period (orange squares) $1000\ln\alpha_{calcite\text{-}water}$ values. **(b)** Deviations from the calcite clumped isotope equilibrium proposed by this study for long-period $\Delta_{47\text{-}RF}$ values. Measurement error of $1000\ln\alpha_{calcite\text{-}water}$ is not published. $\Delta_{47\text{-}RF}$ error bars represent 1SE.

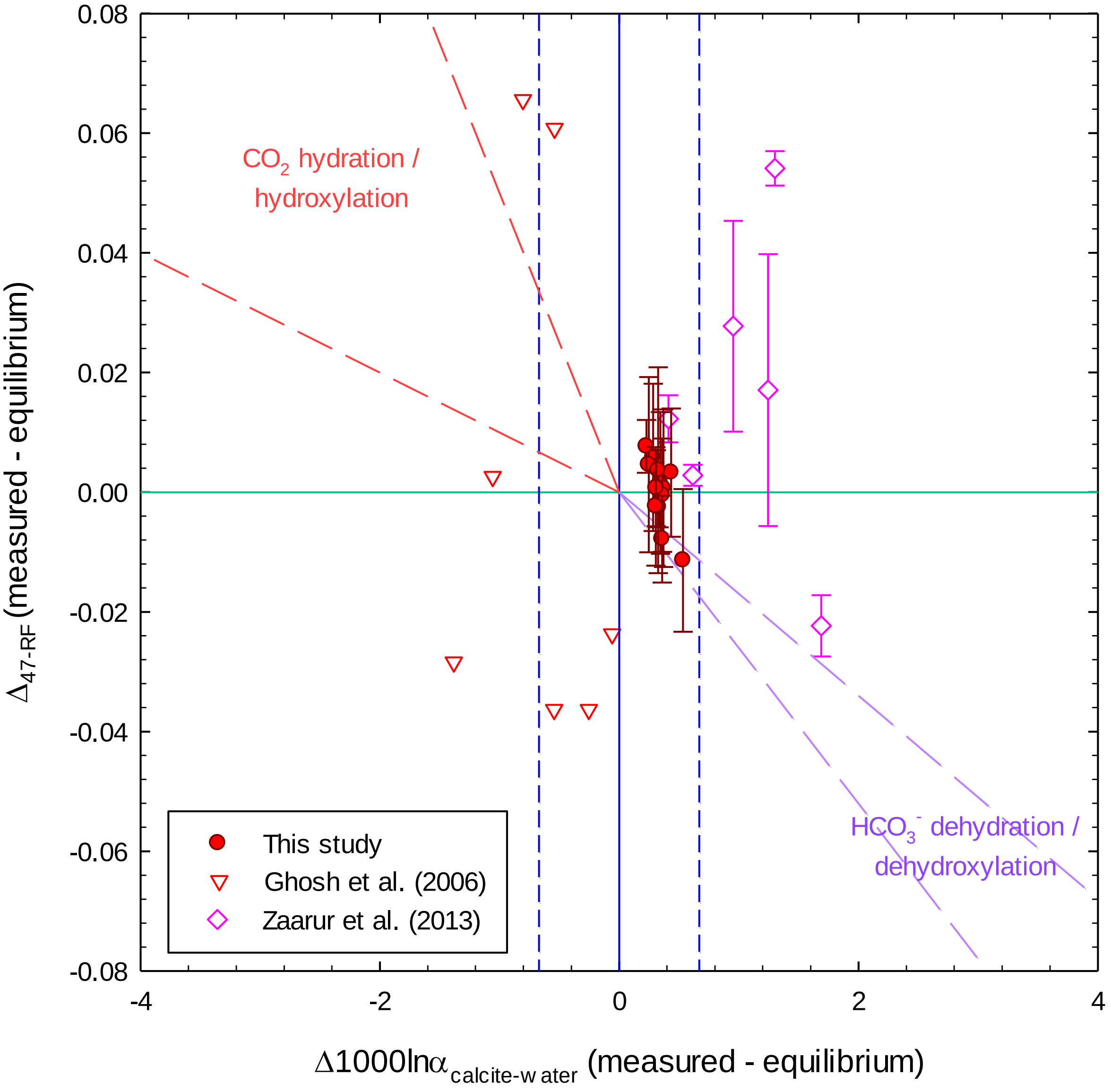

Figure 5: Deviation from clumped and oxygen isotope equilibrium for $CaCO_3$ samples from Ghosh et al. (2006) and Zaarur et al. (2013) whose mineralogy was predominantly calcite. Values are relative to Kim and O'Neil (1997)'s calcite-water oxygen isotope equilibrium and this study's calibration of the calcite clumped isotope paleothermometer. $\Delta_{47\text{-RF}}$ values for Ghosh et al. (2006) have been re-projected to the ARF, thus 1SE error bars are not provided for these samples. Predicted clumped and oxygen isotope co-variance for CO_2 hydration/hydroxylation and HCO_3^- dehydration/dehydroxylation non-equilibrium isotope effects is displayed for reference.

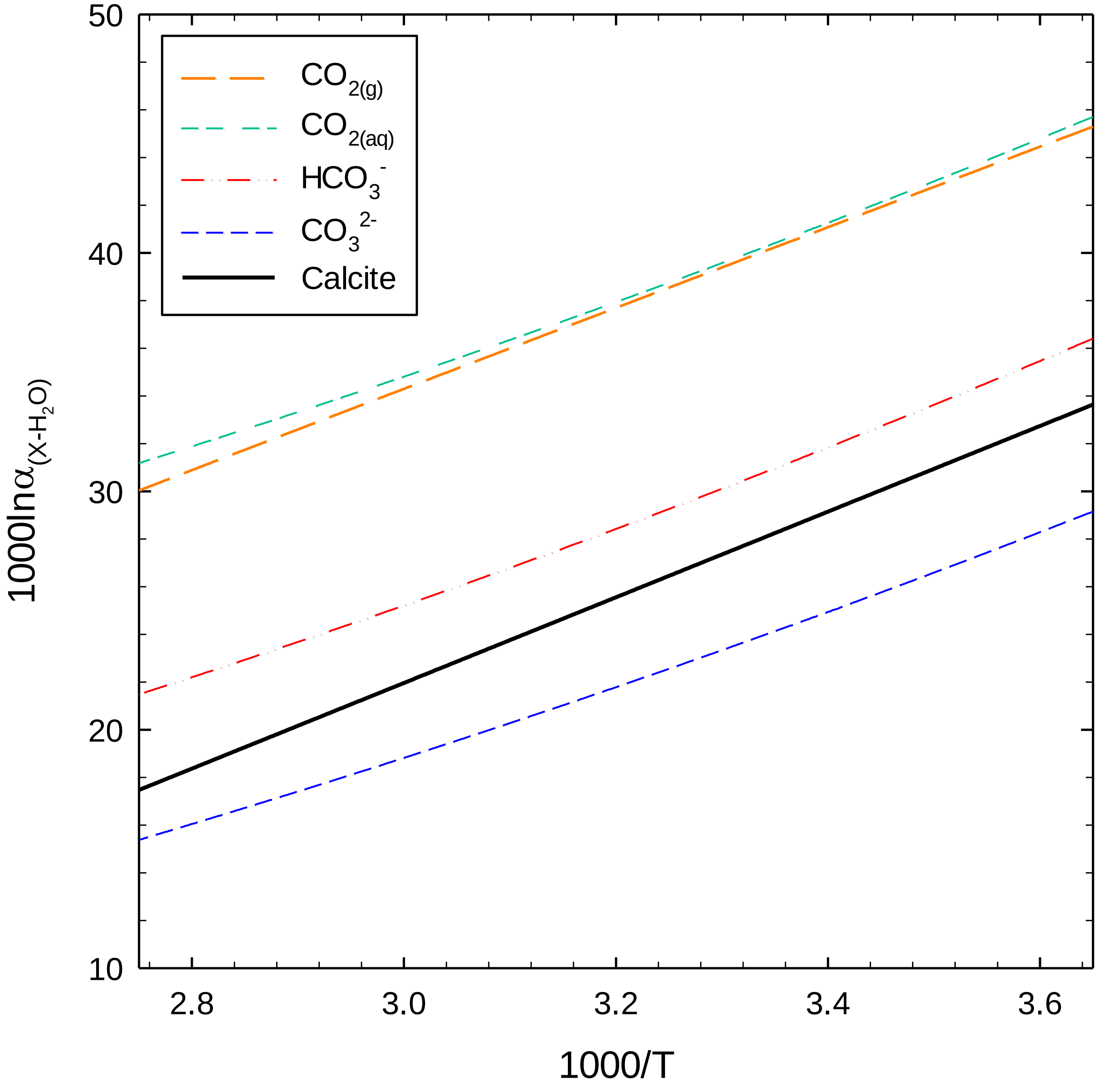

Figure 6a: Experimentally-derived 1000lnα$_{\text{X-water}}$ values for $CO_{2(g)}$ (Brenninkmeijer et al., 1983), $CO_{2(aq)}$, HCO_3^-, CO_3^{2-} (Beck et al., 2005), and calcite (Kim and O'Neil, 1997).

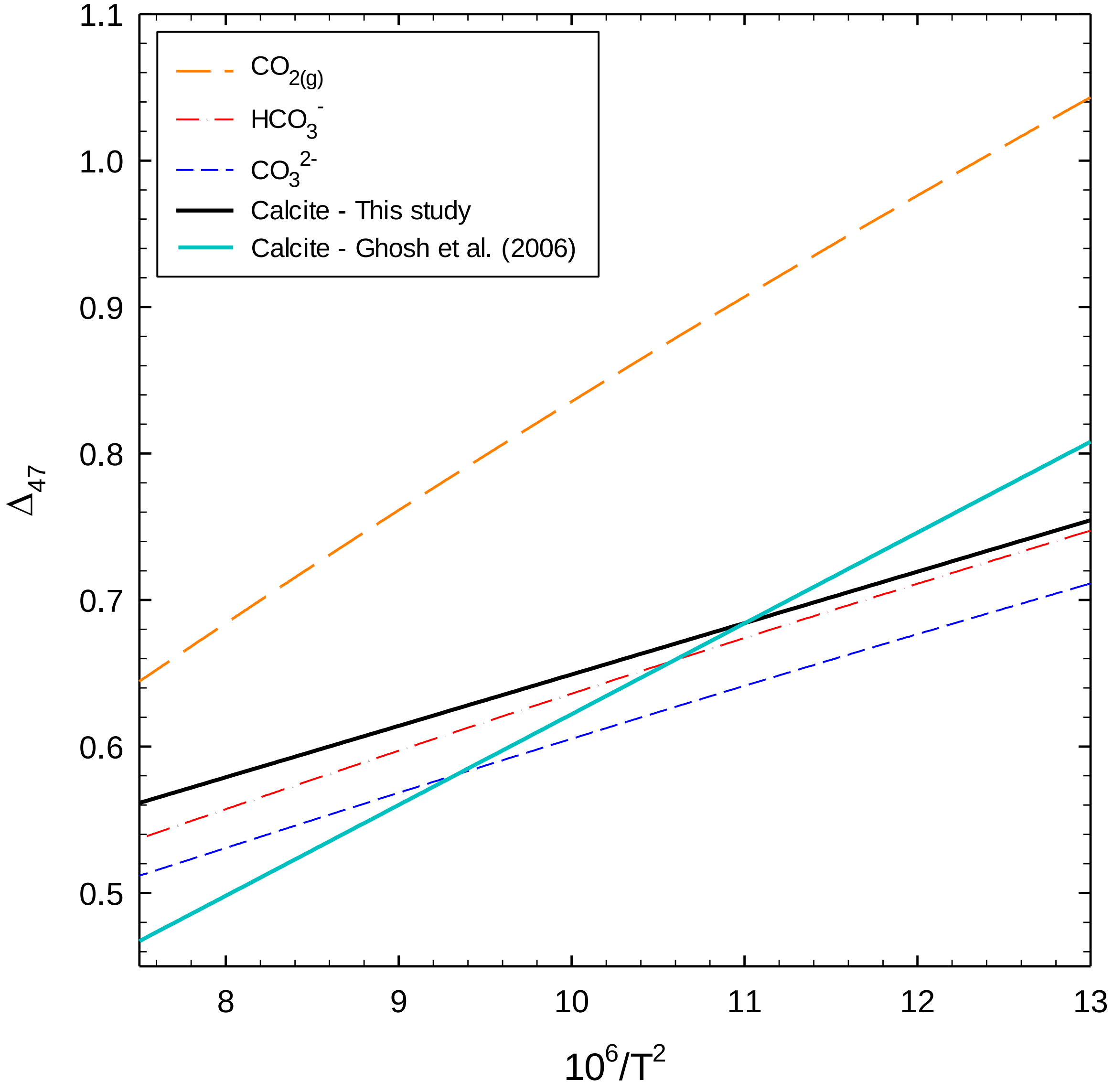

Figure 6b: Theoretical temperature dependence of Δ_{47} values for $CO_{2(g)}$ (Wang et al., 2014), HCO_3^-, and CO_3^{2-} (Hill et al. (2014). Calcite clumped isotope calibrations from this study and Ghosh et al. (2006) are shown for reference. The Δ_{47} values for HCO_3^- and CO_3^{2-} are projected using the Δ_{63}-Δ_{47} AFF of 0.280 ‰ (Tripati et al., 2015).

3.7. Tables

Table 1: Experiment starting chemistry and conditions during calcite precipitation

Sample info		Starting chemistry					Precipitation conditions								
Start date	Experiment name	Sol. $NaHCO_3$ (mmolal)	Sol. $CaCl_2$-H_2O (mmolal)	Avg. titrant $NaHCO_3$ (mmolal)[1]	Titrant $CaCl_2$ H_2O (mmolal)	Initial Ω (Calcite)[2]	Starting pH	Ending pH	Avg. pH	Avg. pH 1σ	Avg Temp (°C)	Avg Temp 1σ	Duration (days)	Titrant injection rate (ml/hr)	Precipitation rate (mg/hr)
2/5/2015	CS-15-T1F[3]	9.997	1.003	29.512	3.403	0.9671	8.13	7.92	8.10	0.15	15.0	0.1	11.06	0.5	0.18
2/19/2015	CS-15-T2E[3,4]	10.000	0.898	29.500	3.148	1.0057	8.20	7.91	8.11	0.20	16.2	0.2	7.08	0.5	0.26
2/19/2015	CS-15-T2F[3,4]	10.000	0.898	29.500	3.148	1.0440	8.24	7.83	8.08	0.22	16.2	0.2	7.08	0.5	0.28
3/13/2015	CS-15-T3E[3]	10.005	0.800	27.737	2.900	1.0389	8.30	8.01	8.23	0.13	15.1	0.1	7.01	0.5	0.18
3/13/2015	CS-15-T3F[3]	10.005	0.800	27.737	2.900	1.0484	8.31	7.95	8.16	0.19	15.1	0.1	7.01	0.5	0.28
1/30/2015	CS-25-T5D[3]	10.002	0.800	29.505	2.933	1.1127	8.24	8.16	8.06	0.13	25.04	0.03	14.01	0.25	0.14
5/6/2015	CS-25-T10C	10.005	0.799	29.497	2.952	1.1956	8.33	8.08	8.12	0.13	25.02	0.06	8.06	0.5	0.25
5/6/2015	CS-25-T10D	10.005	0.799	29.497	2.952	1.2503	8.39	8.06	8.28	0.18	25.02	0.06	8.06	0.5	0.20
5/6/2015	CS-25-T10F	10.003	0.802	29.503	2.944	1.2065	8.34	8.09	8.18	0.09	25.04	0.06	8.06	0.5	0.17
3/20/2015	CS-40-T1C	10.000	0.502	29.518	2.403	1.2806	8.44	8.30	8.30	0.08	40.04	0.04	7.94	0.5	0.17
3/20/2015	CS-40-T1D	10.000	0.502	29.518	2.403	1.2654	8.42	8.25	8.23	0.08	40.02	0.05	7.94	0.5	0.20
4/9/2015	CS-40-T2C	9.999	0.502	29.507	2.394	1.2734	8.43	8.35	8.29	0.09	39.98	0.06	7.71	0.5	0.19
4/9/2015	CS-40-T2D	9.999	0.502	29.507	2.394	1.2988	8.46	8.30	8.28	0.11	39.98	0.09	7.71	0.5	0.20

[1] To minimize the potential for CO_2 offgassing in $NaHCO_3$ titrant solution, refilling of titrant syringe used fresh solution only. This value represents the average of titrants prepared per experiment

[2] Initial Calcite saturation state calculated using Geochemists Workbench® 10. Variables used: Starting chemistry, Starting pH, and Avg. Temp.

[3] Trace amounts of Teflon in collected precipitate

[4] Subsequent temperature calibration of the growth chamber yielded a +1.2 °C offset

Table 2: Isotopic compositions of experimental bulk solutions and calcite relative to the $\delta^{18}O_{VSMOW\text{-}SLAP}$ and $\delta^{13}C_{VPDB}$ scale

Experiment name	Avg. Temp (°C)	10^3/T*	Bulk solution			Calcite		$1000\ln\alpha_{Calcite\text{-}H2O}$
			Avg. $\delta^{18}O_{H2O}$ (‰)**	Initial $\delta^{13}C_{DIC}$ (‰)**	$\delta^{13}C_{DIC}$ drift (‰)***	$\delta^{18}O_{Calcite}$**	$\delta^{13}C_{Calcite}$**	
CS-15-T1F	15.0	3.471	-6.52	-6.12	0.21	24.34	-5.50	30.59
CS-15-T3E	15.1	3.469	-6.48	-6.35	0.04	24.20	-5.67	30.42
CS-15-T3F	15.1	3.469	-6.45	-6.41	0.19	24.20	-5.50	30.38
							Average:	**30.46**
CS-15-T2E	16.2	3.456	-6.46	-6.29	0.24	24.03	-5.55	30.22
CS-15-T2F	16.2	3.456	-6.48	-6.42	0.47	24.02	-5.41	30.24
							Average:	**30.23**
CS-25-T5D	25.04	3.354	-6.48	-5.74	0.55	22.16	-5.43	28.41
CS-25-T10C	25.02	3.354	-6.48	-6.29	0.68	22.15	-5.46	28.41
CS-25-T10D	25.02	3.354	-6.48	-6.19	0.29	22.15	-5.60	28.41
CS-25-T10F	25.04	3.354	-6.50	-6.25	0.19	22.30	-5.56	28.58
							Average:	**28.45**
CS-40-T1C	40.04	3.193	-6.40	-6.36	0.56	19.24	-5.61	25.47
CS-40-T1D	40.02	3.193	-6.38	-6.15	0.38	19.24	-5.59	25.46
CS-40-T2C	39.98	3.194	-6.42	-6.07	0.44	19.13	-5.63	25.39
CS-40-T2D	39.98	3.194	-6.42	-6.21	0.35	19.21	-5.68	25.47
							Average:	**25.45**

* T is presented in Kelvin (°C + 273.15)

**1 SD of $\delta^{18}O$ and $\delta^{13}C$ measurements is ≤ 0.15 ‰ for bulk solution values and ≤ 0.05 ‰ for calcite values

***$\delta^{13}C_{DIC}$ drift = (Final - Initial)

Table 3: Clumped isotope compositions of inorganic calcite

Experiment name	Avg. Temp (°C)	$10^6/T^2$*	Calcite				
			δ^{47}	1 SD	$\Delta_{47\text{-RF}}$**	1 SE	*n*
CS-15-T1F	15.0	12.045	5.49	0.03	0.724	0.011	4
CS-15-T3E	15.1	12.036	5.18	0.01	0.727	0.012	4
CS-15-T3F	15.1	12.036	5.34	0.03	0.725	0.015	4
CS-15-T2E	16.2	11.944	5.12	0.03	0.715	0.003	3
CS-15-T2F	16.2	11.944	5.24	0.04	0.719	0.012	4
CS-25-T5D	25.04	11.246	3.32	0.02	0.694	0.013	4
CS-25-T10C	25.02	11.248	3.29	0.10	0.693	0.009	3
CS-25-T10D	25.02	11.248	3.14	0.01	0.685	0.007	4
CS-25-T10F	25.04	11.246	3.33	0.02	0.682	0.012	4
CS-40-T1C	40.04	10.195	0.18	0.04	0.660	0.017	4
CS-40-T1D	40.02	10.196	0.20	0.01	0.657	0.006	4
CS-40-T2C	39.98	10.199	0.05	0.01	0.664	0.004	3
CS-40-T2D	39.98	10.199	0.07	0.01	0.654	0.010	4

* T is presented in Kelvin (°C + 273.15)

**$\Delta_{47\text{-RF}}$* values are presented with a $\Delta^*_{25\text{-}90}$ acid fractionation factor of 0.069 ‰, as determined by Eq. 23 of Guo et al. (2009)

Table 4: Comparison of various precipitation methods utilized in experimental Δ_{47} calibrations

Author	System description				System conditions	
	Precipitation technique	Technique description	Solution Preparation	Solution thermal equilibration	Temperature (°C)	pH
This study	Modified constant addition technique	Constant addition of $NaHCO_3$ and CaCl titrants to a saturated solution ($\Omega \approx 1$) induces controlled $CaCO_3$ precipitation	**Bulk solution:** 1L 10 mM NaHCO3 and 1-2 mM CaCl produced through mixing of 500ml constituent solutions **Titrant (-):** 27.7 - 29.5 mM NaHCO3 **Titrant (+):** 2.4 - 3.4 mM CaCl	48 hr	15, 25, 40	Starting pH: 8.13 – 8.46, pH drift ≤ 0.41
Ghosh et al. (2006)*	Forced N_2 degassing	Continuous slow bubbling of humidified N_2 (40 bubbles/min) through a saturated $Ca(HCO_3)_2$ solution removes CO_2 and induces $CaCO_3$ precipitation	**HA1:** 5mM $NaHCO_3$:$CaCl_2$ by bubbling CO_2 **Others:** dissolution of ~ 0.5g $CaCO_3$ / 800ml H_2O by bubbling CO_2 for 1-2 hr. Filtered to remove excess $CaCO_3$.	1 hr	1, 23, 33, 50	N/A[1]
Dennis and Schrag (2010)	Passive degassing	Saturated $Ca(HCO_3)_2$ solution exposed to atmosphere, passive degassing of CO_2 induces $CaCO_3$ precipitation	100ml $CaCl_2$ solution slowly added to 900ml $NaHCO_3$ solution to yield final $\Omega \approx 10$ (GWB, V:5)	≥ 2 hr	7.5, 10, 15, 20, 25, 30, 40, 50, 60, 70, 77	N/A[1]
Zaarur et al. (2013)	Forced N_2 degassing	Continuous slow bubbling of humidified N_2 (40 bubbles/min) through a saturated $Ca(HCO_3)_2$ solution removes CO_2 and induces $CaCO_3$ precipitation	Dissolution of $CaCO_3$ / 1L H_2O by bubbling 100% CO_2 for ~ 1 hr. Filtered to remove excess $CaCO_3$.	N/A	5, 8, 15, 25, 35, 50, 65	N/A[1]
Tang et al. (2014)**	CO_2-Diffusion method	An inner (low pH) and outer (high pH) solution is seperated by a diffusive membrane. A pH gradient forces continuous diffusion of DIC-$CO_{2(g),}$ inducing $CaCO_3$ precipitation in the pH-buffered outer solution	**Inner solution**: 0.5L 830 mM $NaHCO_3$ **Outer solution:** 5L 10 mM $CaCl_2$ + 5 mM NH_4Cl + pH titrant 2 M NaOH	N/A	5, 25, 40	Outer solution pH experiment range: 8.3 - 10.5, controlled by 2 M NaOH titrant (± 0.03)

Affek and Zaarur (2014)	Passive degassing	Saturated $Ca(HCO_3)_2$ solution loosely covered from atmosphere, passive degassing of CO_2 induces $CaCO_3$ precipitation	Dissolution of $CaCO_3$ / 1L H_2O by bubbling 100% CO_2 for ~ 1 hr	N/A	7, 11, 16, 17, 26, 32, 40, 50, 55, 65, 69	N/A[1]
Defliese et al. (2015)	**5 °C:** Passive degassing + daily addition **≥ 25 °C:** Passive degassing	**5 °C:** 1 ml of $CaCl_2$ solution added daily to $NaHCO_3$ solution to induce $CaCO_3$ precipitation by passive degassing of CO_2 **≥ 25 °C:** $CaCl_2$ and $NaHCO_3$ solutions mixed and exposed to atmosphere, passive degassing of CO_2 induces $CaCO_3$ precipitation	**5 °C:** 0.4L 270 mM CaCl2 and a 3.6L 27 mM $NaHCO_3$ solution **≥ 25 °C:** 0.4L 3.5 - 14 $CaCl_2$ mixed with 3.6L 3.5 - 1.4 mM $NaHCO_3$	10 days for 5 °C, 48 - 72 hr for ≥ 25 °C	5, 25, 50, 70	N/A[2]
Kluge et al. (2015)	Forced N_2 degassing	Continuous slow bubbling of humidified N_2 (60 bubbles/min) through a saturated $Ca(HCO_3)_2$ solution removes CO_2 and induces $CaCO_3$ precipitation	Dissolution of 360 mg calcite / 500 ml H_2O by bubbling CO_2. Filtered to remove excess $CaCO_3$. CO_2 bubbled during equilibration period. In some cases, NaCl was added.	Minimum 15, 14, 15, 3, 3 and 2 hr for 23.5 + 25.7, 37.5, 49.6, 69.9, 79.9 and 91.0 °C, respectively	23.5, 25.7, 37.5, 49.6, 69.9, 79.9 and 91.0	N/A[1]
Tripati et al. (2015)	Forced N_2 degassing	Continuous slow bubbling of humidified N_2 (40 bubbles/min) through a saturated $Ca(HCO_3)_2$ solution removes CO_2 and induces $CaCO_3$ precipitation	Dissolution of $CaCO_3$ / 1L H_2O by bubbling 100% CO_2 for ~ 1 hr. Filtered to remove excess $CaCO_3$. Carbonic anhydrase added to some experiments.	7 days for 0.5 °C, 72 hr for others	0.5, 25, 27, 30, 40, 50	N/A[1]

---

*Experiment HA1 prepared differently from remaining experiments

**Ionic strength of experiments was altered: 5 and 40 °C = 35 mM, 25 °C = 35, 292 or 832 mM

[1] Starting pH likely low-moderate after 1-2 hr CO_2 bubbling

[2] Starting pH presumably ~ 8.3 (HCO_3^{2-}-dominated starting solution)

Table S1: Clumped isotope measurement statistics of inorganic $CaCO_3$ precipitation experiments used in clumped isotope calibration studies

Reference	Temperature points (°C)	Temp control (± °C)	Experimental reproducibility				
			Repeat experiments	Avg. Δ_{47}	Stdev	Sterr	Avg. Replicate analyses per experiment (*n*)
This study	15	0.1	3	0.726	0.001	0.001	4
	16	0.1	2	0.718	0.003	0.002	3.5
	25	0.05	4	0.689	0.006	0.003	3.75
	40	0.05	4	0.658	0.004	0.002	3.75
		Total experiments:	**13**			**Total individual analyses:**	**49**
Ghosh et al. (2006)	1	0.2	1	0.826	N/A	N/A	11
	23	1	3	0.717	0.048	0.028	5.33
	33	2	1	0.649	N/A	N/A	6
	50	2	2	0.598	0	0	7.5
		Total experiments:	**7**			**Total individual analyses:**	**48**
Dennis and Schrag (2010)	7.5	1	1	0.718	N/A	N/A	2
	10	1	1	0.740	N/A	N/A	3
	15	1	2	0.695	0.021	0.015	2.5
	20	1	2	0.722	0.047	0.033	2
	25	1	1	0.701	N/A	N/A	2
	30	1	2	0.669	0.003	0.002	2.5
	40	1	1	0.644	N/A	N/A	4
	50	2	1	0.605	N/A	N/A	5
	60	2	1	0.619	N/A	N/A	4
	70	2	2	0.598	0.018	0.013	3.5
	77	2	1	0.581	N/A	N/A	3
		Total experiments:	**15**			**Total individual analyses:**	**44**
Zaarur et al. (2013)	5	0.5	1	0.806	N/A	N/A	3
	8	0.5	1	0.770	N/A	N/A	3
	15	0.5	1	0.738	N/A	N/A	3
	25	0.5	1	0.705	N/A	N/A	3
	35	0.5	1	0.671	N/A	N/A	3
	50	0.5	1	0.612	N/A	N/A	3
	65	0.5	1	0.565	N/A	N/A	3
		Total experiments:	**7**			**Total individual analyses:**	**21**
Tang et al. (2014)	5	0.5	11	0.754	0.016	0.005	3.78
	25	0.5	7	0.688	0.019	0.007	3

	40	0.5	7	0.649	0.020	0.008	1.86
		Total experiments:	**25**			**Total individual analyses:**	**76**
Affek and Zaarur (2014)	7	N/A	1	0.732	N/A	N/A	3
	11	N/A	2	0.715	0.002	0.002	2.5
	16	N/A	1	0.667	N/A	N/A	3
	17	N/A	1	0.701	N/A	N/A	4
	26	N/A	2	0.681	0.006	0.004	4
	32	N/A	1	0.648	N/A	N/A	5
	40	N/A	2	0.621	0.017	0.012	3
	50	N/A	1	0.604	N/A	N/A	4
	55	N/A	1	0.611	N/A	N/A	4
	65	N/A	1	0.544	N/A	N/A	3
	69	N/A	1	0.576	N/A	N/A	3
		Total experiments:	**14**			**Total individual analyses:**	**48**
Defliese et al. (2015)	5	N/A	1	0.7400	N/A	N/A	4
	25	N/A	1	0.6953	N/A	N/A	4
	50	N/A	1	0.6195	N/A	N/A	4
	70	N/A	1	0.6100	N/A	N/A	4
		Total experiments:	**4**			**Total individual analyses:**	**16**
Tripati et al. (2015)	0.5		2	0.796	0.006	0.005	2
	25		3	0.678	0.021	0.012	2.67
	27		1	0.684	N/A		3
	30		2	0.663	0.014	0.010	2
	40		2	0.647	0.008	0.006	2
	50		2	0.598	0.011	0.008	2
		Total experiments:	**12**			**Total individual analyses:**	**27**

Table S2: Comparison of published clumped isotope standard material Δ_{47} values

Standard	Reference	Individual aliquot name	$\Delta_{47\text{-RF}}$ (‰)*	1 SE	*n*
NBS-19	This study		0.367	0.005	3
	Dennis et al. (2011) - Harvard		0.373	0.007	7
	Dennis et al. (2011) - Johns Hopkins		0.399	0.005	12
	Dennis et al. (2011) - Yale		0.404	0.006	40
	Petersen and Schrag (2014)		0.366	0.007	9
	Meckler et al. (2014)		0.390	0.005	3
	Henkes et al. (2014)		0.404	0.003	9
		Average:	**0.386**	**0.006**	
NBS-18	This study		0.422	0.009	3
Carrara Marble**	This study		0.389	0.008	14
	Dennis et al. (2011) - CalTech	N/A	0.392	0.007	18
	Dennis et al. (2011) - Harvard	CM2	0.385	0.005	40
	Dennis et al. (2011) - Johns Hopkins	UU-Carrara	0.403	0.006	8
	Dennis et al. (2011) - Yale	YCM	0.400	0.004	49
	Kluge and Affek (2012)	Carrara marble	0.358	0.003	66
	Dennis and Cochran (2013)	CM2	0.388	0.005	53
	Henkes et al. (2013)	UU-Carrara	0.403	0.002	93
	Rosenheim et al. (2013)	IAEA CO-1 and C-1	0.391	0.006	19
	Dale et al. (2014)	ETH-3	0.391	0.005	42
	Henkes et al. (2014)	UU-Carrara	0.402	0.003	27
	Tripati et al. (2015) - Caltech MS 1	N/A	0.394	0.006	12
	Tripati et al. (2015) - Caltech MS 2	N/A	0.395	0.004	10
	Tripati et al. (2015) - UCLA MS	N/A	0.386	0.002	72
		Average:	**0.391**	**0.003**	

*Variability of $\Delta_{47\text{-RF}}$ values may partially relate to the adoption of differing acid fractionation factors ($\Delta^*_{25\text{-Tacid}}$) amongst laboratories

**Separate aliquots of Carrara Marble may possess unique $\Delta_{47\text{-RF}}$ values

3.8. References

Adkins J. F., McIntyre K. and Schrag D. P. (2002) The salinity, temperature, and $\delta^{18}O$ of the glacial deep ocean. *Science* **298**, 1769–1773.

Affek H. P. and Zaarur S. (2014) Kinetic isotope effect in CO_2 degassing: Insight from clumped and oxygen isotopes in laboratory precipitation experiments. *Geochimica et Cosmochimica Acta* **143**, 319–330.

Beck W. C., Grossman E. L. and Morse J. W. (2005) Experimental studies of oxygen isotope fractionation in the carbonic acid system at 15°, 25°, and 40°C. *Geochimica et Cosmochimica Acta* **69**, 3493–3503.

Brenninkmeijer C. A. M., Kraft P., and Mook W. G. (1983) Oxygen isotope fractionation between CO_2 and H_2O. *Isotope geoscience* **1**, 181–190.

Cao X. and Liu Y. (2012) Theoretical estimation of the equilibrium distribution of clumped isotopes in nature. *Geochimica et Cosmochimica Acta* **77**, 292–303.

Chacko T. and Deines P. (2008) Theoretical calculation of oxygen isotope fractionation factors in carbonate systems. *Geochimica et Cosmochimica Acta* **72**, 3642–3660.

Clark I. D., Fontes J.-C., and Fritz P. (1992) Stable isotope disequilibria in travertine from high pH waters: Laboratory investigations and field observations from Oman. *Geochimica et Cosmochimica Acta* **56**, 2041–2050.

Clark I. D. and Lauriol B. (1992) Kinetic enrichment of stable isotopes in cryogenic calcites. *Chemical Geology (Isotope Geoscience Section)* **102**, 217–228.

Daëron M., Guo W., Eiler J., Genty D., Blamart D., Boch R., Drysdale R., Maire R., Wainer K. and Zanchetta G. (2011) $^{13}C^{18}O$ clumped in speleothems: Observations from natural caves and precipitation experiments. *Geochimica et Cosmochimica Acta* **75**, 3303–3317.

Defliese W. F., Hren M. T. and Lohmann K. C. (2015) Compositional and temperature effects of phosphoric acid fractionation on Δ_{47} analysis and implications for discrepant calibrations. *Chemical Geology* **396**, 51–60.

Defliese W. F. and Lohmann K. C. (2015) Non-linear mixing effects on mass-47 CO_2 clumped isotope thermometry: Patterns and implications. *Rapid Communications in Mass Spectrometry* **29**, 901–909.

Dennis K. J., Affek H. P., Passey B. H., Schrag D. P. and Eiler J. M. (2011) Defining an absolute reference frame for 'clumped' isotope studies of CO_2. *Geochimica et Cosmochimica Acta* **75**, 7117–7131.

Dennis K. J. and Schrag D. P. (2010) Clumped isotope thermometry of carbonatites as an indicator of diagenetic alteration. *Geochimica et Cosmochimica Acta* **74**, 4110–4122.

Dietzel M., Tang J., Leis A. and Köhler S. J. (2009) Oxygen isotope fractionation during inorganic calcite precipitation – Effects of temperature, precipitation rate and pH. *Chemical Geology* **268**, 107–115.

Dreybrodt W. and Scholz D. (2011) Climatic dependence of stable carbon and oxygen isotope signals recorded in speleothems: From soil water and speleothem calcite. *Geochimica et Cosmochimica Acta* **75**, 734–752.

Eagle R.A., Eiler J.M., Tripati A.K., Ries J.B., Freitas P.S., Hiebenthal C., Wanamaker Jr. A. D., Taviana M., Elliot M., Marenssi S., Nakamura K., Ramirez P., and Roy K. (2013) The influence of temperature and seawater carbonate saturation state on ^{13}C-^{18}O bond ordering in bivalve mollusks. *Biogeosciences* **10**, 4591–4606.

Eiler J. M. and Schauble E. (2004) $^{18}O^{13}C^{16}O$ in Earth's atmosphere. *Geochimica et Cosmochimica Acta* **68**, 4767–4777.

Fernandez A., Tang J. and Rosenheim B. E. (2014) Siderite 'clumped' isotope thermometry: A new paleoclimate proxy for humid continental environments. *Geochimica et Cosmochimica Acta* **126**, 411–421.

Garzione C. N., Hoke G. D., Libarkin J. C., Withers S., Macfadden B., Eiler J., Ghosh P. and Mulch A. (2008) Rise of the Andes. *Science* **320**, 1304–1307.

Ghosh P., Adkins J., Affek H., Balta B., Guo W., Schauble E. A., Schrag D. and Eiler J. M. (2006) ^{13}C–^{18}O bonds in carbonate minerals: A new kind of paleothermometer. *Geochimica et Cosmochimica Acta* **70**, 1439–1456.

Green M. and Taube H. (1963) Isotopic fractionation in the OH^--H_2O exchange reaction. *Journal of Physical Chemistry* **67**, 1565–1566.

Guo W. (2008). *Carbonate clumped isotope thermometry: application to carbonaceous chondrites and effects of kinetic isotope fractionation*. Ph. D. thesis, Div. of Geology and Planetary Science, Caltech, Pasadena, CA.

Guo W., Mosenfelder J. L., Goddard III W. A. and Eiler J. M. (2009a) Isotopic fractionations associated with phosphoric acid digestion of carbonate minerals: Insights from first-principles theoretical modeling and clumped isotope measurements. *Geochimica et Cosmochimica Acta* **73**, 7203–7225.

Guo W., Kim, S. Thiagarajan N., Adkins J. F. and Eiler J. M. (2009b). Mechanisms for “vital effects” in biogenic carbonates: New perspectives based on abundances of ^{13}C-^{18}O bonds. *Eos Trans. AGU* **90**(52) Fall Meet. Suppl. Abstract PP34B-07.

He B., Olack G. A., and Colman A. S. (2012) Pressure baseline correction and high-precision CO_2 clumped-isotope (Δ_{47}) measurements in bellows and micro-volume modes. *Rapid Communications in Mass Spectrometry* **26**, 2837–2853.

Hill P. S., Schauble E. A. and Tripati A. K. (2014) Theoretical constraints on the effects of pH, salinity, and temperature on clumped isotope signatures of dissolved inorganic carbon species and precipitating carbonate minerals. *Geochimica et Cosmochimica Acta* **125**, 610–652.

Horita J. and Clayton R. N. (2007) Comment on the studies of oxygen isotope fractionation between calcium carbonates and water at low temperatures by Zhou and Zheng (2003; 2005). *Geochimica et Cosmochimica Acta* **71**, 3131–3135.

Huntington K.W., Eiler J.M., Affek H.P., Guo W., Bonifacie M., Yeung L.Y., Thiagarajan N., Passey B., Tripati A., Daëron M., and Came R. (2009) Methods and limitations of ‘clumped’ CO_2 isotope (Δ_{47}) analysis by gas-source isotope ratio mass spectrometry. *Journal of Mass Spectrometry* **44**, 1318–1329.

Jiménez-López C., Cabellero E., Huertas F. J. and Romanek C. S. (2001) Chemical, mineralogical and isotope behavior, and phase transformation during the precipitation of calcium carbonate minerals from intermediate ionic solution at 25°C. *Geochimica et Cosmochimica Acta* **65**, 3219–3231.

Kern D. M. (1960) The hydration of carbon dioxide. *Journal of Chemical Education* **37**, 14–23.

Kim S.-T., Gebbinck C. K., Mucci A. and Coplen T. B. (2014) Oxygen isotope systematics in the aragonite-CO_2-H_2O-NaCl system up to 0.7 mol/kg ionic strength at 25 °C. *Geochimica et Cosmochimica Acta* **137**, 147–158.

Kim S.-T., Coplen T. B. and Horita J. (2015) Normalization of stable isotope date for carbonate minerals: Implementation of IUPAC guidelines. *Geochimica et Cosmochimica Acta* **158**, 276–289.

Kim S.-T., Hillaire-Marcel C. and Mucci A. (2006) Mechanisms of equilibrium and kinetic oxygen isotope effects in synthetic aragonite at 25 °C. *Geochimica et Cosmochimica Acta* **70**, 5790–5801.

Kim S.-T. and O’Neil J. R. (1997) Equilibrium and nonequilibrium oxygen isotope effects in synthetic carbonates. *Geochimica et Cosmochimica Acta* **61**, 3461–3475.

Kim S.-T., O’Neil J. R., Hillaire-Marcel C. and Mucci A. (2007) Oxygen isotope fractionation between synthetic aragonite and water: Influence of temperature and Mg^{2+} concentration. *Geochimica et Cosmochimica Acta* **71**, 4704–4715.

Kluge T. and John C. M. (2015) Effects of brine chemistry and polymorphism on clumped isotope revealed by laboratory precipitation of mono- and multiphase calcium carbonates. *Geochimica et Cosmochimica Acta* **160**, 155–168.

Kluge T., John C. M., Jourdan A.-L., Davis S. and Crawshaw J. (2015) Laboratory calibration of the calcium carbonate clumped isotope thermometer in the 25-250 °C temperature range. *Geochimica et Cosmochimica Acta* **157**, 213–227.

McConnaughey T. (1989) ^{13}C and ^{18}O isotopic disequilibrium in biological carbonates: II. *In vitro* simulation of kinetic isotope effects. *Geochimica et Cosmochimica Acta* **53**, 163–171.

McConnaughey T. A. (2003) Sub-equilibrium oxygen-18 and carbon-13 levels in biological carbonates: carbonate and kinetic models. *Coral Reefs* **22**, 316–327.

McCrea J.M. (1950) On the isotopic chemistry of carbonates and a paleotemperature scale. *The Journal of Chemical Physics* **18**, 849–857.

McManus J. F., Oppo D. W. and Cullen J. L. (1999) A 0.5-million-year record of millennial-scale climate variability in the North Atlantic. *Science* **283**, 971–975.

O'Neil J. R., Clayton R. N. and Mayeda T. K. (1969) Oxygen isotope fractionation in divalent metal carbonates. *The Journal of Chemical Physics* **51**, 5547–5558.

Romanek C. S., Grossman E. L. and Morse J. W. (1992) Carbon isotopic fractionation in synthetic aragonite and calcite: Effects of temperature and precipitation rate. *Geochimica et Cosmochimica Acta* **56**, 419–430.

Saenger C., Affek H. P., Felis T., Thiagarajan N., Lough J. M., and Holcomb M. (2012) Carbonate clumped isotope variability in shallow water corals: Temperature dependence and growth-related vital effects. *Geochimica et Cosmochimica Acta* **99**, 224–242.

Tang J., Dietzel M., Fernandez A., Tripati A. K. and Rosenheim B. E. (2014) Evaluation of kinetic effects on clumped isotope fractionation (Δ_{47}) during inorganic calcite precipitation. *Geochimica et Cosmochimica Acta* **134**, 120–136.

Thiagarajan N., Adkins J., and Eiler J. (2011) Carbonate clumped isotope thermometry of deep-sea corals and implications for vital effects. *Geochimica et Cosmochimica Acta* **75**, 4416–4425.

Tripati A. K., Hill P. S., Eagle R. A., Mosenfelder J. L., Tang J., Schauble E. A., Eiler J. M., Zeebe R. E., Uchikawa J., Coplen T. B., Ries J. B. and Henry D. (2015) Beyond temperature: Clumped isotope signatures in dissolved inorganic carbon species and the influence of solution chemistry on carbonate mineral composition. *Geochimica et Cosmochimica Acta* **166**, 344–371.

Usdowksi E., Michaekus J., Botcher M. and Hoefs J. (1991) Factors for the oxygen isotope equilibrium fractionation between aqueous and gaseous CO_2, carbonic acid, bicarbonate, carbonate, and water (19 °C). *Zeitschrift für Physikalische Chemie* ***170***, *237*–249.

Wacker U., Fiebig J. and Schoene B. R. (2013) Clumped isotope analysis of carbonates: comparison of two different acid digestion techniques. *Rapid Communications in Mass Spectrometry* **27**, 1631–1642.

Wang Z., Schauble E. A. and Eiler J. M. (2004) Equilibrium thermodynamics of multiply substituted isotopologues of molecular gases. *Geochimica et Cosmochimica Acta* **68**, 4779–4797.

Watson B. E. (2004) A conceptual model for near-surface kinetic controls on the trace-element and stable isotope composition of abiogenic calcite crystals. *Geochimica et Cosmochimica Acta* **68**, 1473–1488.

Zaarur S., Affek H. P. and Brandon M. T. (2013) A revised calibration of the clumped isotope thermometer. *Earth and Planetary Science Letters* **382**, 47–57.

Zeebe R. E. (2005) Reply to the comment by P. Deines on “An explanation of the effect of seawater carbonate concentration on foraminiferal oxygen isotopes,” by R. E. Zeebe 1999. *Geochimica et Cosmochimica Acta* **69**, 789–790.

CHAPTER 4: Conclusion

4.1. Advancements and Future Growth of the Carbonate Clumped Isotope Paleothermometer

Carbonate clumped isotope geochemistry offers an invaluable geochemical proxy for assessing the formation temperature of carbonate minerals. Unlike the conventional carbonate-water oxygen isotope paleothermometer, the clumped isotope composition of carbonates is independent of the oxygen isotope composition of parent water. This permits the estimation of carbonate formation temperature in cases where the oxygen isotope composition of parent water is immeasurable or poorly constrained (e.g., Jurassic Sauropods or the Allan Hills 84001 Martian meteorite; Eagle et al., 2011; Halevy et al., 2011). The precise and accurate application of the carbonate clumped isotope paleothermometer is dependent on three primary criteria. First, the clumped isotope composition of the preserved carbonate must still reflect clumped isotope equilibrium relative to its formation temperature. Paleotemperature estimates may be construed if the carbonate has inherited non-equilibrium clumped isotope effects during formation, or if diagenetic alteration has resulted in partial re-equilibration of the clumped isotope signature. Second, given the exceptionally low abundance of the $^{13}C^{18}O^{16}O$ isotopologue (~ 45 ppm) of acid-liberated CO_2, a rigorous purification, measurement, and normalization protocol is necessary to attain reasonable reproducibility for the $\Delta_{47\text{-RF}}$ value. Finally, a suitable well-defined carbonate clumped isotope equilibrium calibration must be applied to determine the carbonate formation temperature.

Carbonate clumped isotope geochemistry is still in its first decade of existence. In this time, innovations associated with the analytical protocol have permitted substantial decreases in necessary sample size, refined carbonate pre-treatment protocols, identified mineralogical and temperature specific isotope effects associated with phosphoric acid digestion, enabled the full automation of clumped isotope measurements, identified and corrected mass spectrometer-specific isotope effects, and provided a robust normalization protocol for inter-laboratory comparison of the $\Delta_{47\text{-RF}}$ value. Beyond these improvements, there still exists several considerations for future clumped isotope studies. To date, there is still substantial disagreement between theoretical and experimental derivations of the clumped isotope acid fractionation factor. Furthermore, although several new acquisition protocols account for machine-specific isotope effects, in some cases, these correction protocols lead to over-compensation, and still require a suitable normalization protocol to reduce unintended isotope effects. Finally, and perhaps most importantly, given the capabilities of current generation mass spectrometers, a method to directly measure the Δ_{63} value of carbonates remains elusive.

Disagreement amongst calibrations of the carbonate clumped isotope paleothermometer complication the estimation of carbonate formation temperatures. Calibrations are distinctly separated into two categories, *'shallow'* slope calibrations similar to Dennis and Schrag (2010), and *'steep'* slope calibrations similar to Ghosh et al. (2006). To elucidate true carbonate clumped isotope equilibrium, inorganic calcites were slowly precipitated at 15, 25, and 40 °C using an upgraded constant addition technique to provide control of both the oxygen and carbon isotopic composition of the parent solution. Calcites conform to the Kim and O'Neil (1997) calcite-water oxygen isotope equilibrium curve, providing a conservative assurance of precipitation in isotopic equilibrium. The calibration of the clumped isotope composition of precipitated calcites is indistinguishable from *'shallow'* slopes calibrations, suggesting these studies observed clumped isotope equilibrium. In comparison, it is plausible that carbonates conforming to the *'steep'* slope calibrations inherited non-equilibrium isotope effects during precipitation.

These isotope effects are possibly linked to precipitation method, where all *'steep'* slope calibration studies employed the forced CO_2 degassing method from a parent solution formed through dissolution of reagent $CaCO_3$ via CO_2 bubbling. The physicochemical properties of this system appear to support non-equilibrium isotope effects associated with CO_2 hydration/hydroxylation as well as HCO_3^- dehydration/dehydroxylation, where the contribution from each effect is dependent on precipitation temperature. Although the observed calcite-water oxygen isotope fractionation from these carbonates commonly reflects non-equilibrium isotope effects, the extent of these effects is uncharacteristic of the predicted behavior of the CO_2 hydration/hydroxylation and HCO_3^- dehydration/dehydroxylation pathways. Instead, it is peculiar that $CO_{2(g)}$, and possibly $CO_{2(aq)}$, share a similar temperature dependency to *'steep'* slope calibrations. This observation could imply that the clumped isotope composition of *'steep'* slope carbonates can partially reflect $CO_{2(aq)}$ if rapidly precipitating from a CO_2-dominated DIC reservoir. Prior to a conclusive understanding of the source of the calibration discrepancy, the precision of carbonate formation temperature determinations is debatable. However, upon resolution, it is clear that the emerging field of carbonate clumped isotope geochemistry holds great promise for future paleoclimate studies.

4.2. References

Dennis K. J. and Schrag D. P. (2010) Clumped isotope thermometry of carbonatites as an indicator of diagenetic alteration. *Geochimica et Cosmochimica Acta* **74**, 4110–4122.

Eagle R. A., Tütken T., Martin T. S., Tripati A. K., Fricke H. C., Connely M., Cifelli R. L., and Eiler J. M. (2011) Dinosaur body temperatures determined from isotopic (^{13}C-^{18}O) ordering in fossil biominerals. *Science* **333**, 443–445.

Ghosh P., Adkins J., Affek H., Balta B., Guo W., Schauble E. A., Schrag D. and Eiler J. M. (2006) ^{13}C–^{18}O bonds in carbonate minerals: A new kind of paleothermometer. *Geochimica et Cosmochimica Acta* **70**, 1439–1456.

Halevy I., Fischer W. W., and Eiler J. M. (2011) Carbonates in the Martian meteorite Allan Hills 84001 formed at 18 ± 4 °C in a near-surface aqueous environment. *Proceedings of the National Academy of Sciences of the United States of America* **108**, 16895–16899.

Kim S.-T. and O'Neil J. R. (1997) Equilibrium and nonequilibrium oxygen isotope effects in synthetic carbonates. *Geochimica et Cosmochimica Acta* **61**, 3461–3475.